ELUCIDATING MECHANISMS OF LIVER DEVELOPMENT AND LIVER PROGENITOR CELL-DRIVEN REGENERATION IN ZEBRAFISH

by

Mehwish Khaliq

B.Sc., University of Michigan, 2008

MPH, University of Michigan, 2011

Submitted to the Graduate Faculty of

University of Pittsburgh in partial fulfillment

of the requirements for the degree of

Doctor of Philosophy

University of Pittsburgh

2017

UNIVERSITY OF PITTSBURGH

SCHOOL OF MEDICINE

This dissertation was presented

by

Mehwish Khaliq

It was defended on

May 19, 2017

and approved by

Paul Monga, MD, Professor, Pathology

Nathan Bahary, MD PhD, Associate Professor, Medicine

Lance Davidson, PhD, Associate Professor, Developmental Biology

Michael Tsang, PhD, Associate Professor, Developmental Biology

Dissertation Advisor: Donghun Shin, PhD, Associate Professor, Developmental Biology

ELUCIDATING MECHANISMS OF LIVER DEVELOPMENT AND LIVER PROGENITOR CELL-DRIVEN REGENERATION IN ZEBRAFISH

Mehwish Khaliq

University of Pittsburgh, 2017

Chronic liver disease encompasses the steady destruction of hepatic tissue over time, resulting in the replacement of healthy liver tissue with damaged fibrotic and cirrhotic tissue. Among other symptoms, cirrhosis manifests itself with regenerative hepatic nodules and portal hypertension, triggering a loss of liver functionality and poor quality of life. Moreover, in the United States, cirrhosis remains the 12th leading cause of death, incurring healthcare costs of billions of dollars. Despite the astronomical costs and limited palliative care, the only effective treatment for cirrhosis is liver transplantation. The demand for liver transplants, however, far exceeds the availability of donor livers, underpinning the need for harnessing the liver's innate regenerative capacity. Using zebrafish as a model organism, the main aim of this dissertation is to elucidate the underlying mechanisms of liver progenitor cell (LPC)-driven liver regeneration as well as liver development, since events involved in the former process can be recapitulated in the latter. Our lab previously characterized the biliary epithelial cell (BEC)-driven liver regeneration in which after extensive hepatocyte ablation, BECs dedifferentiate into LPCs and subsequently, the LPCs can re-differentiate into mature hepatocytes/BECs. During this regenerative process, our RNAseq analysis showed an upregulation of genes mediating the Bone Morphogenetic Protein (BMP) pathway, including a BMP downstream target gene, Inhibitor of DNA binding 2a (Id2a). Using loss- and gain-of-function approaches, we show Id2a to be an important regulator of hepatic outgrowth during liver development as well as an important mediator of BEC repopulation in LPC-driven liver regeneration. In addition, as LPC activation is often accompanied by an inflammatory

cell response, our second focus was on the role of Signal Transducer and Activator of Transcription 3 (Stat3) in the LPC-driven liver regeneration model. By chemically inhibiting Stat3, we show Stat3 signaling regulates not only the differentiation of LPCs into hepatocytes, but also the proliferation of BECs during LPC-driven liver regeneration.

TABLE OF CONTENTS

LIST OF TABLES

LIST OF FIGURES

PREFACE

First, I would like to express my deepest appreciation and gratitude to my advisor, Dr. Donghun Shin, for his patient mentorship, time and ideas throughout my graduate school life. It was an honor to be his first Ph.D. student. I also thank my thesis committee members, Drs. Paul Monga, Nathan Bahary, Michael Tsang, and Lance Davidson for their unwavering support, helpful feedback, and thought-provoking suggestions. Thanks to Dr. Monga for serving as my co-mentor on the CATER and NIH grants. Thanks to Dr. Bahary for providing guidance on my grant application. Thanks to Dr. Tsang for his constant encouragement and for setting aside his time to discuss my projects and future career options. Thanks to Dr. Davidson for guiding me and taking the time to discuss future career prospects with me. Without my mentor and committee members' expert guidance, I would not be here today.

I thank Drs. Michael Tsang, Neil Hukriede and Beth Roman and their respective lab members for sharing reagents, feedback and for making the environment on the 5th floor BST3 an enjoyable one. Thank you to DLAR staff, the fish community and the Department of Developmental Biology. Thank you to my funding sources (NIH and the CATER training program).

I thank my lab members for training me as well as for helpful discussions and advice in troubleshooting experiments.

I especially thank God for His immeasurable guidance.

Last, but not least, I would like to thank my family (my parents and siblings) and friends (here and abroad) for their support, encouragement and patience during the highs and lows.

1.0 INTRODUCTION

The liver performs several key regulatory and metabolic functions important for maintaining homeostasis, such as: immune regulation, synthesis and secretion of cholesterol, bile and blood clotting factors, metabolism of urea and glucose as well as drug detoxification. As blood from the intestine has direct contact with the liver, the liver is easily exposed to harmful substances throughout an organism's lifetime. Furthermore, due to the importance of the liver in homeostatic processes, any injurious exposure or congenital manifestation can be debilitating to the human health. Liver disease can arise from various etiologies, including metabolic, congenital and infectious (hemochromatosis, alpha-1 anti-trypsin deficiency, acute hepatitis A, B, E and acute HSV hepatitis), leading to severe morbidity and mortality. Considering the importance of the liver in homeostatic maintenance, it is not surprising to find the liver possesses the incredible capacity to regenerate. In unfolding the process of liver regeneration, it is equally significant to simultaneously study the process of liver development. In fact, several signaling pathways and genes active during hepatogenesis are also important for liver regeneration. Therefore, using zebrafish as a model organism, the primary focus of this dissertation is to understand the mechanisms involved in liver development and liver regeneration.

1.1 SIGNIFICANCE AND RELEVANCE TO HUMAN HEALTH

Chronic liver disease and cirrhosis are the 12th leading cause of death in the United States and the 4th most common among middle-aged adults [1]. Currently in the United States, for the approximate 40,000 patients suffering from end-stage chronic liver disease, liver transplantation remains the primary, proven and effective therapy. Unfortunately, the increasing demand for transplantable livers cannot solely be fulfilled by the available donors, a cohort that continues to plunge dramatically: from 7017 in 2006 to 6683 in 2011 [2]. Furthermore, the US health care cost associated with advanced liver disease or cirrhosis demands attention: direct costs (hospitalization/drug therapies) amount to $2.5 billion and indirect costs (quality of life, work productivity) can amount as high as $10.6 billion annually [3]. In addition, patients suffering from chronic liver disease are at an increased risk of developing hepatocellular carcinoma, the second leading cause of all cancer deaths worldwide [4].

Undoubtedly for these patients, there exists a pressing need to fully recognize the underlying mechanisms involved in the intricate processes of liver development and regeneration. Since processes and mechanisms active during development can often be recapitulated during regeneration, it is vital to study both events in unison to address the ultimate goal of liver research: identify novel targets that will enhance or restore the liver's innate regenerative capacity in patients suffering from chronic liver diseases.

1.2 ZEBRAFISH AS A MODEL ORGANISM

Originally used as a research model organism in 1937, zebrafish (*Danio rerio*) are now used extensively to study developmental and regenerative processes as well as human diseases, such as cancer [5-9]. Specifically, zebrafish are a useful in vivo model for studying liver development and disease for several reasons. Zebrafish embryos develop outside of the mother. Embryos are large and initially optically transparent, allowing for easy visualization and accessibility during early development. Each mating opportunity can produce hundreds of embryos from a single clutch and these embryos can develop rapidly with a short generation time from birth to adulthood (about 3 months). In fact, organ development in zebrafish is relatively rapid: the heart begins beating by 24 hours post fertilization (hpf) and a functional liver forms by 5 days post fertilization (dpf). The zebrafish also have organs relevant for the study of human disease, including eyes, kidneys, heart and liver.

Zebrafish are especially important for small molecule in vivo chemical screening [10]. Due to their small size, zebrafish embryos can be efficiently utilized for high throughput assays to screen for clinically relevant drugs with therapeutic potential [11, 12]. Previously successful screens have included effects of compounds on increasing hematopoietic stem cell numbers [13], tumor growth suppressors [14], kidney cyst formation [15] and liver injury [16].

Many developmental and disease mechanisms as well as signaling pathways observed in humans and rodents have been successfully recapitulated in zebrafish [17]. Indeed, although the zebrafish teleost group experienced a genome duplication event between 250-400 million years ago [18], zebrafish still share about 70% of their genomes with humans and > 80% of disease-associated genes. The zebrafish genome has been fully sequenced [19]. Due to the maternal contribution of mRNA during early development, zebrafish mutants can also bypass the zygotic

demand for specific genes during development, allowing for the study of a genetic deficiency at later stages.

Several powerful tools and techniques have been developed to modify zebrafish genetics and investigate effects on development and disease. These techniques include generation of transgenic fish and forward and reverse genetic approaches. Using the Tol2 transposase system, numerous transgenic zebrafish lines have been produced for easy visualization of organs (i.e., liver, pancreas, heart), active signaling pathways (i.e., BMP, Notch, Wnt) and genetic injury models [20-25].

Forward genetic screening is an unbiased approach in which random mutations are introduced into the zebrafish genome following N-ethyl-N-nitrosourea (ENU) mutagenesis or retroviral insertion. Subsequent generations of zebrafish mutants of unknown genetic variation are analyzed for deleterious phenotype in an organ or gene of interest. Once a phenotype has been established, the mutant is further studied to pinpoint the corresponding mutated or defective gene. This approach in forward genetics has led to the discovery of several zebrafish mutants with liver-specific phenotypes [26], including *uhrf1* [27], *wnt2bb* [28] and *fgf10* [29].

Besides forward genetics screening, reverse genetics has also been successfully applied in zebrafish. For transient, knockdown studies, morpholino oligonucleotides (MOs) are used to block either mature mRNA translation or mRNA splicing of a gene of interest. Typically, MOs are injected at the 1-4-cell stage, making them especially powerful for developmental studies [30, 31]. Although MOs can provide useful information about effects of temporary gene knockdown, they have also been subject to criticism for off-target effects [32]. In addition, zebrafish have been targets of knockout (KO) studies. Targeted mutagenesis has come to the forefront in recent years with the discovery of Transcription Activator-Like Effector Nuclease (TALEN) and Clustered

Regularly Interspaced Short Palindromic Repeats (CRISPR) Type II system [33, 34]. Due to its improved knockout efficiency, CRISPR has replaced previous methods of genetic manipulation, including TALENs and zinc finger nucleases (ZFNs). Originally adapted from the bacterial defense mechanism, CRISPR technology allows for gene manipulation with the design of site-specific guide RNAs that direct the nonspecific CRISPR-associated endonuclease (Cas9) to the genomic site of interest. DNA cleavage by Cas9 endonuclease results in double strand breaks (DSB) at the genomic target sequence, which activates the non-homologous end joining (NHEJ) repair pathway. NHEJ is an error-prone repair pathway that results in a range of mutations due to random insertions or deletions (indels) at the cleaved site.

1.3 LIVER DEVELOPMENT

1.3.1 Overview of Liver Structure

As the largest internal organ in humans, the liver comprises 2-5% of the whole-body weight. The mammalian liver is organized into a lobular structure of hexagonal shape with each lobe containing bi-layered plates of parenchymal, polarized epithelial cells, termed hepatocytes [*see Figure 1*]. Hepatocytes are the main functional cells of the liver and conduct a multitude of functions, including bile and cholesterol synthesis and drug detoxification. At each corner of the hexagonal lobule is a portal triad, consisting of a hepatic artery, portal vein and a bile duct. From the intestine, blood rich in toxins and nutrients enters the liver at the portal vein; however, since this blood does not come directly from the heart, it contains mostly deoxygenated blood. Hence, the hepatic artery is necessary for providing an oxygenated blood supply to the liver. Blood then travels towards the

center of the lobule, termed the central vein, where it is eventually returned to circulation. Surrounding the hepatocytes are fenestrated endothelial cells termed sinusoids. Blood flows through the sinusoids from the portal triad towards the central vein.

Hepatocytes secrete bile into the canaliculi channels located at their apical membrane. Bile travels in a reciprocal direction to the blood flow, through the canals of Hering to the bile duct located in the portal triad [35, 36]. The bile duct is lined with biliary epithelial cells (BECs or cholangiocytes), which are important for bile and fluid secretion. The bile ducts will converge into the common hepatic duct, which transports bile from the liver to the gallbladder for storage.

In addition to hepatocytes, BECs and endothelial cells, additional cell types in the liver include hepatic stellate cells (HSCs) and Kupffer cells. HSCs are peri-sinusoidal pericytes found in the space of Disse and major contributors to liver fibrosis. Kupffer cells are specialized resident macrophages.

Although many of the hepatic cell types are evolutionarily conserved in zebrafish and humans, the zebrafish hepatic architecture is notably different from the human architecture. In contrast to the lobular structure, zebrafish liver is organized in a tubular shape with hepatocytes arranged in cords surrounding a single biliary channel composed of a single BEC. Bile travels from the hepatocytes through the pre-ductular intrahepatic bile channels to the extrahepatic and common hepatic duct. Endothelial cells line the basal side of the hepatocytes. Instead of the hepatic artery/portal vein present at the edge of the lobule, these structures are interspersed throughout the zebrafish liver. Upon injury, HSCs, typically quiescent vitamin A-storing cells, are activated and transform into myofibroblast-like cells. Myofibroblast-like cells secrete extracellular matrix (ECM) components such as collagen into the hepatic environment, which can be the basis of liver fibrosis. HSCs have also been identified in zebrafish and similar to humans and rodents, activated

HSCs are important for ECM deposition [37]. No resident macrophages (i.e., Kupffer cells) have yet been identified in zebrafish.

Besides the technical differences, metabolic zonation is also absent in zebrafish. The human liver displays functional plasticity, whereby differential gene expression results in hepatocyte-specific functional heterogeneity. This plasticity and variation in expression is caused by the location of hepatocytes and their proximity to either the portal triad or the central vein [38]. Unlike mammals, fetal hematopoiesis and early vasculogenesis do not occur in the zebrafish livers. Due to the absence of these two processes, the zebrafish can be used to study genes important in hepatogenesis, independent of hematopoiesis-related or early vasculogenesis-related phenotypes [39].

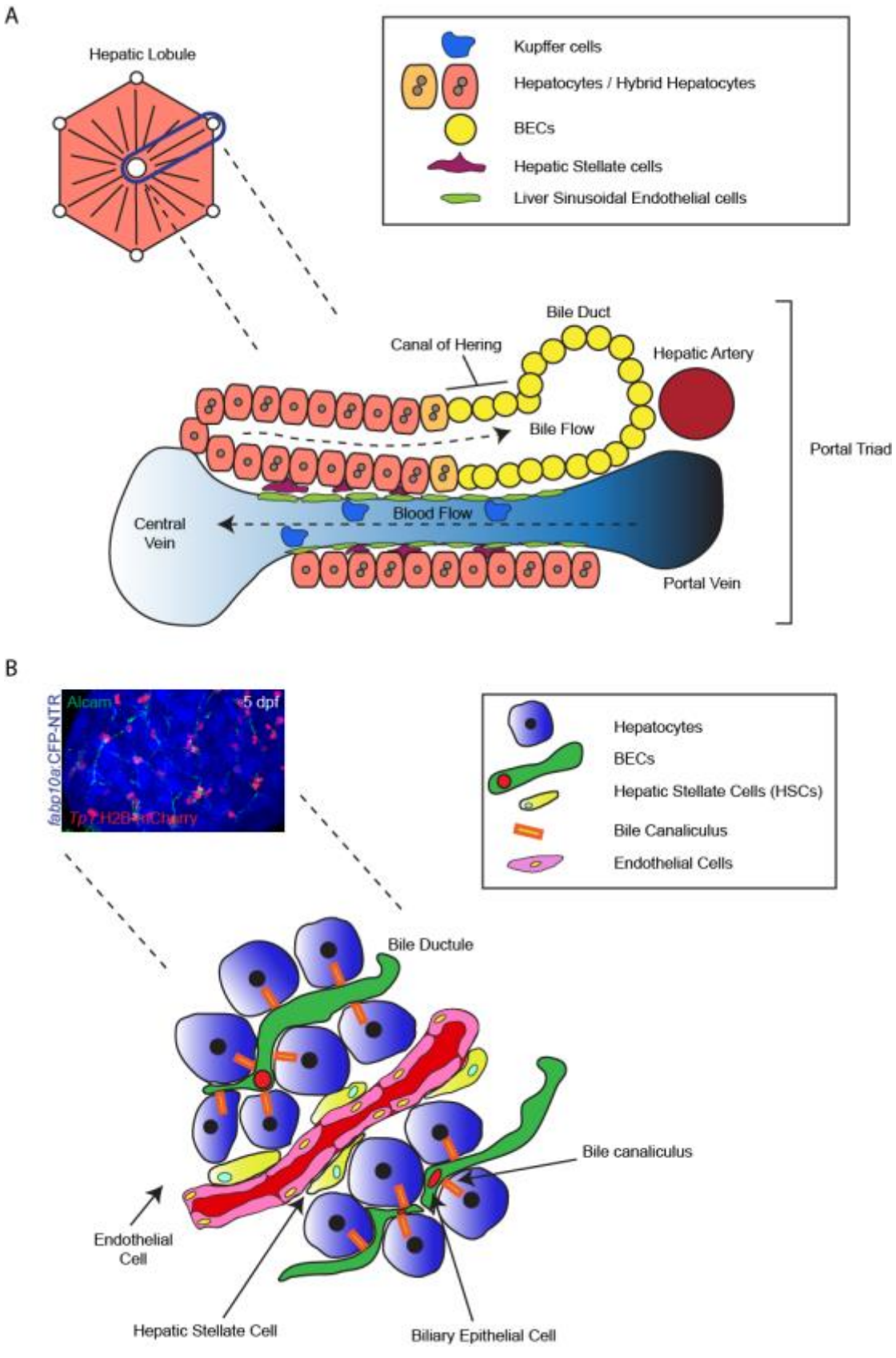
A
Hepatic Lobule
Kupffer cells
Hepatocytes / Hybrid Hepatocytes
BECs
Hepatic Stellate cells
Liver Sinusoidal Endothelial cells
Bile Duct
Canal of Hering
Hepatic Artery
Bile Flow
Portal Triad
Blood Flow
Central Vein
Portal Vein
B
fabp10a:CFP-NTR
Alcam
5 dpf
Tp1:H2B-RFPCherry
Hepatocytes
BECs
Hepatic Stellate Cells (HSCs)
Bile Canaliculus
Endothelial Cells
Bile Ductule
Bile canaliculus
Endothelial Cell
Hepatic Stellate Cell
Biliary Epithelial Cell

Figure 1: Overview of the mammalian and zebrafish liver structure

(A) The mammalian liver is organized into a lobular structure with the portal triads (containing hepatic artery, portal vein and bile duct) situated at each corner of the lobule. A zoomed-in view shows that while blood flows from the portal vein towards the central vein, bile flows in the opposite direction towards the portal triad. In addition to the two epithelial cell types found in the liver (i.e., hepatocytes and biliary epithelial cells (BECs)), the liver also contains Kupffer cells, hepatic stellate cells (HSCs) and liver sinusoidal endothelial cells. **(B)** The zebrafish liver is organized into a tubular structure. (Left) Confocal image of a 5-dpf liver stained with Alcam (BEC marker) in *Tg(fabp10a:CFP-NTR; Tp1: H2B-mCherry)* transgenic fish highlighting hepatocytes (blue) and BEC nuclei (red). (Right) Zoomed-in schematic of zebrafish liver structure with hepatocyte layers (blue) surrounding a single BEC (red), which projects its ductule (green). At their apical side, hepatocytes contain bile canaliculi (yellow/red outline), while at the basal end, hepatocytes are adjacent to the liver sinusoidal vessels (red). The HSCs can be found adjacent at the basal side of the hepatocytes, adjacent to the vessels (yellow). Note: Cell size not drawn to scale.

1.3.2 Overview of Liver Development in Mammals and Zebrafish

During gastrulation, three primary germ layers are formed: ectoderm, mesoderm and endoderm. The endoderm gives rise to several organs, including the stomach, pancreas and liver. The definitive endoderm forms when epiblast cells migrate into the cell interior through the primitive streak, displacing the visceral endoderm. During organogenesis, the definitive endoderm forms the primitive gut tube epithelium adjacent to mesodermal-derived tissue. Along the anterior-posterior and dorsal-ventral axes, the gut tube is patterned into 3 different domains: foregut, midgut and hindgut. This endodermal patterning is Wnt- and FGF-dependent as Wnt ligands (Wnt8, Wnt8b and Wnt3) and FGF4 signals from the adjacent mesoderm promote hindgut formation and suppress

foregut identity [40, 41]. Since the liver arises from the ventral/anterior foregut endoderm, Wnt signaling must be repressed to allow foregut endoderm formation [40, 42, 43].

Following endoderm patterning, foregut endodermal cells gain the competence to respond to inductive signals from the surrounding mesenchyme mainly due to the expression of specific pioneer transcription factors (i.e., FOXA and GATA). Prior to hepatoblast specification, FOXA and GATA regulate hepatic competence by occupying regulatory sites on chromatin gene enhancer regions, including that of the liver-specific gene, *Albumin* [44-46]. In the absence of enhancer site occupation, chromatin remains compact and *Albumin* gene transcription does not occur [47]. In the liver, FOXA/GATA binding facilitates chromatin accessibility for liver-specific factors.

Expressed in the foregut endoderm, GATA4, 5 and 6 are zinc finger transcription factors regulating endoderm differentiation as well as cardiac development [48-50]. *Gata4*$^{-/-}$ and *Gata6*$^{-/-}$ single knock-out embryos are embryonic lethal due to an impairment of extraembryonic endoderm differentiation and failure of gastrulation [51, 52]. To bypass this defect, *Gata6*$^{-/-}$ embryos were generated from via the tetraploid complementation assay. The embryos were obtained from *Gata6*$^{-/-}$ ES cells and wild-type extraembryonic tissues. In these embryos, although endoderm specification occurs normally, the liver bud fails to expand [53, 54]. In zebrafish, single knockdown of *gata4* or *6* also exhibit impaired liver expansion. Interestingly, *Gata4/6* double knockdowns fail to develop a liver bud altogether. These data suggest the redundant roles of *Gata4/6* in liver development [55].

Highly expressed in the liver, FOXA, also known as hepatocyte nuclear factor 3 (HNF3), is a transcription factor composed of forkhead DNA-binding motif (i.e., winged helix) as part of the helix-turn-helix class of proteins. Similar to the GATA factors, FOXA factors also play redundant roles during hepatogenesis. Both FOXA1 and A3 are expressed in the foregut endoderm

but FOXA1 or FOXA3 depletion alone appears to have no detrimental effect on liver development [56, 57]. Even when *FoxA1* or *A3* are simultaneously mutated in mice, liver development still occurs normally. *FoxA2* single-KO mice die prematurely due to aberrant notochord/node development [58, 59]. Interestingly, when *FoxA1/A2* are both deleted (*FoxA2* conditionally from the foregut endoderm at embryonic day (E) 8.5), hepatoblast specification is compromised and the liver bud fails to form. This highlights that single depletion of FOXA factors has little effect on hepatic competence and hepatoblast specification; together, however, FOXA1/A2 regulate the early liver developmental process [60].

Once competent endodermal cells are identified, liver development in zebrafish and mammals proceeds in three main stages: (1) hepatoblast specification; (2) hepatoblast differentiation; and (3) hepatic outgrowth.

Hepatoblast specification occurs when signals from the surrounding mesenchyme, such as the cardiac mesoderm and the septum transversum mesenchyme (STM), prompt the competent endodermal cells to commit to a hepatic fate. At E9.0 following specification, the hepatic diverticulum forms and is lined by hepatic endodermal cells at the anterior end. These cells, termed hepatoblasts, are a single layer of cuboidal-shaped epithelium that eventually transforms into a pseudostratified epithelium. Hepatoblasts proliferate and, together with mesenchymal tissues, produce matrix metalloproteinases (MMPs) that aid in degrading the extracellular matrix (ECM) in the basal lamina [61]. As the basal layer degrades, hepatoblasts delaminate and migrate into the septum transversum mesenchyme (STM). Subsequently, this newly formed liver bud undergoes immense growth as hepatoblasts continue to proliferate between E10-15. Also, during this time process, between E9.5 to 12.5, the bi-potent progenitor hepatoblasts differentiate into either hepatocytes or BECs.

In zebrafish, no hepatoblast migration occurs. Instead at 24 hpf, the endoderm-derived intestinal rod forms a bar of midline cells. Between 24-28 hpf, the intestinal rod thickens and loops as cells at the anterior region aggregate. The cell aggregate begins to bud leftward, away from the intestinal rod, forming the liver primordium. In zebrafish, the initiation of hepatoblast specification can be detected as early as 22-24 hpf with the onset of *hhex* and *prox1a* expression [62, 63]. Hepatoblast-to-hepatocyte differentiation can be detected as early as 32 hpf with the ceruloplasmin (*cp*) marker [64] or at 48 hpf with the fatty acid binding protein (*fabp10a*) [65]. Hepatoblast-to-biliary differentiation can be detected with the 2F11 or Keratin-18 staining [66, 67]. Following differentiation, hepatic outgrowth occurs at 50 hpf and consists of the rapid proliferation of hepatocytes and BECs as well as the morphogenesis of the biliary network.

The next section will examine the signaling pathways and factors important for the three stages of liver development.

1.3.3 Signaling Pathways and Factors Regulating Liver Development

Liver specification initiates once the ventral foregut endoderm receives inductive signals, including fibroblast growth factor (FGF) and bone morphogenetic protein (BMP) from the surrounding cardiac mesoderm and STM, respectively [68]. During hepatogenesis, as zebrafish do not possess a STM, embryos receive inductive BMP signals from the lateral plate mesoderm (LPM). Although FGF signals are also important for zebrafish hepatoblast specification, the source of these FGFs has not yet been identified [69, 70]. *Fgf10* is expressed in the mesenchymal tissue of the extrahepatic structures as well as the liver itself. Since *Fgf10*$^{-/-}$ mice have smaller livers, *Fgf10* is dispensable for hepatoblast specification, but important for hepatoblast proliferation [71]. This process involves Wnt/β-catenin signaling since *Fgf10* gain-of-function experiments results

in an upregulation of β-catenin during liver development, which may be AKT-dependent [72]. *fgf10a* signaling has also been implicated in regulating hepatic competence during zebrafish hepatogenesis [73].

Around E8.25 in mice, FGF signaling (specifically, FGF1 and 2) from the cardiac mesoderm [69, 74] were first identified as important for hepatoblast specification in mouse explants of foregut endoderm, which also expressed FGF receptors 1 and 4. FGF concentration is strictly regulated by the positioning of the STM, which separates the cardiac mesoderm from the endoderm [75]. In zebrafish embryos, FGF inhibition resulted in defective hepatoblast specification (reduced *hhex* and *prox1a* expression) and differentiation (no hepatocyte-specific marker expression) [70].

In addition to FGF, which is necessary but not sufficient for hepatoblast specification, BMP signaling from the STM is required for proper endodermal patterning, hepatoblast specification and hepatic differentiation [76]. Further information about the role of BMP signaling in liver development and liver regeneration is discussed in Section 1.5.

Wnt signaling also plays an important role in early hepatogenesis. In zebrafish, Wnt2bb and Wnt2 are secreted Wnt ligands expressed in the LPM that contribute to hepatoblast specification. Wnt signaling mutants, Prometheus (*prt*), which have defective *wnt2bb* are characterized by small or absent liver buds [28]. However, the defect is transient as these mutants eventually recover and can grow into adulthood. This observation indicates multiple Wnts may contribute to liver specification: for instance, when *wnt2* was additionally knocked down in *wnt2bb* mutants, *hhex* was not expressed and the liver failed to develop altogether [77]. In mice, however, double KOs of *Wnt* and *Wnt2b* has no effect on liver development [78, 79]. The study of *apc*$^{-/-}$ zebrafish mutants, which have dysregulated β-catenin degradation [80], uncovered the temporal

role of Wnt signaling in liver development: induction of Wnt at early somitogenesis blocked liver specification, whereas post-somitogenesis Wnt induction is important for hepatoblast proliferation, affecting the liver size [40, 81, 82].

Hepatic competence is retained in the zebrafish endodermal region posterior to the foregut endoderm, although this capacity is gradually lost over time. When *wnt8a* is overexpressed, both hepatoblast specification and differentiation are affected: (1) ectopic hepatoblast induction occurs in regions previously reserved for intestinal and pancreatic tissues; and (2) hepatoblast differentiation markers (*sox9b*, *cp*) are induced [73]. At later stages of liver development, Wnt/β-catenin signaling is critical for cell proliferation, survival, hepatocyte maturation and biliary differentiation in embryonic liver cultures [83].

Following hepatoblast specification, liver bud morphogenesis involves the contribution of several factors, including HEX and PROX1. HEX is a homeobox family of transcription factors that is expressed in the ventral foregut endoderm and in the liver [84]. *Hex* KO embryos lack several endodermal organs, including liver and ventral pancreas. Although hepatic endoderm specification still occurs in *Hex* KO embryos, the endodermal cells fail to proliferate, causing a defect in liver development [85]. Moreover, as *Hex* is necessary for hepatoblast delamination, *Hex*$^{-/-}$ hepatoblasts fail to delaminate and migrate into the STM [85-87]. If *Hex* is conditionally deleted in hepatoblasts, the embryos survive but display an increased BEC proliferation and defective morphogenesis of the intrahepatic bile ductules [88]. In zebrafish, *hhex* morphants showed that although hepatoblast specification may have be unaffected, the liver bud failed to form. In fact, *hhex* morphants had additional biliary ductular development defects and did not survive past 2 dpf [63].

Prospero homeoprotein (PROX1) is a homeobox-containing transcription factor with a helix-turn-helix structure and is important for hepatoblast differentiation and delamination. *Prox1*$^{-/-}$ hepatoblasts have elevated levels of E-cadherin, which causes a lack of ECM degradation. As a result, these hepatoblasts fail to delaminate and migrate into the STM [89]. Moreover, when *Prox1* is specifically depleted in the hepatoblasts, the mice die at birth due to a defective liver morphology. Expression of mature hepatocyte markers (HNF4A, GS, KLF15, APOC2) is decreased in *Prox1*-deficient livers and biliary-related genes are increased (SOX9, KRT19). This implicates PROX1 as an important regulator of hepatoblast differentiation in addition to its role in hepatoblast migration. Even though biliary differentiation-related genes are upregulated, biliary formation is still defective with prematurely formed, large intrahepatic bile ducts. Once hepatoblast differentiation has occurred, however, no gene expression differences are observed [90].

Most of the focus thus far has been on signaling important in the early stages of liver development. For later stages of hepatogenesis, such as hepatoblast differentiation, one signaling pathway that has emerged as a key regulator of BEC differentiation is the Notch signaling pathway. Notch is important for BEC development, proliferation, differentiation and biliary morphogenesis [67, 91, 92]. Notch signaling promotes a biliary fate, while suppressing a hepatocyte fate [93]. In humans, defects in Notch signaling can lead to biliary-associated diseases, such as Alagille syndrome, characterized by bile accumulation in the liver. The syndrome is caused by mutations in the JAG1 Notch ligand or NOTCH2 receptor proteins [94, 95].

1.4 LIVER REGENERATION

1.4.1 Overview of Liver Regeneration

The liver possesses an innate and robust capacity to regenerate. Liver regeneration can manifest in one of two ways: (1) hepatocyte-driven or (2) BEC-driven [*see Figure 2*]. Typically following liver injury, hepatocytes proliferate to restore the lost liver mass. This process is termed hepatocyte-driven liver regeneration. However, if hepatocyte proliferation is blocked, then the BECs undergo dedifferentiation into hepatoblast-like cells (HB-LCs), also termed LPCs. LPCs can then differentiate into functional hepatocytes. These two types of liver regeneration will be discussed in detail in sections 1.4.3 and 1.4.4, respectively.

As HB-LCs/LPCs share both hepatocyte and BEC markers, they possess a bipotential capacity similar to hepatoblasts. Hence, these progenitor cells have been referred to as 'hepatoblast-like cells,' 'oval cells,' 'ductular cells,' 'hepatic progenitor cells' or 'liver progenitor cells.' The term 'oval cell' was first coined in a rat model of chemical-induced liver carcinogenesis. In this liver injury model, the newly-emerging oval cells possessed distinct morphological traits, including ovoid nuclei, small size and high nuclei to cytoplasmic ratio [96]. LPCs are also thought to reside in a phenomenon termed the ductular reaction (DR). DRs are a heterogeneous cluster of duct/cord-like structures that include extracellular matrix components and inflammatory cells [97].

Throughout the dissertation, these progenitor cells will be referred to as LPCs for ease of clarity.

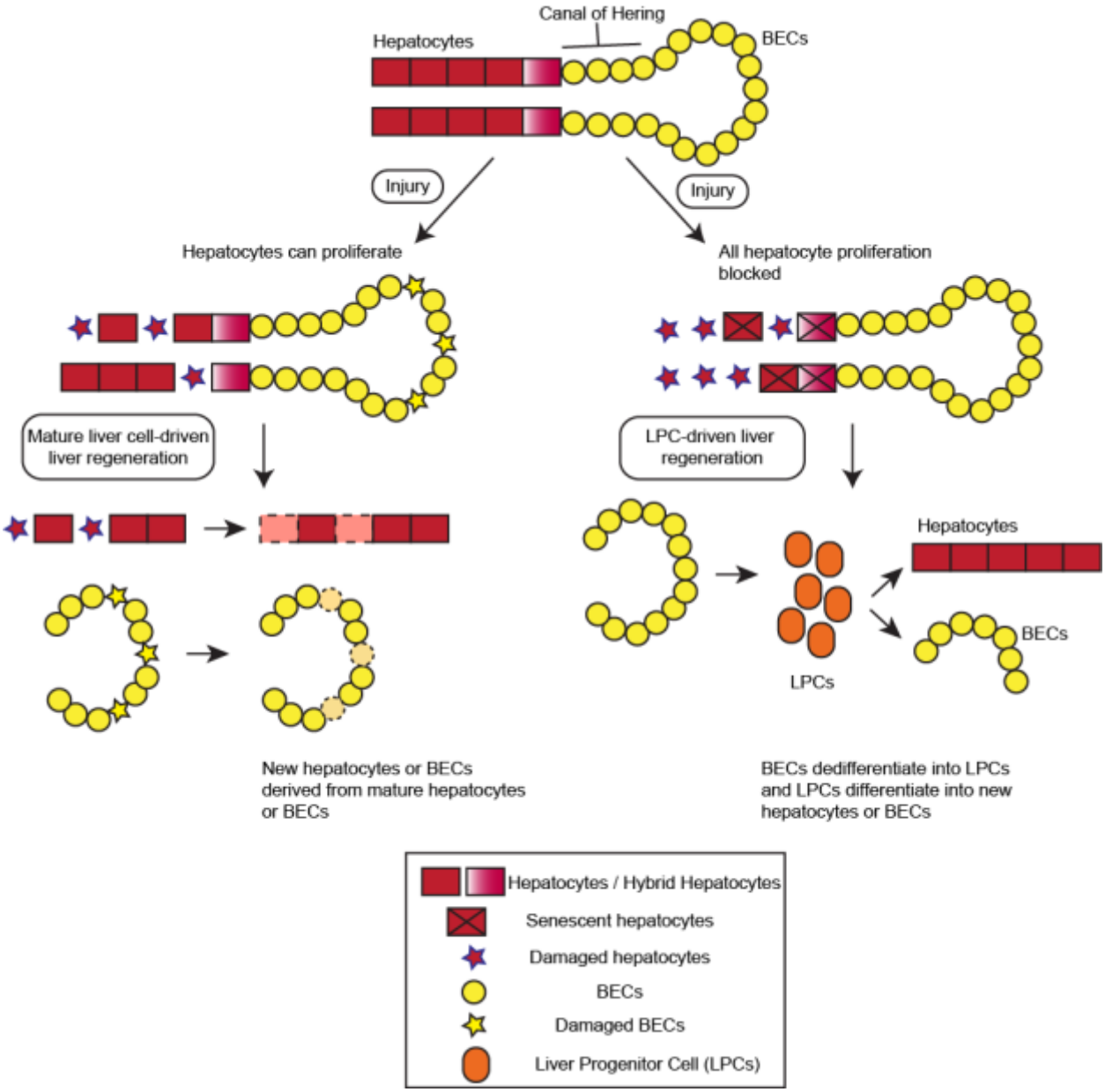

Figure 2: A model for the types of liver regeneration

In mature cell-driven liver regeneration, when hepatocytes or BECs are injured, the remaining cells can respectively proliferate and regenerate the lost cells. In contrast, under severe or chronic liver injury, when most hepatocytes are damaged and/or become senescent and lose the ability to proliferate, LPC-driven liver regeneration occurs. In this regeneration process, the remaining BECs can dedifferentiate into liver progenitor cells (LPCs), which proliferate and differentiate into mature hepatocytes and/or BECs.

1.4.2 Hepatocyte Turnover in Physiological Conditions

No true resident stem cell has been identified in the liver. This is hardly surprising considering that under physiological homeostatic conditions and most pathological conditions, hepatocytes can quickly execute a regenerative response to replace the functional tissue. Moreover, hepatocyte turnover rate is relatively low in adult livers, with a half-life in the range of 8-12 months [98, 99]. One explanation for hepatocyte turnover in physiological conditions is the streaming liver hypothesis. According to this hypothesis, new hepatocytes originate from the periportal zone proximal to the bile ducts. These new hepatocytes then migrate towards the central vein, populating the liver parenchyma [100]. Evidence for this hypothesis remains controversial. In one lineage tracing study with X-gal staining, the tamoxifen-inducible CreERT2 construct was inserted into the *Sox9* (a BEC marker) locus [101]. Initially, X-gal positive hepatocytes were observed spreading from the periportal bile ducts towards the central vein region; over time, X-gal positive hepatocytes could be detected throughout the entire liver parenchyma. However, separate studies which used different strains to label BECs, such as the SOX9-CreERT2 BAC transgenic or the osteopontin (OPN)-CreERT2, found no evidence to prove the streaming liver model of hepatocyte turnover [36, 102]. Hence, further study is needed to unequivocally name the liver cell responsible for hepatocyte turnover in homeostatic, physiological conditions.

1.4.3 Hepatocyte-driven Liver Regeneration

In pathological conditions and most liver injury models, such as partial hepatectomy (PHx), there is no involvement of resident ‘stem cells.’ Instead, mature hepatocytes proliferate to restore the liver parenchyma. First described in 1931 by Higgins and Anderson, PHx is an example of a

compensatory mechanism of regeneration [103]. After a 70% excision – or a 2/3 resection – of the liver lobes, the remaining hepatocytes proliferate to compensate for the lost liver mass. The liver fully recovers by 5-7 days post-PHx. Initial research studies using radiolabeled thymidine incorporation in hepatocytes showed that nearly all hepatocytes proliferate post-PHx [104, 105]. However, mouse studies of PHx with lineage tracing has shown that although most hepatocytes enter the S phase of the cell cycle, not all hepatocytes proceed to the M phase and divide. In fact, liver regeneration post-PHx initially manifests as a hypertrophic event and later as a proliferation event [106].

The regenerative response post-PHx involves a priming and a replicative phase. The priming phase is marked by cytokine production and release of growth factors that activate downstream transcription factors, such as signal transducer and activator of transcription 3 (STAT3). The replicative phase involves two rounds of DNA replication events with the peak hepatocyte replication occurring at 24h post-PHx in rats and 36h in mice. Hepatocytes are the first liver cells to enter DNA synthesis followed by BECs, HSCs and then endothelial cells. Several factors have been identified to be important mediators of the regenerative response post-PHx. These include hepatocyte growth factor (HGF)/tyrosine-protein kinase Met (c-Met) [107, 108], epidermal growth factor (EGF)/EGFR, interleukin-6 (IL6)/STAT3 [109, 110], tumor necrosis factor (TNF)/tumor necrosis factor receptor 1 (TNFR1) [111] and transforming growth factor beta (TGFB) [112]. Following PHx, known hepatocyte mitogens, HGF and EGF, are activated [113]. If their cognate receptors, c-Met or EGFR, are both inhibited prior to PHx, then proper regeneration fails to occur [114]. In addition, PHx also results in an upregulation of non-mitogenic factors, such as IL-6, norepinephrine, insulin and TNF. These factors enhance signals regulating hepatocyte proliferation.

In addition to mice and rats, PHx has also been modeled in adult zebrafish. In zebrafish, following a 1/3 resection of the liver lobes, the liver recovers to its original size 7 days post-PHx [27]. Hepatocyte regeneration manifests as the re-entry of the remaining hepatocytes into the cell cycle. In zebrafish, the cell cycle regulator, Uhrf1, was found to be an important regulator of hepatic outgrowth and liver regeneration; in fact, after PHx, *uhrf1*$^{+/-}$ mutants failed to recover their liver size. Although zebrafish exhibit epimorphic regeneration upon injury in several organs (i.e., heart, eye), Interestingly, it remains unclear whether following PHx, zebrafish liver regeneration is a compensatory (as occurs in higher vertebrates and involves proliferation of remnant lobes) or an epimorphic (true regeneration in which hepatocytes proliferate from the missing lobe) event [27, 115].

Clinically, although PHx does not represent any pathological condition of human liver disease, this model of liver injury still provides relevant information about mechanisms involved in hepatocyte-driven liver regeneration for living donors providing partial liver transplants.

1.4.4 BEC- or LPC-driven Liver Regeneration

Although mature liver cells possess the incredible ability to regenerate, this ability is in jeopardy once hepatocyte proliferation is compromised, as occurs in cases of chronic viral hepatitis or alcoholic liver disease. In such scenarios, oval cells or LPCs emerge as the progenitor cells accountable for mediating liver regeneration. Thought to arise from the periportal regions (or canals of Hering), LPCs are bi-potent, facultative resident progenitor cells with the ability to differentiate into hepatocytes and BECs [116, 117]. LPCs express hepatocyte (M2-PKm, Albumin), BEC (EpCAM, CK-19, Osteopontin, Sox9) [116, 118] and markers specific to their progenitor cell status (LGR5, FOXL1, TROP2) [119, 120]. TROP2 expression only appears in

LPCs after DDC-induced liver injury and is absent in BECs of uninjured livers. Using transgenic, knockin mouse lines, leucine-rich repeat-containing G-protein coupled receptor 5 (LGR5) was also shown to be expressed specifically in LPCs post-liver injury. Additional co-markers used to identify LPCs include CD133 and MIC1-1C3 [121-124].

Due to the bi-potential progenitor cell nature of LPCs, it is reasonable to consider the canal of Hering, a junctional region located strategically between the hepatocyte parenchyma and the biliary compartment, as a niche from which post-injury-specific LPCs arise. However, this notion remains to be proven. LPCs are thought to arise from pre-existing BECs since LPCs and BECs are phenotypically alike [125]. However, hepatocytes can also act as facultative progenitor cells in cases of BEC injury, such as bile duct ligation (BDL), to restore the BEC number and function [126, 127].

Several animal models of LPC activation have been established, including the rat 2-acetylaminofluorene (2-AAF)/PHx model of liver injury [128], the mouse 3,5-diethyoxycarbonyl-1,4-dihidro-collidine (DDC)-containing diet, the choline-deficient ethionine-supplemented diet (CDE) of liver injury [129, 130], the hepatocyte-specific deletion of *Mdm2* (a p53 inhibitor) model of liver injury [131] and the zebrafish hepatocyte-specific genetic ablation model [20, 132]. In the 2-AAF/PHx rat model, 2-AAF is administered before PHx to block hepatocyte proliferation, as measured by the absence of PCNA-positive nuclei, p53 induction and increased p21 levels [133]. Although the 2-AAF/PHx rat model effectively activates an oval cell response, it is limited by the difficulty of pursuing lineage tracing experiments in rats. Alternative options include the mouse DDC and CDE diet models of liver injury. In the DDC diet, heme biosynthesis is blocked, inducing hepatocyte damage and subsequent periportal cell proliferation. On the other hand, the CDE diet causes fatty liver disease in mice and models alcoholic liver disease or nonalcoholic

steatohepatitis. Initial injury manifests as steatosis and LPC activation/proliferation, while long-term exposure results in a fibrotic and cirrhotic phenotype, eventually leading to hepatocellular carcinoma (HCC) [134]. Although the aforementioned models activate LPCs, the main concern is that the induced LPCs are not all the same, with rat oval cells displaying distinct markers (*Dlk*/*Pref-1*, *AFP*) not observed in the mouse liver injury models [135]. In the mouse *Mdm2* KO genetic-inducible model, AhCre system with an *Mdm2* floxed genetic system was used to express Cre recombinase upon B-napthoflavone treatment. Upon Cre activation, *Mdm2*, which promotes p53 degradation, was blocked in the majority (>98%) of hepatocytes. Thus, *p53* was upregulated and resulted in hepatocyte apoptosis, necrosis and even senescence. As a result, there was a robust response of LPC activation, proliferation and subsequent differentiation into mature hepatocytes. Finally, the zebrafish hepatocyte-specific genetic ablation model involves complete hepatocyte ablation and subsequent LPC activation, proliferation and differentiation into hepatocytes and BECs. This zebrafish model will be discussed further in section 1.4.5.

Using these models, several studies have sought to elucidate key factors and pathways relevant for the regulation of LPC-driven liver regeneration. These factors and pathways include TWEAK, HGF/c-Met, BET proteins, NOTCH, WNT and FGF pathways. Among these factors, the LPC mitogen, TNF-like weak inducer of apoptosis (TWEAK), acts through its receptor, FN14 [136-138]. In transgenic mice with TWEAK overexpression, oval cell and BEC proliferation (with no mitogenic effect on mature hepatocytes) was significantly increased even in the absence of any liver injury. Moreover, in a DDC diet model of liver injury, inhibition of TWEAK also prevented oval cell proliferation. Whereas in a *Mdm2* KO model of liver injury and LPC activation, a deficiency in FN14 prevented the proper induction of a ductular reaction, addition of TWEAK enhanced the ductular reaction response [131].

Another factor, FGF7, is also important for regulating LPC expansion. In serum samples obtained from human patients of fulminant hepatic failure/acute hepatitis, FGF7 levels were increased. In mouse DDC and BDL models of liver injury, expression of *Fgf7* was highly upregulated near the LPCs [139]. Similar to TWEAK, forced overexpression of *Fgf7* in non-injured livers caused significant increase in the number of CK19-positive LPCs near the periportal regions. *Fgf7* KO mice on a DDC diet or BDL injury exhibited low survival, a block of LPC activation and a decrease in proliferation of CK19-positive LPCs.

Besides its known role in hepatocyte-driven liver regeneration, the growth factor signaling pathway involving HGF/c-Met is also important for LPC-driven liver regeneration [140]. In a DDC model of liver injury, upon deletion of *Met* in LPCs using the Alb-Cre (epithelial cells) and Mx1-Cre (stromal) lines, LPC proliferation, migration and differentiation into hepatocytes was significantly impaired. MET or EGFR deletion and overexpression *in vitro* established the contrasting roles these receptors play in cell fate decisions [141]. While MET – via STAT3/AKT – is an important regulator of LPC-to-hepatocyte differentiation, EGFR – through its mediation of NOTCH1 – is important for LPC-to-biliary cell fate commitment and ductular morphogenesis.

NOTCH and WNT signaling can also regulate LPC-mediated liver regeneration [142]. In a DDC model of liver injury, LPCs require NOTCH signaling for proper biliary cell fate commitment and WNT for proper hepatocyte cell fate commitment during regeneration. Following biliary injury, a Notch-associated ligand, JAGGED1, is released from myofibroblasts and interacts with the Notch receptor present on proximal LPCs. For hepatocyte recovery, hepatic Kupffer cells release WNT3A proximal to activated LPCs, which produce Numb to block Notch signaling and instead activate a hepatocyte differentiation pathway.

In addition to murine models, the zebrafish model has been used successfully to elucidate underlying mechanisms of LPC-driven liver regeneration. Blocking bromodomain and extraterminal (BET) proteins negatively affects several key steps of LPC-driven liver regeneration, including BEC dedifferentiation into LPCs, LPC proliferation and subsequent LPC differentiation into mature hepatocytes [143].

Furthermore, Stueck et al. recently reported on evidence for LPC/BEC-driven liver regeneration in human liver samples of chronic liver disease patients. The progression of 'bud' development was recorded. Bud development was defined as clusters of hepatocytes and bile ductules derived from BEC-sourced LPCs. Newly generated hepatocytes (70% from buds) were found near the terminal ducts from which they emerged to populate the liver parenchyma. Immature hepatocytes expressed both EpCAM and GS (glutamine synthetase), BEC-specific and hepatocyte-specific markers, respectively. However, this dual expression later disappeared as hepatocytes matured [144]. The authors concluded that in cirrhotic livers the LPCs, which are most likely derived from the BECs, contribute to hepatocyte repopulation of the liver parenchyma.

Insights about LPC-mediated liver regeneration derived from these important studies will help in the creation of novel therapeutics to enhance innate liver regeneration and combat liver disease in patients.

1.4.5 Zebrafish LPC-driven Regeneration Model

Using lineage tracing methods, a recently established model of LPC activation in larval and adult zebrafish is characterized by BEC contribution to LPC activation after total hepatocyte loss [20, 132] [*see Figure 3*]. In this model the transgenic line, *Tg(fabp10a:CFP-NTR)*, is used to express *Escherichia coli* bacterial nitroreductase (NTR) enzyme fused with the cyan fluorescent protein

(CFP) from the hepatocyte-specific *fabp10a* promoter. When fish are treated with metronidazole (Mtz), a prodrug, cells expressing NTR metabolize Mtz into a cytotoxic metabolite. At first, NADH or NADPH can both reduce NTR [145]. Upon Mtz addition, NTR reduces Mtz and converts it into a cytotoxic agent – essentially a powerful DNA interstrand cross-linking compound – that induces cell death in NTR-expressing cells [146-148]. In *Tg(fabp10a:CFP-NTR)* zebrafish, CFP can be detected as early as 2.5 dpf and Mtz is treated at 3.5 dpf for a 36-hour treatment [149]. After Mtz treatment, all hepatocytes expressing CFP-NTR will undergo cell death (i.e., apoptosis), corresponding to severe liver damage. Following Mtz washout at 5 dpf, since hepatocytes can no longer contribute to the regenerative response, BECs now assume control of liver regeneration in a three-step process: (1) All BECs dedifferentiate into LPCs, which co-express Hnf4a (a hepatoblast/hepatocyte marker) and Prox1 (a hepatoblast/hepatocyte/BEC marker) in Alcam-positive (a BEC marker) BECs; (2) LPCs proliferate; and (3) LPCs differentiate into hepatocytes and BECs to reconstitute the lost liver mass. Using this zebrafish liver injury model, we sought to elucidate the underlying mechanisms of LPC-driven liver regeneration, specifically focusing on BMP and Stat3 signaling pathways.

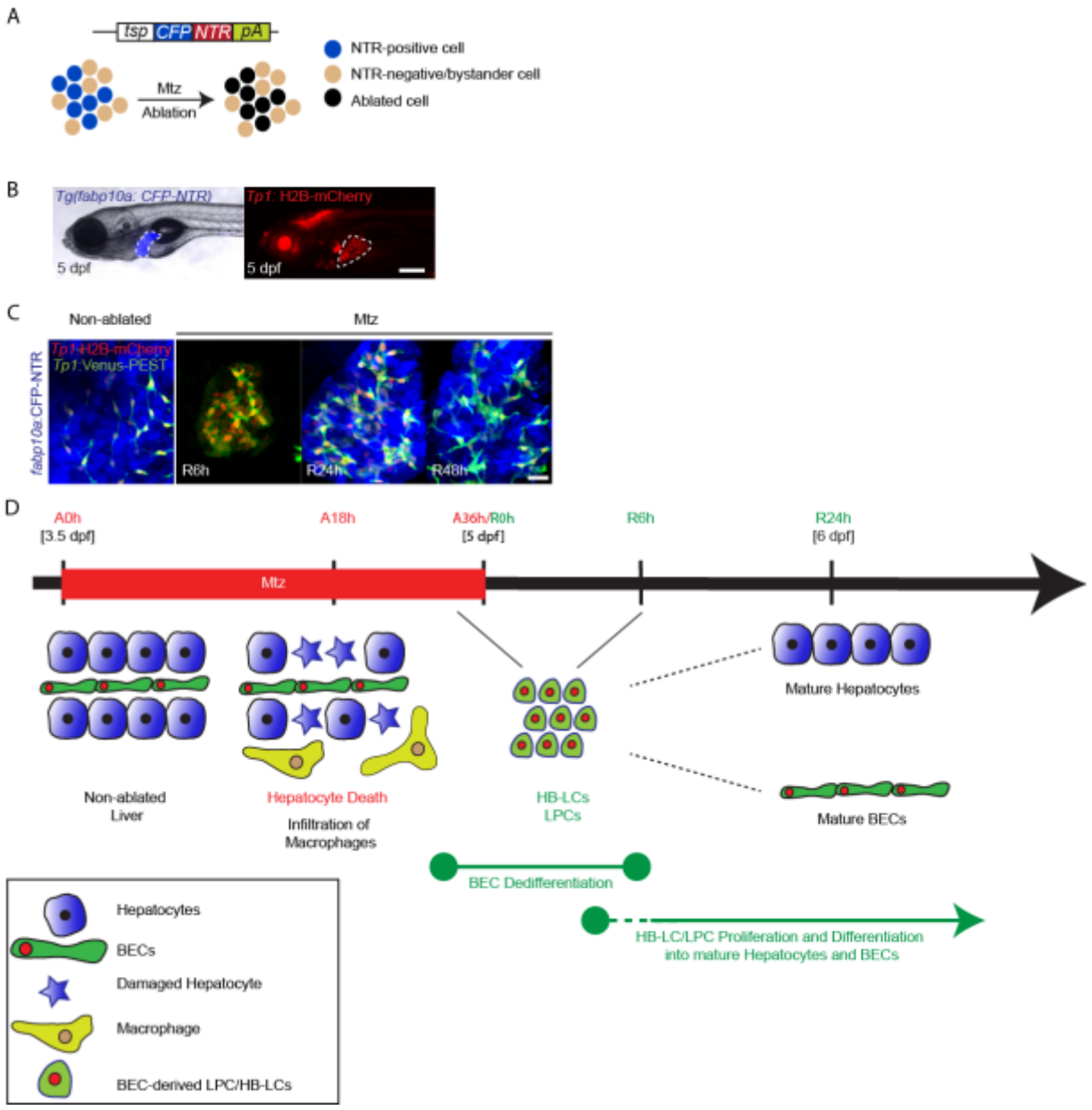

Figure 3: LPC-driven liver regeneration model in zebrafish

(A) Schematic for the cassette expressing the cerulean fluorescent protein (CFP) fused to the nitroreductase (NTR) gene from a tissue-specific (tsp) promoter. Specific cells (blue) express this transgene prior to ablation. After metronidazole (Mtz) treatment, cells expressing this transgene (blue) are specifically and genetically ablated (black). Bystander or surrounding NTR-negative cells are unharmed. **(B)** Epifluorescence images of a 5-dpf zebrafish larvae expressing CFP (blue) fused to NTR from the hepatocyte-specific promoter, *fabp10a*, and nuclear mCherry (red) in Notch-signaling cells. The white dashed lines outline the liver region. **(C)** Confocal time-course images of control (non-

ablated) and regenerating livers following a 36-hour Mtz treatment. After Mtz washout, liver regeneration (R) begins. In addition to *Tg(fabp10a:CFP-NTR)* and *Tg(Tp1:H2B-mCherry)* lines, the *Tg(Tp1:Venus-PEST)* highlights active Notch signaling in the BECs. The liver fully regenerates by R102h post-Mtz washout. **(D)** Overview of the hepatocyte damage (ablation: A) and steps of liver recovery (regeneration: R). Larvae are treated with Mtz at 3.5 dpf for 36 hours. Upon Mtz washout at 5 dpf, liver regeneration can be monitored. At A18h, due to intense hepatocyte cell ablation, macrophages infiltrate into the liver. At A36h/R0h, all BECs have dedifferentiated into HB-LCs/LPCs to begin the regeneration process. Following dedifferentiation, the liver undergoes intensive periods of proliferation and differentiation of LPCs into either hepatocytes or BECs. Scale bars: 250 μm (B); 20 μm (C).

1.5 BMP SIGNALING PATHWAY

1.5.1 Overview of the BMP Signaling Pathway

Originally discovered in 1965 and now classified as regulators of bone formation, Bone Morphogenetic Proteins (BMPs) are extracellular cytokines and members of the superfamily of Transforming Growth Factor-B (TGF-B) [150]. The evolutionarily conserved canonical TGF-B/BMP signaling pathway is involved in a diverse array of vertebrate physiology, including homeostasis, embryo patterning, cell fate determination, injury response and organ development [151-154].

In the canonical BMP pathway, BMP ligands are synthesized in an inactive precursor form. Following a proteolytic cleavage event, inactive BMP ligands dimerize and become active. Active BMPs bind to the serine/threonine BMP type I and type II receptors (BMPRs). The kinase domain of type II BMPR phosphorylates type I BMPR; the latter then activates the SMAD signaling

pathway by phosphorylating SMAD1/5/8. A heteromeric complex forms when SMAD1/5/8 associate with the common SMAD, SMAD4, which translocates to the nucleus and activates expression of downstream target genes, such as *id2a* and *tbx2b* [155, 156] [*see Figure 4*]. Alternative, non-canonical BMP, SMAD-independent pathways also exist, signaling through MAPK cascade, the PI3K/AKT and/or Rho-GTPases [157-159]. Both the non-canonical and canonical pathways can be regulated by the BMP ligands extracellularly or intracellularly via phosphatases, inhibitory SMADs, miRNAs, Chordin/Noggin proteins, as well as crosstalk with other signaling pathways [160].

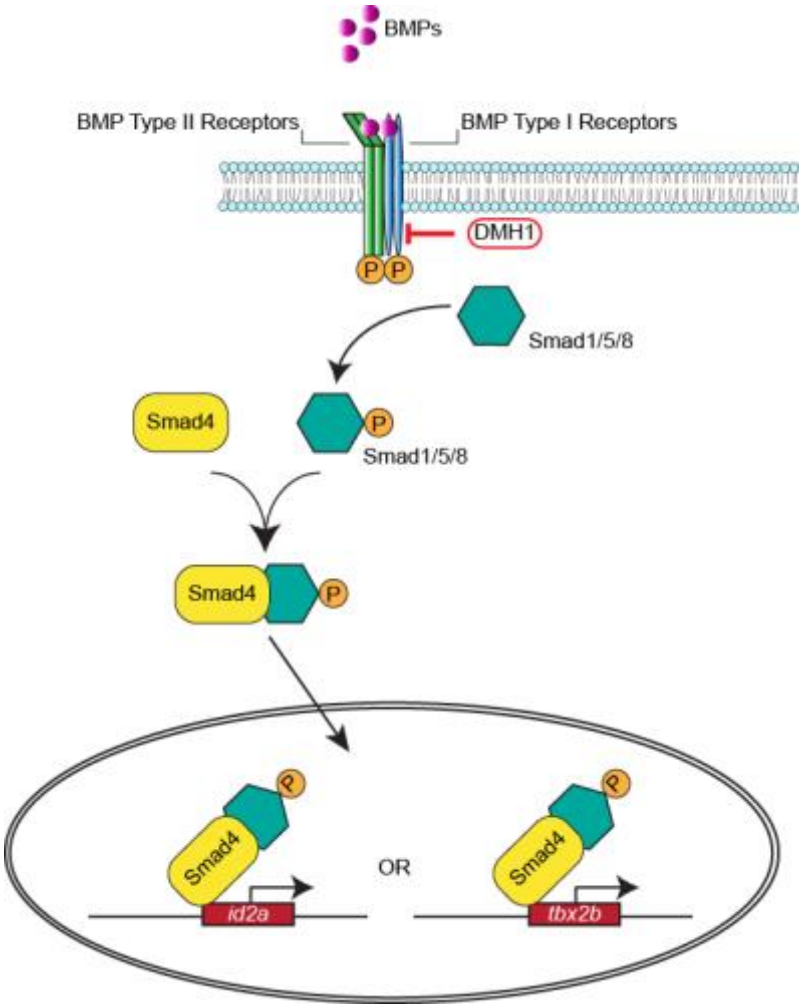

Figure 4: Schematic of the canonical BMP signaling pathway

In canonical BMP signaling, BMP ligands dimerize and bind to the serine/threonine BMP type I and type II receptors, activating them. Type I BMP receptor phosphorylates Smad 1/5/8. Upon activation, Smad 1/5/8 associates with Smad4 and the entire heterotrimeric complex translocates to the nucleus and activates expression of downstream target genes (i.e., *id2a* and *tbx2b*). DMH1, a small molecule inhibitor, blocks BMP signaling by specifically targeting BMP Type I receptors.

1.5.2 BMP Signaling in Liver Development

Due to their pleiotropic effect, BMPs are essential for the proper development and function of various organs (reviewed in [160]) [161, 162], as evidenced by the non-viability of *Bmp2* or *Bmp4* knockout mice. For example, complete absence of *Bmp2* or *4* is embryonic lethal due to defects in heart and mesoderm development, respectively [163, 164]. In mammalian liver development, BMP signaling from the STM is essential, but not sufficient, for induction of hepatic cell fate [76, 165] over pancreas specification [166]. Moreover, BMP signaling may affect *Gata4* levels, thereby regulating hepatic competence during liver development [70]. Specifically, BMP4 is one of the few secreted proteins that are involved in standard morphogenesis and growth of the hepatic endoderm as well as formation of the liver bud [76]. Inhibition of the BMP pathway blocks hepatic induction in mice [76, 165].

In zebrafish, a common endodermal progenitor cell was identified that can give rise to both the ventral pancreas and the liver. The location of cells from the *bmp2b*-secreting LPM determines the cell fate: cells located medially adopted a pancreatic/intestinal fate, whereas cells located laterally adopted a hepatic fate. Bmp2b regulates cell fate by blocking *pdx1* expression in cells adjacent to the medial cells, which will give rise to the liver [167]. In addition, Bmp2a is required for liver formation. In zebrafish studies, when BMP signaling was blocked early using either a dominant-negative BMPR or *alk8* mutants, hepatoblast specification was inhibited, most likely

due to decreased expression of Gata4. If, however, BMP signaling is blocked at the post-hepatic specification stage, there is little effect on the maintenance of the liver progenitors [70].

1.5.3 BMP Signaling in Liver Regeneration

Although TGF-B and activin A have been characterized as negative regulators of liver regeneration, BMPs are thought to promote liver regeneration. For example, in a mouse model of partial hepatectomy, regeneration was regulated, in part, by the BMP signaling pathway. Not only was the expression of the type II BMP receptor, Alk3, upregulated, but treatment with recombinant human BMP7 led to enhanced hepatocyte proliferation and liver regeneration. Moreover, blocking endogenous BMP7 resulted in a delayed liver regenerative response [168].

In contrast to the requirement of BMP7 for liver regeneration after partial hepatectomy, BMP4 must be downregulated. In fact, if BMP4 expression is artificially enhanced after partial hepatectomy, then hepatocyte proliferation is significantly decreased and liver regeneration impaired. On the other hand, if BMP4 was blocked, hepatocyte proliferation was increased, indicative of enhanced liver regeneration [169]. One way to consolidate the two differing observations of BMPs is the thought that BMP7 and BMP4 act through different receptors, with the latter inhibiting and the former enhancing, respectively, liver regeneration. For example, when ALK3 is blocked prior to partial hepatectomy, hepatocyte proliferation is increased; however, when ALK2 is blocked there is no effect, or even a slight decrease, in hepatocyte proliferation [170].

Similarly, when BMP signaling is blocked in the adult zebrafish partial hepatectomy model, the liver mass is transiently reduced at day 7 days post-partial hepatectomy, but is back to normal size by 9 days post-partial hepatectomy. Moreover, *in vitro* treatment of BMP2 enhances

hepatocyte proliferation and upon co-treatment of BMP2 and the BMP antagonist, Noggin, the enhanced proliferation effect is gone [115].

One known downstream target gene of the BMP pathway is the Inhibitor of DNA binding 2 (ID2) protein. In zebrafish, since Id2a is expressed in the hepatoblasts and BECs of the liver, Chapter 2 of this dissertation will focus on the effect of *id2a* deficiency on liver development. Although the role of BMP signaling in liver development has been established, its role in LPC-driven liver regeneration has not yet been elucidated. In our zebrafish LPC-driven liver regeneration model, we found several components of the BMP pathway as well as *id2a* to be upregulated at multiple stages of the regeneration process. Thus, Chapter 3 of this dissertation will focus on the effect of BMP signaling and its downstream target gene, *id2a*, on LPC-driven liver regeneration.

1.5.4 Helix-loop-helix Factors and Inhibitor of DNA Binding Proteins BMP Signaling in Liver Regeneration

Conserved from yeast to humans, helix-loop-helix (HLH) group of proteins consists of more than 240 members categorized into 7 groups, including Class I (E proteins with E-box sites), Class II (heterodimerize with E-proteins), Class III (leucine zipper-containing in addition to the HLH motif), Class IV (dimerize with Myc, Mad, Max or Mxi), Class V (Id proteins), Class VI (proline-containing) and Class VII (contain a bHLH-PAS domain). Common among all classes of HLH is the helix-loop-helix domain – also termed the dimerization domain [171]. Most HLH proteins possess a basic domain, which allows for DNA binding to specific DNA target sequences, such as E-boxes (CANNTG) or N-boxes (CACNAG). Some HLH proteins contain a PAS domain, which is a signaling sensor of environmental conditions and stress and provides additional dimerization

motifs, while some HLH factors possess a domain at the C-terminus that is involved in co-repressor interactions. Still others, like the Id proteins, lack the DNA-binding domain and instead act as negative regulators [172, 173]. HLH proteins form either homo- or heterodimers and function in regulating cell cycle control, cell fate commitment and differentiation; moreover, HLH proteins are involved in important developmental processes, such as pancreatogenesis, myogenesis and neurogenesis [174-176].

Typically, organogenesis requires regulatory signals, extracellular or intracellular, to properly control cell proliferation and differentiation. Id proteins belong to the HLH family that lacks the basic DNA binding domain. Besides their known function to positively regulate proliferation and negatively regulate differentiation in vertebrates and invertebrates [177-180], Id proteins are also involved in the regulation of senescence, cell fate commitment, apoptosis and tumorigenesis [181-184]. In mammals, four Id proteins have been discovered, including ID1, ID2, ID3 and ID4 [172, 180, 185, 186]. Mechanistically, Id proteins act in a dominant negative fashion by dimerizing with other bHLH transcription factors through their HLH domain, essentially sequestering the bHLH factors, preventing their dimerization with their partner and subsequently regulating transcription [177].

The structure of Id proteins consists of the HLH domain and variable N and C-terminal regions. The N-terminal region of Id2 protein can be ubiquitinated and primed for degradation [187] and is also involved in inducing apoptosis [188], whereas the C-terminus contains a nuclear-cytoplasmic transport [189]. Id2 can bind both bHLH (E proteins) as well as non-bHLH proteins, such as the Retinoblastoma protein (Rb); in the latter case, Id2 antagonizes Rb protein's ability to act as a growth suppressor. Because of its role in regulating the cell cycle, Id expression has been

shown to be upregulated in various types of cancers, including neuroblastoma [190], pancreatic cancer [191] and prostate cancer [192].

The zebrafish genome contains five Id proteins, including Id1, Id2a, Id2b, Id3 and Id4. Previously, two developmental studies in zebrafish have implicated *id2a* in the role of retinogenesis regulating the cell cycle. In particular, Id2a was essential in the transition from the S to M phase of the cell cycle and subsequent retinal cell differentiation [193]. During the G1-S transition, it is thought that ID proteins are released from phosphorylated Rb protein to negatively regulate other bHLH factors [182]. In our zebrafish model of LPC-driven liver regeneration model, *id2a* was upregulated throughout the regeneration process. Since many pathways active during development may also be recapitulated during regeneration, we sought to investigate the role of Id2a in liver development as well as regeneration.

1.6 INFLAMMATORY SIGNALING IN LPC-DRIVEN LIVER REGENERATION

1.6.1 Overview of the Stat3 Signaling Pathway

Signal transduction and activator of transcription (STAT) protein 3, also termed the acute phase response factor (APRF), is an important transcription factor and mediator of development, homeostasis, disease pathology and response. The STAT family of proteins consists of 7 members in mammals (STAT1, 2, 3, 4, 5a, 5b and 6) and, due to a genome duplication event, 8 members in zebrafish (Stat1a, 1b, 2, 3, 4, 5a, 5b and 6). Zebrafish Stat3 contains 3 splice variants and is 86.5% homologous to the mouse STAT3 protein [194]. Stat3 is composed of 6 distinct domains, including

coiled-coil, Src homology domain (SH2), DNA-binding, N-terminal and the transactivation domains.

STAT3 signaling initiates when cytokines or growth factors bind to their cognate receptors, resulting in downstream autophosphorylation and subsequent activation of the Janus kinases (JAKs) [195]. Activated JAKs then phosphorylate STATs at the Tyr705 site, which homo- or heterodimerize to other STATs through binding to the SH2 domain, and translocate to the nucleus to regulate transcription of numerous target genes [*see Figure 5*]. Besides being activated by JAKs, STAT3 proteins can also be phosphorylated (i.e., activated) at the Ser727 site by ERK, ATR and CDK1 [196]. Interestingly, unphosphorylated STAT3 can also translocate to the nucleus and influence transcription of downstream genes [197]. Traditionally, the downstream genes have been reported to be important for survival, proliferation and differentiation [198]. In the liver, IL-6 family of cytokines, IL-22 from Th17 cells, and IFN-A/B from virus-infected cells [199] can all activate STAT3 in hepatocytes, which aids in survival, proliferation and regeneration.

Multiple cytokines can activate STAT3 in Kupffer cells, including the IL-6 family of cytokines (IL-6, LIF-1, IL-11) [11]. Liver Kupffer cells express both IL-6 and IL-10 receptors (IL-6R, IL-10R). As both IL-6 and IL-10 can activate STAT3, but can have varying effects downstream (pro-inflammatory vs. anti-inflammatory, respectively), the question arises how such an activation is mediated. One study suggests that when IL-6 cytokines, released from multiple cell types, bind to IL-6R, STAT3 is transiently activated, causing a pro-inflammatory response. In contrast, when IL-10 binds to IL-10R, STAT3 activation is lengthened, resulting in an anti-inflammatory response. Moreover, this response appears to be modulated by SOCS3 [200, 201].

One of the key negative regulators and downstream targets of STAT3 is the family of suppressor of cytokine signaling (SOCS) genes. In a negative feedback manner, SOCS proteins

aim to inhibit cytokine signaling by one of two methods: (1) Through their SH2 domains or kinase inhibitory region (KIR) [202], SOCS proteins can directly bind to active JAKs or phosphorylated tyrosine 757 (Tyr757) on gp130/cytokine receptors and inhibit their kinase activity or (2) Through their SOCS box, SOCS proteins can also target their binding partner for proteosomal degradation [203]. However, independent of cytokine signaling, SOCS proteins can also be activated by alternative stimuli, including cyclic AMP (cAMP), LPS and statins and can also regulate other pathways, such as TLR signaling independent of STAT3 [204, 205]. While mammalian SOCS proteins consist of eight members (SOCS1-7, CIS), the zebrafish SOCS protein family is composed of 12 members (Socs1a, 1b, 2, 3a, 3b, 4, 5a, 5b, 6a, 6b, 7 and 9). Each SOCS protein contains a central SH2 domain, variable N-terminal domain and a conserved C-terminal SOCS box. The SOCS box is important for the recruitment of ubiquitin transferases, which may allow SOCS proteins to function as E3 ubiquitin ligases [206].

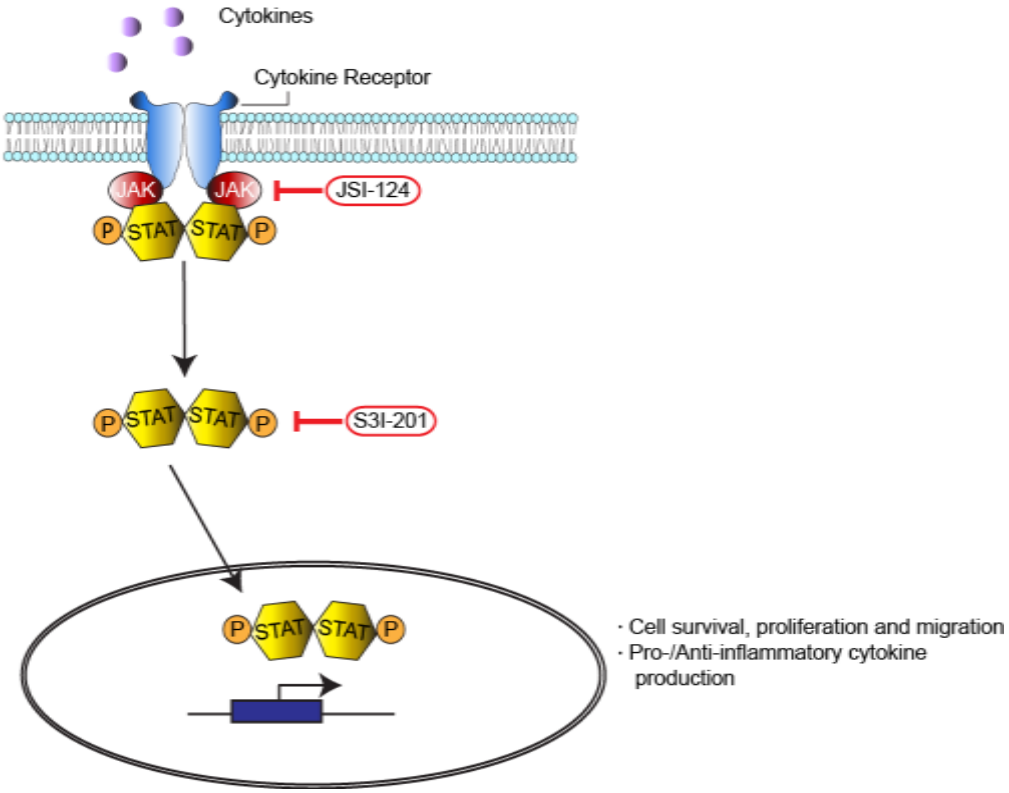

Figure 5: Schematic of the Stat3 signaling pathway

Upon binding of cytokines (i.e., interleukin-6) to their cognate cytokine receptors (i.e., interleukin-6 receptor), the receptors dimerize and undergo a conformational change. Downstream, the Janus kinases (Jaks) are phosphorylated and subsequently phosphorylate Stat3 proteins at the Tyr705 site, resulting in their activation. Stat3 proteins dimerize and translocate to the nucleus where they bind to gene promoters to regulate downstream transcription of many cellular processes, including cell proliferation, survival and migration. Two Stat3 inhibitors include JSI-124 (cucurbitacin I) and S3I-201. While JSI-124 specifically targets the Jaks upstream of the Stat3 pathway, S3I-201 prevents the dimerization of Stat3 proteins.

1.6.2 Role of Stat3 and Socs3 in Liver Regeneration

During the liver regeneration process at 12-18h post-PHx, the initiation step involves the recruitment and release of numerous immune cells, cytokines and components of the innate

immune system. Shortly after PHx, IL-6 is upregulated and this activation results in STAT3 activation downstream. Moreover, *Socs3* expression is also enhanced during this time, indicating the *Stat3* and *Socs3* activation are IL-6 dependent [207].

Socs3 KO mice are embryonic lethal, whereas hepatocyte-specific (using Albumin-Cre) *Socs3* KO mice display enhanced liver regeneration. After PHx, *Socs3* KO mice exhibited an increase in hepatocyte proliferation, cell cycle progression and develop hepatocellular carcinoma (HCC). In addition, when hepatocytes were isolated from the *Socs3* KO mice in culture, they proliferated at an increased rate compared to the wild-type [208].

In most animal models of liver injury tested, interruption of the components in the inflammatory signaling pathway, such as oncostatin M (OSM), IL-6/gp130, IL-11 or STAT3, can further exacerbate the injury. For instance, IL-11, a member of the IL-6 family of cytokines, was found to be upregulated by hepatocytes following acetaminophen-induced acute liver injury as a result of dying hepatocytes releasing reactive oxygen species (ROS). This caused the released IL-11 to bind to IL-11R on neighboring healthy hepatocytes, activating STAT3 downstream and resulting in a compensatory proliferation for liver recovery [209]. Moreover, when the pro-inflammatory cytokine, IL-22, is overexpressed in the mouse liver, hepatocellular damage induced by T-cell-mediated hepatitis is non-existent [210].

In hepatocyte-specific *Stat3* KO mice, depending on the type of liver injury, different responses were observed: (1) in a CCl_4 model of liver injury, liver inflammation was increased; (2) in a LPS-induced liver injury, liver inflammation was decreased. However, the role IL-6 plays in liver regeneration has had several conflicting reports. During PHx-induced liver regeneration, one study reported that IL-6 KO mice displayed an absence of *Stat3* activation, increased mortality, decreased hepatocyte proliferation and downregulation of multiple cell cycle genes, including

Myc, Cyclin D and AP1 [211]. A separate group reported that following PHx in IL-6 KO mice, hepatocyte proliferation was only decreased by 20-30% with no change in mortality rate between sham controls and injured mice [212]. A third group reported that following PHx in IL-6 KO mice, no difference in hepatocyte proliferation was observed; however, IL-6 KO mice had increased mortality compared to wild-type mice [109].

Following acute liver injury, such as PHx, *Socs3* expression was upregulated almost 40 times compared to sham controls. Interestingly, deletion of *Socs3* in the liver resulted in hyperactivation of STAT3 in the liver as it caused an increase in IL-6-mediated phosphorylation of STAT3. Moreover, *Socs3* deletion in the liver enhanced hepatic fibrosis through production of TGF-B1 [213].

In a CDE-diet mouse model of liver injury and oval cell activation, IL-6 levels were also upregulated and IL-6 KO mice displayed a reduction in total oval cell numbers. In fact, similar to the PHx liver injury case, *Socs3* levels were also enhanced in mice given a CDE diet. When CDE-diet mice were stimulated with IL-6, *Socs3* expression was increased in liver progenitor cells in vivo. *In vitro*, when oval cells in culture were stimulated with IL-6, *Socs3* expression was also increased [214].

1.7 MAJOR HYPOTHESIS

Using the zebrafish LPC-driven liver regeneration model, we were interested in studying the process of LPC differentiation into hepatocytes and BECs. To elucidate mechanisms underlying LPC differentiation, we used RNAseq to narrow our focus onto two main pathways, including (1) the BMP signaling pathway and its downstream target gene, *id2a*, and (2) the Stat3 immune

signaling pathway. No previous literature discusses the role of Id2a in liver development and the role of Id2a or Stat3 following complete hepatocyte ablation injury and subsequent LPC-driven liver regeneration.

For this dissertation, we had two main hypotheses. First, we hypothesized that Id2a was an important regulator of hepatoblast/hepatocyte proliferation and biliary morphogenesis in liver development and an important mediator of LPC-driven liver regeneration, acting downstream of the BMP signaling pathway. Second, we hypothesized that Stat3 and Socs3a were important mediators of LPC-to-hepatocyte and -BEC differentiation during LPC-driven liver regeneration.

1.7.1 AIM 1: Elucidate the Role of Id2a in Zebrafish Liver Development

Preliminary studies suggest that *id2a* is expressed in the developing zebrafish liver beginning 30 hpf and is maintained in the structure of the biliary network following hepatoblast differentiation. Moreover, it is known that Id proteins act downstream of the BMP signaling pathway in various developmental processes [F31 55]. Hence, we hypothesized that Id2a is not only required for hepatoblast/hepatocyte proliferation and in the formation of a proper biliary network, but it is also the downstream target of BMP signaling during liver development. To evaluate this hypothesis, we sought to examine the outcome on hepatoblast/hepatocyte proliferation, survival and biliary morphogenesis following *id2a* knockdown and in *id2a* mutants. The findings from these studies are highlighted in Chapter 2.

1.7.2 AIM 2: Determine the Impact of the BMP Signaling Pathway and Downstream Target Gene, *id2a,* in Zebrafish LPC-driven Liver Regeneration

Following hepatocyte-specific genetic ablation in zebrafish and during LPC-driven liver regeneration, RNAseq analyses and RT-PCR data indicate an upregulated expression of *id2a* and BMP pathway components in the regenerating livers. This upregulation is maintained during the dedifferentiation of BECs, appearance of HB-LCs/LPCs and the redifferentiation step of HB-LCs/LPCs into hepatocytes. Furthermore, preliminary data from our lab suggest that inhibition of the BMP signaling pathway compromises LPC-driven liver regeneration. Hence, we hypothesized that Id2a is an important downstream target of BMP signaling during LPC-driven liver regeneration and that Id2a is also an important regulator of this process. To evaluate this hypothesis, we sought to: (1) determine whether the process of BECs dedifferentiation, HB-LCs/LPCs proliferation and/or hepatocyte redifferentiation is compromised in *id2a* mutants; and (2) chemically and genetically inhibit BMP signaling using DMH1 and *smad5* mutants, respectively, to examine effect on LPC-driven liver regeneration, including proliferation, survival, differentiation and functional recovery of hepatocytes and BECs. The findings from these studies are highlighted in Chapter 3.

1.7.3 AIM 3: Elucidate the Role of Stat3 in LPC-driven Liver Regeneration

The final aim of this dissertation was formulated with the interest of studying the initial stages of BEC dedifferentiation after liver injury. RNAseq data generated in our lab showed that both *stat3* and *socs3a* were upregulated during LPC-driven liver regeneration. To address the importance of Stat3/Socs3a signaling in LPC-driven liver regeneration, we blocked Stat3 using a chemical

inhibitor, JSI-124, and examined the effect on LPC-driven liver regeneration. Preliminary data indicated that treatment with Stat3 inhibitor decreased the size of regenerating livers. Thus, we hypothesized that Stat3 and its negative feedback regulator, Socs3a, were necessary mediators for proper LPC-driven liver regeneration. Specifically, we utilized both JSI-124 inhibitor treatment as well as *stat3* TALEN mutants to explore the effect of *stat3* deficiency on LPC-driven liver regeneration. The result of smaller regenerating livers was indicative of either a retention of LPCs in their progenitor state or a defect in hepatocyte/BEC differentiation, proliferation and/or apoptosis. The data highlighting the findings from this hypothesis are presented in Chapter 4 and Appendix B.

2.0 ID2A IS REQUIRED FOR HEPATIC OUTGROWTH DURING LIVER DEVELOPMENT IN ZEBRAFISH

2.1 BACKGROUND

Liver organogenesis is a multifaceted process involving hepatoblast specification from the ventral foregut endoderm, budding and outgrowth of the liver bud, and hepatoblast differentiation into either hepatocytes or biliary epithelial cells (BECs) [41, 215]. In both mice [69, 76] and zebrafish [70, 167], inductive signals of Fibroblast Growth Factors (FGFs) and Bone Morphogenetic Proteins (BMPs) are essential for hepatoblast specification. In conjunction with the BMP and FGF signaling pathways, several homeobox transcription factors, including HHEX and PROX1, also regulate the initial stages of liver organogenesis [216]. HHEX regulates hepatoblast proliferation and delamination from the foregut endoderm as *Hhex*$^{-/-}$ mice lack a liver bud and the hepatoblasts fail to migrate into the surrounding septum transverse mesenchyme [85]. PROX1 also regulates hepatoblast delamination from the liver diverticulum as hepatoblasts fail to migrate in *Prox1*$^{-/-}$ mice [89]. Hepatocyte metabolic gene expression is altered in favor of biliary gene expression when *Prox1* is ablated in post-delaminated hepatoblasts [90]. *hhex* [63] and *prox1a* also regulate liver development in zebrafish. *prox1a*, specifically, marks the initiation of hepatoblast specification in zebrafish [28]. Besides HHEX and PROX1, zebrafish and mammals share additional transcription factors critical for liver organogenesis, such as GATA6 and hepatic nuclear factors (HNFs) [44, 55, 217, 218]. However, a comprehensive understanding of the molecular mechanisms underlying transcriptional regulation during liver development still needs to be defined.

One family of transcriptional regulators essential in developmental processes, including cell lineage commitment, proliferation and differentiation, is the helix-loop-helix (HLH) family of transcription factors [178, 219]. The HLH domain, essential for dimerization, is important in the formation of homo- or hetero-dimers. While some HLH proteins are ubiquitously expressed (*e.g.*, E proteins), other HLH proteins are tissue-specific (*e.g.*, PTF1, HES1). HES1, in particular, downstream of Notch signaling, is essential for digestive system development, especially in extrahepatic bile duct development [220]. In *Hes1*$^{-/-}$ mice, no tubular structures form in the ductal plate during intrahepatic bile duct development [221]. In addition, the bHLH factor, heart and neural crest derivatives expressed 2 (Hand2), is expressed in tissues that surround the liver primordium, such as the lateral plate mesoderm in zebrafish, which later contributes to the hepatic stellate cells [222]. Moreover, bHLH-PAS (Per-ARNT-Sim) factors, such as the hypoxia inducible factors (HIFs), participate in hepatic disease, regeneration, fibrosis, and hepatocellular carcinoma [223]. Hif2α (renamed as Epas1b) binds hypoxia response elements (HREs) and regulates hepatic outgrowth in zebrafish [224]. The activity of bHLH factors can be regulated by the inhibitor of DNA binding (ID) family of proteins.

ID proteins lack the basic DNA binding domain and regulate HLH factors *via* heterodimerization and subsequent creation of nonfunctional, dominant negative complexes that lack DNA-binding capability [171]. By heterodimerizing and sequestering ubiquitously expressed HLH factors, such as E-proteins (E47, E2-2, HEB, E12), or tissue-restricted HLH factors, ID proteins can thereby regulate cell proliferation, differentiation and apoptosis in a cell-context dependent manner [225]. In the pancreas, for instance, by binding and sequestering NeuroD, a bHLH factor implicated in pancreatic beta cell survival and differentiation, ID2 regulates pancreatic progenitor expansion [226]. Non-bHLH factors can also bind and

regulate ID protein function. For example, hypophosphorylated Retinoblastoma (Rb) tumor-suppressor protein interacts with ID2 during cell cycle arrest, preventing the latter from sequestering other transcription factors and consequently allows differentiation to occur [182, 190]. Mice with a genetic deletion of *Id2* display a reduced number of natural killer cells, lack lymph nodes and experience 25% neonatal lethality [227]. To date, no study has examined the role of ID2 in hepatogenesis.

2.2 RESULTS

2.2.1 *id2a* Expression in the Developing Liver

Using whole-mount *in situ* hybridization (WISH), we examined *id2a* expression during liver development in detail. We first detected *id2a* expression in the liver-forming region from 30 hours post fertilization (hpf) (Figure 6A), when hepatoblast specification has already occurred. At this stage, the liver tissue consists of hepatoblasts, which are liver progenitor cells, capable of differentiating into either hepatocytes or BECs. Following hepatoblast differentiation, around 72 hpf, we noted that *id2a* expression displayed a branching pattern in the liver, indicative of the intrahepatic biliary network consisting of BECs. The BEC-specific expression was maintained even at 5 days post fertilization (dpf) (Figure 6A). To confirm *id2a* expression in BECs, we conducted immunostaining in conjunction with WISH utilizing the *Tg*(*prox1a*:*YFP*), *Tg*(*Tp1*:*GFP*), and *Tg*(*kdrl*:*GFP*) lines, which express fluorescent proteins in hepatoblasts [228], BECs [24], and liver endothelial cells [229], respectively. As initially observed, *id2a* was specifically detected in *prox1a*:YFP-positive (Figure 6B) and *Tp1*:GFP-

positive cells (Figure 6C), but not in the endothelial cells (Figure 6D), indicating that in the liver, *id2a* is initially expressed in hepatoblasts and later restricted to BECs.

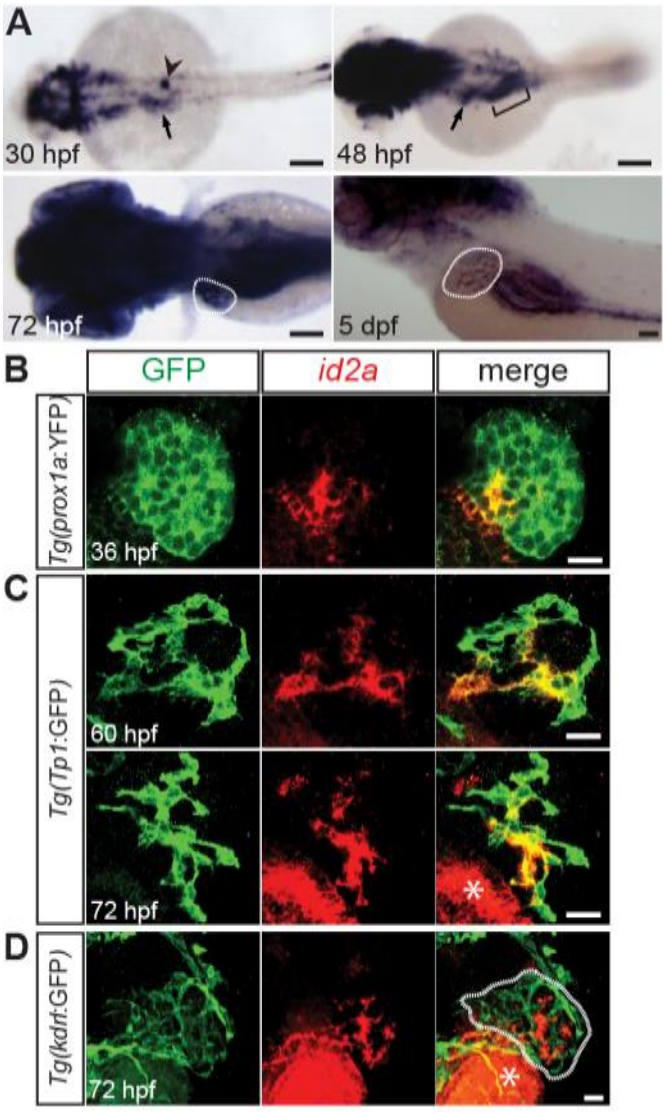

Figure 6: *id2a* expression in the developing liver

(A) WISH reveals *id2a* expression in the liver-forming region at 30 hpf (arrow) and in the liver at 48 hpf (arrow), 72 hpf and 5 dpf (dotted lines). From 72 hpf to, at least, 5 dpf, *id2a* expression in the liver appears to be restricted to BECs. Arrowhead points to the interrenal primordium; bracket denotes the intestinal bulb. Dorsal (30–72 hpf) or lateral (5 dpf) views, anterior to the left. **(B–D)** *id2a in situ* hybridization (red) combined with anti-GFP immunostaining (green) in *Tg*(*prox1a*:*YFP*)

(B), *Tg*(*Tp1*:*GFP*) (C), or *Tg*(*kdrl*:*GFP*) (D) embryos reveals *id2a* expression in hepatoblasts at 36 hpf and BECs at 60 and 72 hpf, but not in the endothelial cells of the liver (dotted line), respectively. Asterisks mark *id2a* expression in the intestinal bulb. Single confocal section (B) or projections of z-stack confocal sections (C, D). Scale bars: 100 (A), 20 (B–D) μm.

Since the zebrafish genome contains five *id* genes, we further investigated the expression patterns of the remaining four *id* genes, *id1*, *id2b*, *id3*, and *id4*, in the liver during embryonic development. At 30 hpf, *id2b*, *id3*, and *id4* are not expressed in the liver-forming region; however, it was not clear whether *id1* is expressed in the liver-forming region due to its broad expression (Figure 7A). Double labeling of *id1* and *sox17*:GFP, which labels all endodermal cells [230], showed *id1* expression in the liver-forming region (Figure 7E; brackets). At 48 hpf, none of the four genes are expressed in the liver. At 72 hpf, *id2b*, and *id3*, but not *id1* or *id4*, are expressed in the liver (Figure 7B and C; arrows); however, their expression does not mimic the biliary branching pattern of *id2a* expression. Altogether, these expression data indicate that both *id1* and *id2a* are expressed in the liver-forming region at 30 hpf and that only *id2a* expression is restricted to BECs.

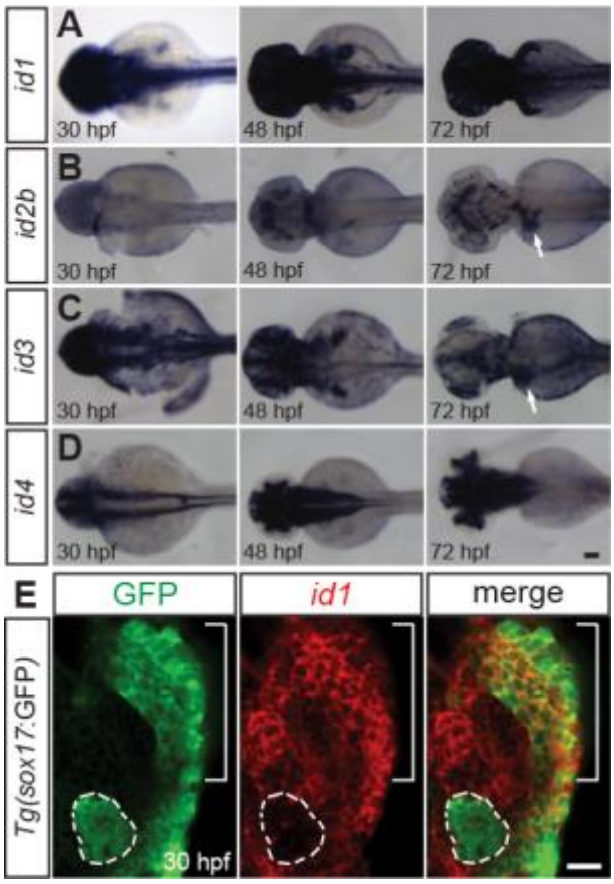

Figure 7: The expression patterns of *id1*, *id2a*, *id2b*, *id3* and *id4* during liver development in zebrafish

(A-D) Wild-type embryos were processed for WISH analysis with *id1* (A), *id2b* (B), *id3* (C), and *id4* (D) probes. *id1* appears to be ubiquitously expressed at 30 hpf, but its expression is absent in the liver at 48 and 72 hpf. *id2b* and *id3* expression in the liver was detected at 72 hpf (arrows), but not at 30 or 48 hpf. *id4* is not expressed in the liver. Dorsal views, anterior to the left. **(E)** *id1 in situ* hybridization (red), combined with anti-GFP immunostaining (green), in *Tg*(*sox17*:*GFP*) embryos reveals *id1* expression in the liver-forming region (brackets), but not in the dorsal pancreas (dotted lines) at 30 hpf. Single confocal optical section, ventral view, anterior up. Scale bars: 100 (A–D), 20 (E) μm.

2.2.2 *id2a* Knockdown Causes an Intrahepatic Biliary Network Deficit in the Developing Liver

Given the restricted expression pattern of *id2a* in BECs, we sought to determine whether *id2a* is important for intrahepatic biliary development. We conducted loss-of-function analyses using published *id2a* morpholino oligonucleotides (MO) [193, 231, 232]. Consistent with previous reports, *id2a* MO-injected embryos were microcephalic and microphthalmic [193], a phenotype also observed in *Id2*$^{-/-}$ mice [227]. Importantly, the small liver phenotype observed in *id2a* MO-injected embryos was partially rescued by *id2a* mRNA injection (Figure 8A and 8B), further validating the *id2a* MO. Since *id2a* is expressed specifically in BECs at later stages of liver development, we used the *Tg*(*Tp1*:*GFP*) line to examine BECs.

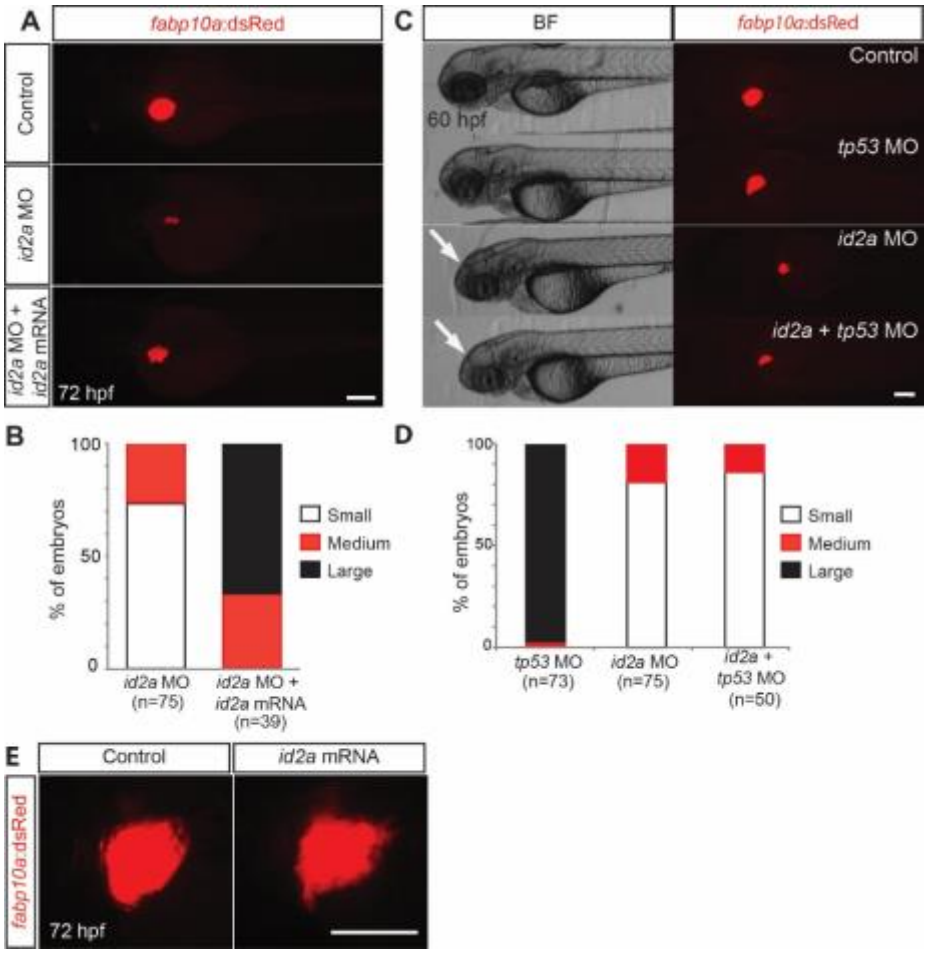

Figure 8: *id2a* mRNA, but not *tp53* MO, injection rescues the reduced liver size in *id2a* MO-injected embryos

(A, B) Epifluorescence images showing *fabp10a*:dsRed expression (red) in control, *id2a* MO-injected, and *id2a* MO + mRNA-co-injected embryos (A) and their quantification (B). Although the liver of the co-injected embryos was still smaller than the control liver, it was much larger than the liver of the single MO-injected embryos, indicating a partial rescue of the liver size defect exhibited in *id2a* MO-injected embryos. For quantification, embryos were divided into three groups based on liver size: small, medium, and large. The *id2a* MO-injected liver size shown in A was considered as small; the liver size of the co-injected embryo shown in A was considered as large. Dorsal view, anterior to the left. (C) Bright-field and epifluorescence images showing the overall morphology of embryos and *fabp10a*:dsRed expression (red), respectively, in control, *tp53* MO-injected, *id2a* MO-injected, and *id2a* MO + *tp53* MO-co-injected embryos. Liver size as well as eye and head size (arrows) in *id2a* MO-injected embryos was

similar to that in embryos co-injected with *id2a* and *tp53* MOs. (D) Quantification of the results in C. For quantification, the liver size of the control embryo shown in C was considered as large and the liver size of the *id2a* MO-injected embryo shown in C was considered as small. Lateral view, anterior to the left. (E) Epifluorescence images showing the *fabp10a*:dsRed expression (red) in control and *id2a* mRNA-injected embryos at 72 hpf. Liver size in *id2a*-mRNA injected embryos was similar to that of control embryos. Lateral view, anterior to the left. Scale bars: 100 μm.

Using epifluorescence microscopy, we detected very few GFP-positive cells in the livers of *id2a* MO-injected embryos (Figure 9A; squares), suggesting BEC number was greatly reduced. To further analyze the intrahepatic biliary structure, whole-mount immunostaining combined with confocal microscopy was used. In *id2a* MO-injected embryos, not only was the liver size reduced, but the intrahepatic biliary network failed to branch, appearing aggregated (Figure 9B). Taken together, these data imply that lack of *id2a* results in defective biliary structure and reduced BEC number, suggesting that *id2a* may regulate intrahepatic biliary development.

2.2.3 *id2a* Knockdown Reduces Liver Size but does not Block Hepatoblast Specification or Hepatocyte Differentiation

The main steps of liver development include hepatic competence, hepatoblast specification, hepatocyte or BEC differentiation, and hepatic outgrowth [41]. Since *id2a* is expressed in the liver-forming region from 30 hpf (Figure 6A) after hepatoblast specification, which occurs around 22 hpf in zebrafish [28], it is unlikely that *id2a* is implicated in hepatic competence. Thus, we examined the expression of the following markers in *id2a* MO-injected embryos: the early hepatoblast markers, *hhex* and *prox1a* [28, 233], for hepatoblast specification and maintenance;

and the hepatocyte markers, *fabp10a*, *cp*, and *sepp1b*, for hepatocyte differentiation and hepatic outgrowth. *hhex* and *prox1a* expression was detected in the livers of the MO-injected embryos at 36 hpf (Figure 9C and D, arrows), suggesting that *id2a* does not regulate hepatoblast specification or its maintenance (Figure 9C and D, arrows).

Hepatic *fabp10a*, *cp*, and *sepp1b* expression was also detected in the MO-injected embryos at 48 hpf (Figure 9E–G, arrows), suggesting that *id2a* does not regulate hepatocyte differentiation. However, the liver size was reduced following *id2a* knockdown, implicating *id2a* in regulating hepatic outgrowth. Additionally, since *id2a* is expressed strongly in the gut and intestinal regions during development (Figure 6A; bracket), we examined the expression of *cdx1b*, an intestinal bulb marker [234], expecting a similar outgrowth phenotype as observed in the liver. As expected, lack of *id2a* had no effect on *cdx1b* induction; however, the intestinal bulb failed to grow at 48 hpf in *id2a* MO-injected embryos (Figure 9H, brackets), indicative of an intestinal outgrowth defect. We further sought to determine whether *id2a* knockdown resulted in a general outgrowth defect of all endoderm-derived organs or specific organs in which *id2a* is expressed. Since *id2a* is not expressed in the dorsal pancreas (Figure 6A and 10A), we performed WISH to examine the expression of insulin, which marks the pancreatic beta cells of the dorsal pancreas [235]. We found no difference in the size of the dorsal pancreas between control and *id2a* MO-injected embryos (Figure 10B).

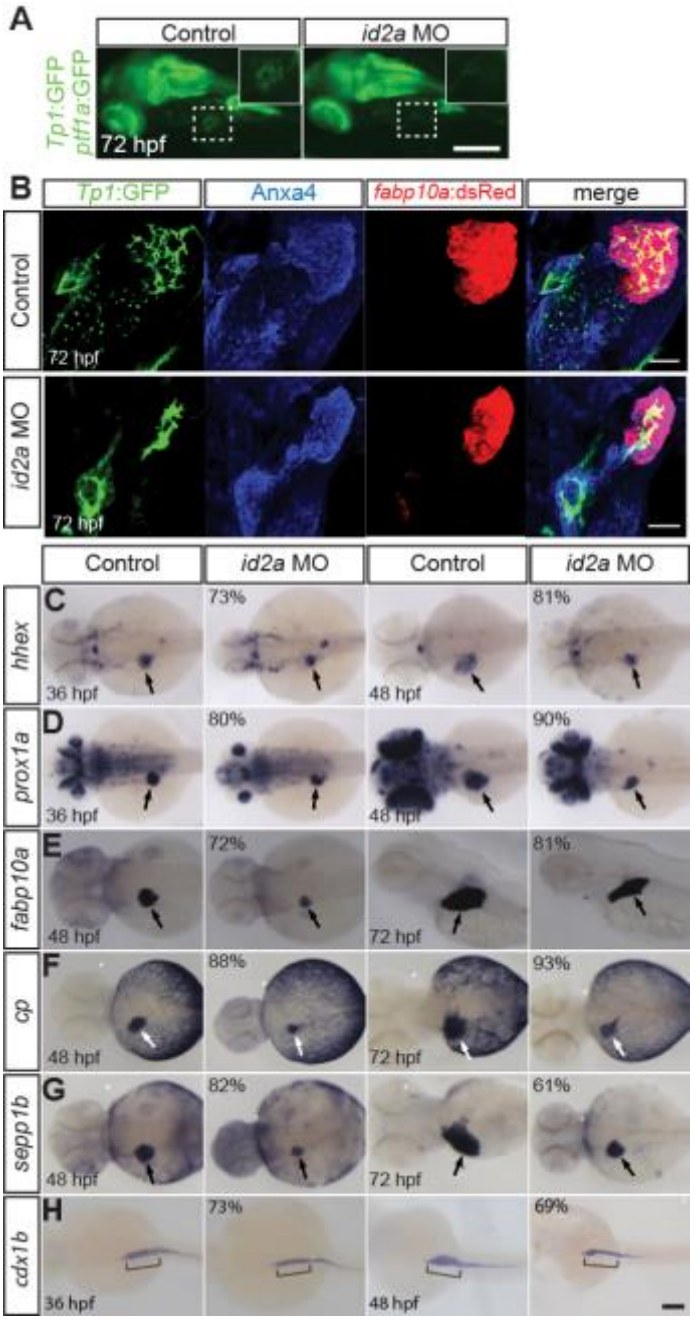

Figure 9: *id2a* knockdown reduces liver size but does not block hepatoblast specification or hepatocyte differentiation

(A) Epifluorescence images revealing a decreased number of *Tp1*:GFP^{+} BECs in the liver of *id2a* MO-injected embryos at 72 hpf compared with controls (squares). Higher magnification images of the square regions are shown in insets. Lateral view, anterior to the left. **(B)** Confocal projection images revealing *fabp10a*:dsRed (hepatocytes; red), *Tp1*:GFP (BECs; green) and Anxa4 (the hepatopancreatic ductal

system; blue) expression [236]. In *id2a* MO-injected embryos, liver size was greatly reduced and intrahepatic BECs appeared aggregated, displaying a branching defect. **(C-H)** *id2a* MO-injected and uninjected control embryos were processed for WISH with *hhex* (C), *prox1a* (D), *fabp10a* (E), *cp* (F), *sepp1b* (G), and *cdx1b* (H) probes. Overall liver size was greatly reduced in *id2a* MO-injected embryos as revealed by the hepatoblast markers (*hhex* and *prox1a*) and the hepatocyte markers (*fabp10a*, *cp*, and *sepp1b*). However, the expression of these genes was clearly detected in the MO-injected embryos (C–G, arrows), indicating unaltered hepatoblast specification and hepatocyte differentiation upon *id2a* knockdown. The induction of the intestinal bulb as assessed by *cdx1b* expression appeared unaffected in *id2a* MO-injected embryos at 36 hpf; however, the intestinal bulb failed to grow at 48 hpf (H, brackets). The percentage of *id2a* MO-injected embryos exhibiting the representative phenotype shown is indicated in the upper left corner (n = 10–20). The remaining percentage of embryos exhibited an intermediate liver/intestinal bulb phenotype: their liver/intestinal bulb size was still smaller than that of the control embryos. Arrows point to the liver. Scale bar: 250 (A), 20 (B), and 100 (C–H) μm.

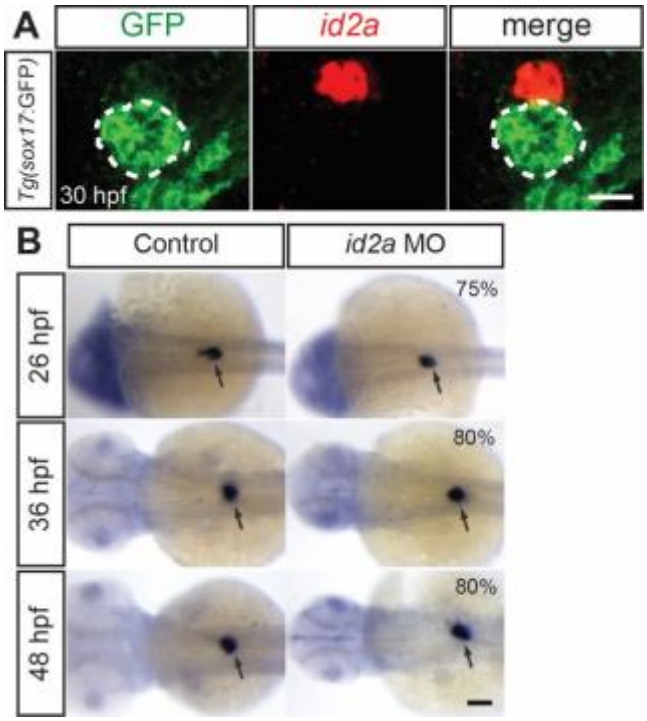

Figure 10: *id2a* knockdown does not result in a general endoderm-derived organ defect

(A) *id2a* in situ hybridization (red) combined with anti-GFP immunostaining (green) in *Tg(sox17:GFP)* embryos reveals that *id2a* is highly expressed in the interrenal primordium but not in the dorsal pancreas (dashed lines) at 30 hpf. Single confocal section images. **(B)** *id2a* MO-injected and control embryos were processed for WISH with the *insulin* probe, which marks pancreatic β-cells of the dorsal pancreas (arrows). Overall size of the dorsal pancreas appeared unaffected in the MO-injected embryos compared to controls. The percentage of *id2a* MO-injected embryos exhibiting the representative phenotype shown is indicated in the upper left corner (n=10-20). The remaining percentage of embryos exhibited an intermediate or slightly larger dorsal pancreas phenotype. Arrows point to the dorsal pancreas. Scale bars: 20 μm (A) and 100 μm (B).

Previous studies have implicated ID proteins in the maintenance of neural stem cells. *Id1* and *Id3* double-knockout mice exhibit precocious neuronal differentiation, whereas *ID2* overexpression in the chick hindbrain inhibits neuronal differentiation [237]. Thus, it is still possible that *id2a* knockdown may result in precocious hepatocyte differentiation. To test

this possibility, we examined *fabp10a* expression at 36 hpf, when *fabp10a* expression is not yet detected in the livers of wild-type embryos. However, *fabp10a* expression was not detected in *id2a* MO-injected embryos (data not shown), ruling out this possibility. Moreover, we examined whether Id2a overexpression could increase liver size. However, liver size was not further increased in *id2a* mRNA-injected embryos at 72 hpf compared with controls (Figure 8E), indicating that Id2a is not sufficient for liver outgrowth.

Altogether, these data indicate that during liver development, *id2a* is not required for hepatoblast specification or hepatocyte differentiation, but rather for hepatic outgrowth. Moreover, the outgrowth defect observed in *id2a* MO-injected embryos may also apply to the development of other organ systems, such as the intestinal bulb.

2.2.4 *id2a* Knockdown Reduces Liver Size via Decreased Hepatoblast Proliferation and Increased Cell Death

To determine whether the small liver observed in *id2a* MO-injected embryos was caused by reduced proliferation and/or enhanced cell death, we conducted anti-phospho-Histone 3 (pH3) immunostaining and EdU labeling for proliferation and TUNEL labeling for cell death. Although the percentage of $pH3^+$ cells among *prox1a*:YFP^+ hepatic cells in *id2a* MO-injected embryos at 40 hpf was not significantly different from that in controls, there was a trend of reduced $pH3^+$ cell number in the MO-injected liver compared to the control liver (0–3 *versus* 3–5) (Figure 11A and B). EdU labeling revealed about a 40% decrease in the percentage of EdU^+ cells among *sox17*:GFP^+ hepatic cells in *id2a* MO-injected embryos at 40 hpf compared with controls (Figure 11C and D), indicating reduced proliferation. In addition, we observed TUNEL

and Prox1 double-positive cells in *id2a* MO-injected embryos at 40 hpf, but not in controls (Figure 11E and F). MO-mediated knockdown can often induce apoptosis mediated *via* aberrant p53 activation; thus, concurrent knockdown of *tp53* can ameliorate apoptosis induced by MO off-targeting [238]. Therefore, we performed simultaneous knockdown of *tp53* and *id2a*. We did not detect any differences in microphthalmic, microcephalic, or small liver phenotypes between single *id2a* and double *id2a*/*tp53* MO-injected embryos at 60 hpf (Figure 8C and 8D), indicating that *id2a* knockdown phenotypes are independent of the p53 pathway. Altogether, these data indicate that *id2a* regulates hepatic outgrowth by promoting hepatoblast proliferation and repressing cell death.

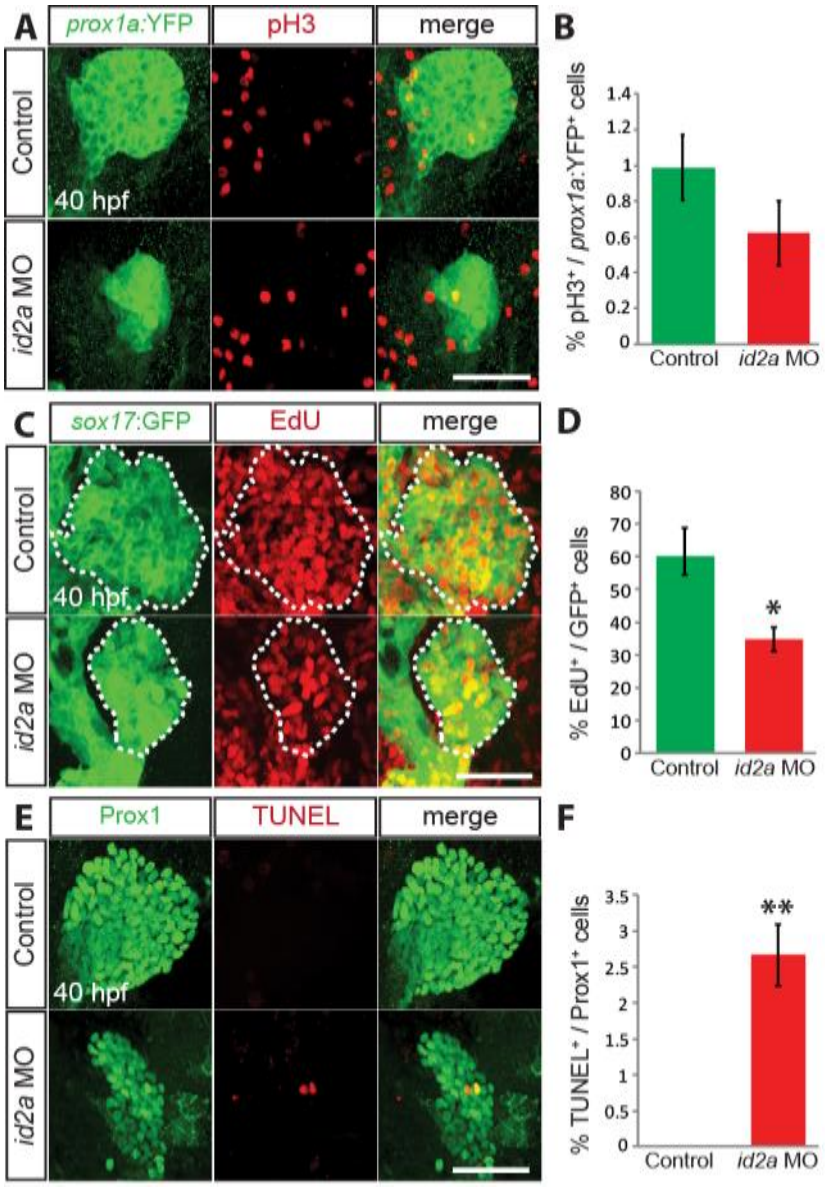

Figure 11: *id2a* knockdown decreases hepatoblast proliferation and increases cell death in the developing liver

(A) Whole-mount immunostaining with anti-pH3 (red) anti-GFP (green) antibodies in *Tg*(*prox1a*:*YFP*) embryos. The total number of *prox1a*:YFP^{+} hepatic cells per liver is 316 ± 8.5 in controls and 156 ± 5.6 in *id2a* MO-injected embryos. **(B)** A graph showing the percentage of pH3^{+} cells among *prox1a*:YFP^{+} hepatic cells (n = 10). **(C)** EdU labeling (red), combined with anti-GFP immunostaining (green), in *Tg*(*sox17*:*GFP*) embryos reveals a significant reduction of proliferation in the liver of *id2a* MO-injected embryos at 40 hpf compared with controls. Dotted lines outline the liver.

The total number of *sox17*:GFP$^+$ cells per liver is 220 ± 16.6 in controls and 127 ± 12.7 in *id2a* MO-injected embryos. **(D)** A graph showing the percentage of EdU$^+$ cells among GFP$^+$ hepatoblasts (n = 10). **(E)** TUNEL labeling (red) combined with anti-Prox1 immunostaining (green) reveals apoptosis in the liver of *id2a* MO-injected embryos at 40 hpf, but not in controls. The total number of Prox1$^+$ cells per liver is 276 ± 20.5 in controls and 140 ± 8.6 in *id2a* MO-injected embryos. **(F)** A graph showing the percentage of TUNEL$^+$ cells among Prox1$^+$ hepatoblasts (n = 10). *p < 0.05, **p < 0.005; error bars, ± s.e.m. Scale bars: 50 μm.

2.3 METHODS

2.3.1 Zebrafish Maintenance

Embryos and adult zebrafish (*Danio rerio*) were raised and maintained under standard laboratory conditions [239] with protocols approved by the University of Pittsburgh IACUC.

2.3.2 Zebrafish Strains

We used the following transgenic lines: *TgBAC*(*prox1a*:*Citrine*)^{hu338} [228] [referred to as *Tg*(*prox1a*:*YFP*)], *Tg*(*EPV.Tp1-Mmu.Hbb*:*EGFP*)^{um14} [24] [referred to as *Tg*(*Tp1*:*GFP*)], *Tg*(*kdrl*:*EGFP*)^{s843} [229] [referred to as *Tg*(*kdrl*:*GFP*)], *Tg*(*ptf1a*:*EGFP*)^{jh1} [240] [referred to as *Tg*(*ptf1a*:*GFP*)], *Tg*(*sox17*:*GFP*)^{s870} [230] and *Tg*(*fabp10a*:*dsRed,ela31*:*GFP*)^{gz12} [39] [referred to as *Tg*(*fabp10a*:*dsRed*)].

2.3.3 Morpholino and mRNA Injections

id2a MO (*5′*-GCCTTCATGTTGACAGCAGGATTTC-3′) [193] and *tp53* MO (*5′*-GCGCCATTGCTTTGCAAGAATTG-3′) [241] were purchased from GeneTools (Philomath, OR, USA). 3–4 ng of *id2a* MO or 2 ng of *tp53* MO was injected into one-cell stage embryos. For rescue experiments, 3 ng of the *id2a* MO and 150 pg of *id2a* mRNA, which is resistant to the *id2a* MO, was sequentially injected into one-cell stage embryos. The *id2a* mRNA was generated using the mMessage mMachine SP6 kit (Life Technologies, Grand Island, NY, USA).

2.3.4 Whole-mount *In Situ* Hybridization and Immunohistochemistry

Whole-mount *in situ* hybridization was performed as previously described [242]. cDNA from 24-hpf embryos was used as a template for PCR to amplify *id1*, *id2a*, *id2b*, *id3*, and *id4* genes. We also used the following probes: *hhex* [243], *prox1* [244], *fabp10a* [245], *sepp1b* [246], *cp* [64], and *cdx1b* [247]. Whole-mount immunostaining was performed as previously described [29], using the following antibodies: chicken polyclonal anti-GFP (1:100; Aves Labs, Tigard, OR, USA), rabbit polyclonal anti-Prox1 (1:1000; Millipore, Billerica, MA, USA), mouse monoclonal anti-Anxa4 (also named as 2 F11; 1:100; Abcam, Cambridge, MA USA), rabbit polyclonal anti-dsRed (1:200; Clontech, Mountain View, CA, USA), mouse monoclonal anti-phospho-Histone H3 (1:100; Cell Signaling, Danvers, MA, USA) and conjugated secondary antibodies, including Alexa Fluor 405, 488, 568, and 647 (1:300; Life Technologies, Grand Island, NY, USA). Hoechst 33342 (2.5 ng/ml; Sigma-Aldrich, St. Louis, MO, USA) was used for DNA staining. Zeiss LSM700 was used for confocal microscopy.

2.3.5 TUNEL and EdU Assays

Apoptotic cell death was analyzed according to the protocol of the *In Situ* Cell Death Detection Kit, TMR Red (Roche, Switzerland). Following whole-mount immunostaining, TUNEL labeling was applied. Cell Proliferation was performed using the protocol outlined in the Click-iT EdU Alexa Fluor 647 Imaging Kit (Life Technologies, Grand Island, NY, USA). Larvae were incubated with EdU solution at 39 hpf for one hour, and at 40 hpf, they were harvested for EdU staining. Unpaired two-tailed Student's t-tests were used for statistical analysis; $p < 0.05$ was considered statistically significant.

2.4 DISCUSSION

In this study, we sought to determine the role of Id2a in liver development. We report three important findings. First, by using WISH followed by immunostaining, we discovered that *id2a* is initially expressed in the liver-forming region from 30 hpf and following hepatoblast differentiation at 48 hpf, *id2a* expression is restricted to BECs. Second, *id2a* knockdown did not affect hepatocyte differentiation or hepatoblast specification, which correlates with a lack of *id2a* liver expression during the hepatoblast specification stage (*i.e.*, 22 hpf). Lastly, our data revealed that *id2a* knockdown inhibited hepatic outgrowth during development as supported by the reduced liver size in *id2a* MO-injected embryos.

Similar to the phenotype observed in *id2a* MO-injected embryos, in which hepatic outgrowth was compromised while hepatoblast specification and hepatocyte differentiation appeared unaffected, additional genes are also implicated in regulating hepatic outgrowth in

zebrafish. Classified as a tumor suppressor gene that functions as a transcriptional activator, core promoter element binding protein (*copeb*; renamed as *klf6a*) is expressed in the zebrafish digestive organs, including the liver, the pancreas, and intestine. In *copeb* MO-injected embryos, the expansion of the liver is impaired [248]. Moreover, the failure of hepatic outgrowth in *copeb* MO-injected larvae is also attributed to a decrease in cell proliferation, as observed in *id2a* MO-injected embryos [248]. A similar phenotype is observed in the cell cycle modulator ubiquitin-like with PHD and ring finger domains 1 (*uhrf1*) mutants, which exhibit smaller livers as a result of a proliferation defect during the hepatic outgrowth phase [27]. In addition, knockdown of either *sfrp5* [249] or *nav3a* [250] also results in a defect in hepatoblast outgrowth and subsequent liver size in 40-hpf zebrafish embryos. These results correlate with the well-known role of ID proteins as master regulators of cell proliferation [251], especially evident during early development.

Early development is a process defined by rapid cell proliferation followed by cell differentiation, generating distinct, mature tissues. Generally, *Id* expression is usually upregulated during the cell proliferation phase of early tissue development, and subsequently downregulated in mature, differentiated cells [252, 253]. However, exceptions exist; therefore, ID protein-mediated proliferation is cell context-dependent. For example, overexpression of *Id1*, *Id2*, or *Id3* in neural stem cells derived from the mouse embryonic forebrain maintains the cortical neural stem cells in a proliferative, self-renewing state, and simultaneously inhibits neuronal differentiation [254]. In contrast, upon differentiation of hematopoietic progenitor cells, *Id2* expression increases [255]. Previously, Uribe et al. reported on the role of *id2a* in zebrafish retinogenesis. Upon *id2a* knockdown, proliferative retinoblasts (in the S-phase) increased as mitotic retinoblasts (in the M-phase) decreased, which demonstrates a

role of Id2a in regulating the S- to M-phase progression during the cell cycle [193]. In contrast, we noted a significant decrease in the number of proliferating hepatoblasts at 40 hpf in *id2a* MO-injected embryos. As aforementioned, this phenotypic difference observed in proliferative cells during retinogenesis and liver development alludes to the dependence on cellular contexts in which *id* genes were studied. Nonetheless, *id2a* appears to play an important role in regulating proliferation in diverse tissue contexts including the developing liver.

In addition to proliferation, ID proteins also regulate apoptosis in a cell-dependent manner [188, 256]. While apoptosis is significantly increased in mammary epithelial cells of *Id2*$^{-/-}$ pregnant mice [257], overexpression of *Id1*, *Id2*, or *Id3* induces apoptosis in serum-deprived rat embryonic fibroblasts [258]. In *id2a* MO-injected embryos, we observed a significant increase in the number of TUNEL-positive hepatoblasts at 40 hpf, highlighting the role of Id2a in regulating apoptosis in the developing liver.

Although intrahepatic biliary defects were also observed in *id2a* MO-injected embryos, it is unclear if the defects are either attributed to (1) a primary phenotype due to *id2a* knockdown or (2) a secondary phenotype due to compromised hepatic outgrowth. BEC-specific knockdown or knockout of *id2a* should conclusively establish a direct or indirect role of *id2a* in intrahepatic biliary morphogenesis. Currently, however, it is a challenge to create such a tool in zebrafish. As *id2a* expression is restricted in BECs during liver development, it will be interesting to explore the role of *id2a* in biliary-driven liver regeneration. Previously, we reported on a novel hepatocyte-specific genetic ablation model in zebrafish: following severe hepatocyte loss, BECs contribute to the repopulation of the liver [20]. Few reports have explored the role of ID2 in liver regeneration. In two different models of liver injury in rats, partial hepatectomy and bile duct ligation, *Id2* is immediately upregulated during the hepatocyte priming phase and ID2 expression is detected in

the proliferating hepatocytes, respectively [259]. However, the role of *Id2* in liver regeneration has not been reported yet. In addition, although ID2 has been shown to interact with various factors, including MyoD during myogenesis [260], future analysis should consider the currently unknown binding factor of Id2a in the developing zebrafish liver. Since *id2a* knockdown reduced the liver size, we speculate the binding partner of Id2a to function as a suppressor of hepatic outgrowth and a negative regulator of hepatoblast proliferation.

Our findings validate the role of *id2a* in promoting hepatic outgrowth and development. Future studies should explore the mechanism of action of Id2a, including its binding partner, in liver development. Discerning the molecular mechanisms regulating liver development will improve our comprehension of the biological relevance of hepatic diseases and methods to enhance innate liver regeneration.

2.5 ACKNOWLEDGEMENTS

This chapter was adapted and modified from the following published work:
Khaliq M.K., Choi T.Y., So J., and Shin D. (2015) Id2a is required for hepatic outgrowth during liver development in zebrafish. *Mech Dev*. **138**, 399-414.

We thank Michael Tsang for critical reading of the manuscript. This research was supported in part by grants from the NIH (T32EB001026) to M.K. and from the American Liver Foundation and the NIH (R01DK101426) to D.S.

3.0 BMP SIGNALING GOVERNS BILIARY-DRIVEN LIVER REGENERATION IN ZEBRAFISH VIA TBX2B AND ID2A

3.1 BACKGROUND

As a highly regenerative organ, the liver can undergo either hepatocyte- or biliary-driven regeneration. In the former case, upon partial hepatectomy or mild liver injury, hepatocytes proliferate to restore the lost liver mass [112]. However, in the latter case, upon severe liver injury in which hepatocyte proliferation is compromised, biliary epithelial cells (BECs) dedifferentiate into liver progenitor cells (LPCs), also called oval cells or hepatoblast-like cells (HB-LCs), and subsequently give rise to hepatocytes [261]. Previously, controversies existed regarding the relative contribution of BEC-driven liver regeneration [262]; however, recent studies in zebrafish [20, 132] and mice [263] have resolved this controversy by showing the extensive contribution of BECs to hepatocytes upon severe liver injury. In mice, hepatocyte-specific *Mdm2* deletion completely blocks hepatocyte proliferation, additionally induces hepatocyte senescence and apoptosis, and subsequently elicits oval cell activation. These oval cells later give rise to hepatocytes, leading to a full liver recovery [263]. In the zebrafish studies, the near-complete ablation of hepatocytes elicits the extensive contribution of BECs to hepatocytes through the dedifferentiation of BECs into HB-LCs and subsequent differentiation of the HB-LCs into hepatocytes [20, 132].

Oval cells are frequently observed in diseased livers and their number positively correlates with disease severity [264]. Since patients suffering from severe liver diseases have limited treatment options and present with an abundance of hepatic oval cells, promoting the

differentiation of oval cells into hepatocytes is deemed an effective therapeutic strategy. Developing such therapies requires a deeper understanding of the mechanisms by which oval cells differentiate into hepatocytes in vivo. Although several factors, such as FGF7 [139] and TWEAK [265], which can induce oval cell activation in vivo, have been identified, factors that regulate oval cell differentiation into hepatocytes in vivo are unknown, mainly due to the lack of an animal model for BEC-driven liver regeneration. However, the recent reports of zebrafish and mouse liver injury models, in which BECs extensively contribute to regenerated hepatocytes, present an opportunity to investigate the mechanisms underlying oval cell differentiation into hepatocytes.

Using the zebrafish BEC-driven liver regeneration model combined with targeted chemical screening, we recently reported on the role of bromodomain extraterminal (BET) proteins in BEC dedifferentiation into HB-LCs and the proliferation of newly-generated hepatocytes [266]. Using the same zebrafish model, we now show the essential role of Bmp signaling in HB-LC differentiation into hepatocytes. Bmp signaling plays important roles in early liver development, such as hepatoblast specification and proliferation [70, 76]. Despite its clear role in early liver development, the role of Bmp signaling in liver regeneration has not been clearly defined. Current literature provides confounding results that BMP2 [267] and BMP4 [169] negatively while BMP7 [268] positively regulate hepatocyte-driven liver regeneration after partial hepatectomy in rodents. Moreover, there is no report on the role of Bmp signaling in BEC-driven liver regeneration. Given the important role of Bmp signaling in early liver development and its positive effect on regeneration of other organs, including the heart [269], we hypothesized that Bmp signaling might regulate BEC-driven liver regeneration. Our finding that the hepatic expression of several genes implicated in Bmp signaling, including *smad5*, was upregulated during BEC-driven liver regeneration further supported our hypothesis. In this study, we report that Bmp signaling

regulates two distinct steps of BEC-driven liver regeneration: (1) HB-LC differentiation into hepatocytes, and (2) the proliferation of newly-generated BECs.

3.2 RESULTS

3.2.1 BMP Signaling is Required for BEC-driven Liver Regeneration

We have established a zebrafish liver injury model in which BECs extensively contribute to hepatocytes [20]. Specifically, *Tg(fabp10a:CFP-NTR)* fish express nitroreductase (NTR) under the hepatocyte-specific *fabp10a* promoter; the treatment of metronidazole (Mtz), which is converted into a cytotoxic drug by NTR, results in hepatocyte-specific ablation in the transgenic fish. In this model, severe hepatocyte ablation induces the dedifferentiation of BECs into HB-LCs, which then differentiate into hepatocytes, thereby leading to a full liver recovery. To understand the molecular mechanisms underlying BEC-driven liver regeneration, we performed RNAseq analyses and compared gene expression profiles between control and regenerating livers at multiple time points during the regeneration. Through this analysis and subsequent validation with RT-PCR and whole-mount in situ hybridization (WISH) (Figure 12), we found that genes implicated in the Bmp signaling pathway, such as *smad5*, *id2a*, and *tbx2b*, were upregulated in regenerating livers at regeneration (R) 6h compared with controls (Figure 13A-13C).

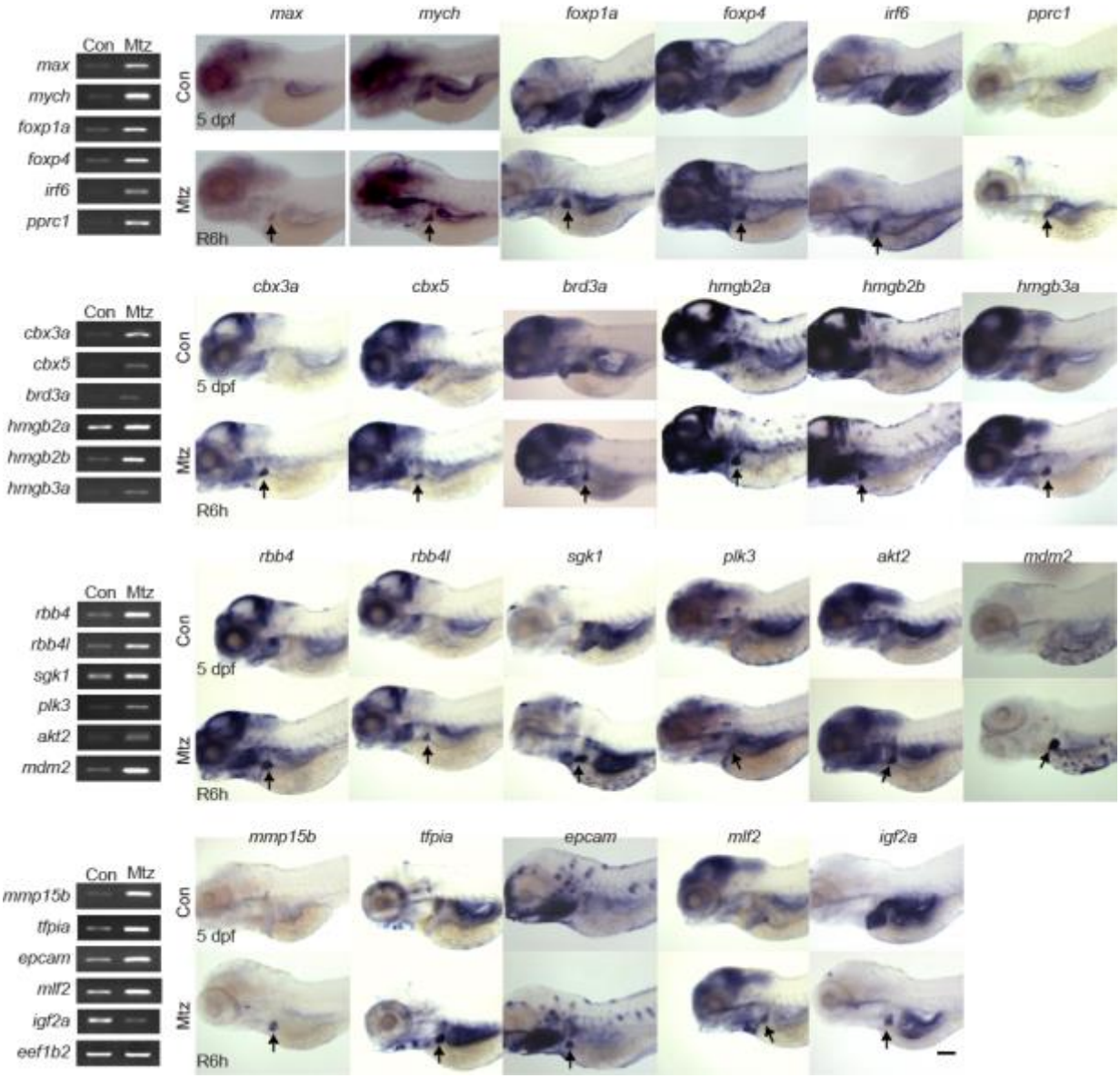

Figure 12: Validation of RNAseq data using RT-PCR and WISH

RT-PCR and WISH were performed to validate genes-of-interest from RNAseq analysis. For RT-PCR, cDNA was prepared from control livers at 5 dpf and from Mtz-treated regenerating livers at R6h. For in situ hybridization, control larvae at 5 dpf and regenerating larvae at R6h were used. Arrows point to regenerating livers. Scale bar: 150 µm.

Bmp signaling plays an essential role in hepatoblast specification and liver growth during liver development [70, 76], but its role in liver regeneration has not been clearly defined. Thus, to

determine whether Bmp signaling was required for BEC-driven liver regeneration, we applied the selective Bmp inhibitor, DMH1, which has been widely used in zebrafish. During BEC-driven liver regeneration, a hepatoblast/hepatocyte marker, Hnf4a, is induced in BECs and the expression of Prox1, a marker for hepatoblasts, hepatocytes, and BECs, is also upregulated in BECs [20]. In addition, the expression of Alcam, a good marker of zebrafish BECs [270] is sustained in HB-LCs, but disappears from HB-LCs when these cells differentiate into hepatocytes [20]. DMH1 treatment from ablation (A) 0h greatly repressed Hnf4a, but not Prox1 or Alcam, expression, at R0h (Figure 13D). Intriguingly, DMH1 treatment after hepatocyte ablation (from R0h) significantly increased the number of BECs at R30h, as assessed by Alcam and *Tp1:*H2B-mCherry expression (Figure 13E). The *Tg(Tp1:H2B-mCherry)* line, which expresses stable H2B-mCherry fusion proteins under the *Tp1* promoter containing the Notch-responsive element, reveals BECs in the liver [271]. Collectively, these data indicate the essential roles of Bmp signaling in BEC-driven liver regeneration.

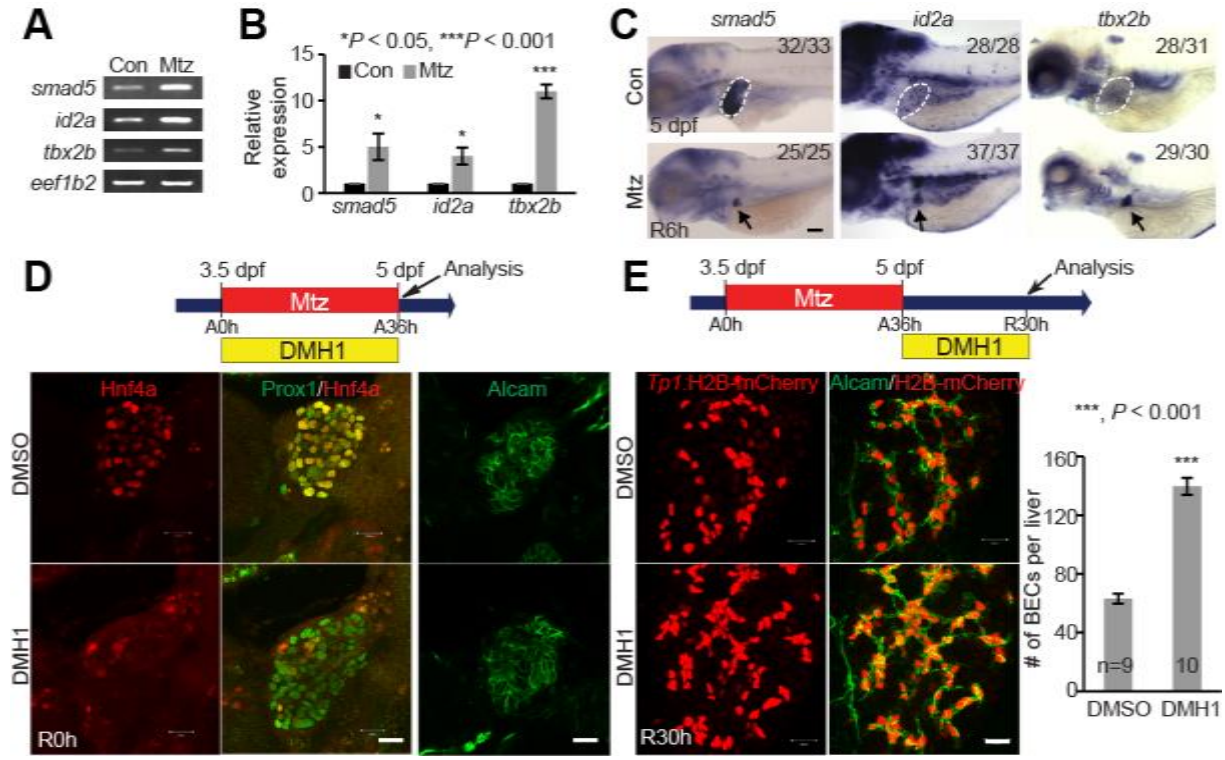

Figure 13: Bmp signaling is required for BEC-driven liver regeneration

(A, B) RT-PCR (A) and qPCR (B) data showing the expression levels of *smad5*, *id2a* and *tbx2b* between control and regenerating livers at R6h. **(C)** WISH images showing the expression of *smad5*, *id2a* and *tbx2b* in control (dashed lines) and regenerating (arrows) livers. Numbers indicate the proportion of larvae exhibiting the expression shown. **(D)** Single-optical section images showing the expression of Hnf4a and Prox1 or Alcam in regenerating livers. **(E)** Confocal projection images showing *Tp1:*H2B-mCherry and Alcam expression in regenerating livers. Quantification of the number of H2B-mCherry/Alcam double-positive cells (i.e., BECs). Scale bars: 150 (C), 20 (D, E) μm; error bars: ±SEM.

3.2.2 Inhibition of BMP Signaling Blocks HB-LCs Differentiation into Hepatocytes

Next, we investigated in detail the effect of Bmp inhibition on earlier stages of BEC-driven liver regeneration. We first determined if Bmp inhibition blocked the dedifferentiation of BECs into HB-LCs. By examining Hnf4a expression at various time points between A24h and A36h, we

found that Hnf4a induction in BECs occurred around A33h and that its expression became stronger at A36h (Figure 14A, arrows). As Hnf4a induction in BECs is indicative of BEC dedifferentiation [20], these data suggest that BECs dedifferentiate into HB-LCs around A33h. This observation was further supported by the expression of *fabp10a:*rasGFP (Figure 14B), which is not expressed in hepatoblasts during liver development but induced in BECs during BEC-driven liver regeneration [266]. At A33h, there were *fabp10a*:rasGFP^{+} cells negative for Hnf4a (Figure 14C, arrows), but not vice versa, indicating that *fabp10a* induction in BECs precedes Hnf4a induction. Although Hnf4a expression in BEC-derived cells was greatly reduced at A36h in DMH1-treated regenerating livers compared with their controls (Figure 13D), the initial induction of Hnf4a and *fabp10a:*rasGFP in BECs at A33h in DMH1-treated regenerating livers occurred similarly to DMSO-treated controls (Figures 14A and 14B). These data together with the Prox1 expression in HB-LCs indicate that Bmp inhibition does not block the dedifferentiation of BECs.

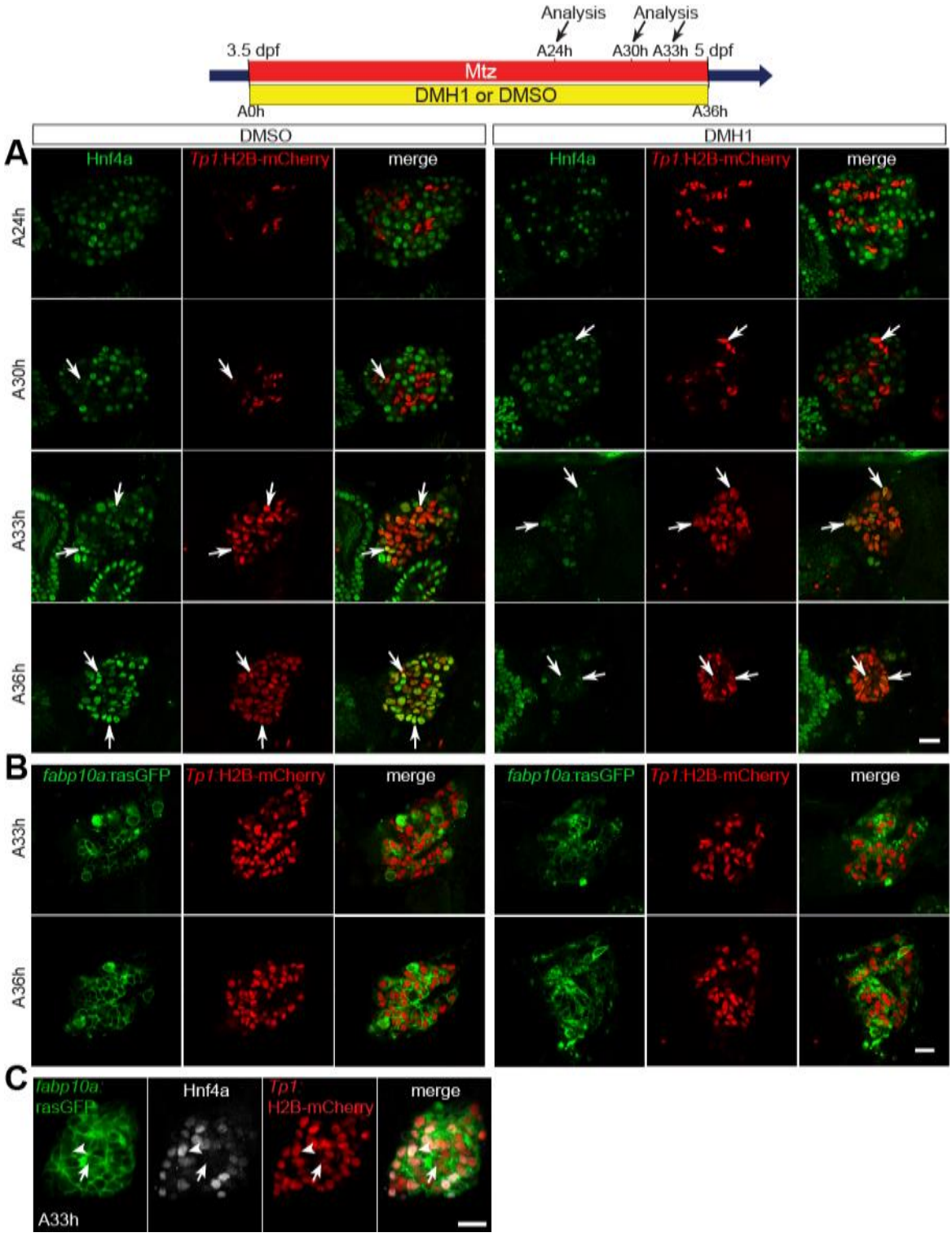

Figure 14: Inhibition of Bmp signaling does not block BEC dedifferentiation into HB-LCs

(A) Single-optical section images showing Hnf4a (green) and *Tp1:*H2B-mCherry (red) expression in ablating livers of DMH1- or DMSO-treated larvae at A24h, A30h, A33h and A36h. Arrows point to

Hnf4a^{+}/H2B-mCherry^{+} cells. **(B)** Single-optical section images showing *fabp10a:*rasGFP (green) and *Tp1:*H2B-mCherry (red) expression in ablating livers at A33h and A36h. **(C)** Single-optical section images showing the expression of *fabp10a:*rasGFP (green), Hnf4a (gray), and *Tp1:*H2B-mCherry (red) in ablating livers at A33h. Arrows point to rasGFP^{+}/Hnf4a^{+}/H2B-mCherry^{+} cells; arrowheads point to rasGFP^{+}/Hnf4a^{-}/H2B-mCherry^{+} cells. Scale bars: 20 μm.

Given that Hnf4a is the master regulator of hepatocyte differentiation [216], the reduced Hnf4a expression upon Bmp inhibition (Figure 13D) suggests a role for Bmp signaling in HB-LC differentiation into hepatocytes. To address this possibility, we sought to examine DMH1-treated regenerating larvae at later stages, such as R24h. However, the continuous DMH1 treatment from A0h killed most regenerating larvae before R24h, preventing the examination of the regenerating livers at later stages. By treating ablating larvae with DMH1 from different time points, we found that DMH1 treatment from A33h also reduced Hnf4a expression at R6h (Figure 15A) but did not kill regenerating larvae as late as R24h. At R24h, A33h DMH1-treated regenerating livers exhibited the following phenotypes: (1) sustained Alcam expression in most BEC-derived *Tp1:*H2B-mCherry^{+} cells, not just in BECs (Figure 15B); (2) sustained Notch activity throughout regenerating livers (Figure 15C); and (3) no expression of hepatocyte markers, Bhmt, *cp,* and *gc* (Figures 15D and 15E), indicating a defect in HB-LC differentiation into hepatocytes. Despite a lack of hepatocyte marker expression, genes expressed in hepatoblasts, such as *foxa3* and *prox1a*, were expressed similarly in DMSO- and DMH1-treated regenerating livers (Figure 15E). *fabp10a*, which is expressed in HB-LCs (Figure 14B), was also normally expressed (Figures 15D and 15E). In addition to the pharmacologic inhibition, we blocked Bmp signaling using the *Tg(hs:dnBmpr1)* line that expresses dominant-negative Bmpr1 under the *hsp70l* heat-shock promoter. The overexpression of dnBmpr1 via a single heat-shock at A30h resulted in sustained Notch activity

and reduced Hnf4a expression in regenerating livers at R12h (Figure 15F). All these data indicate the role of Bmp signaling in HB-LC differentiation into hepatocytes.

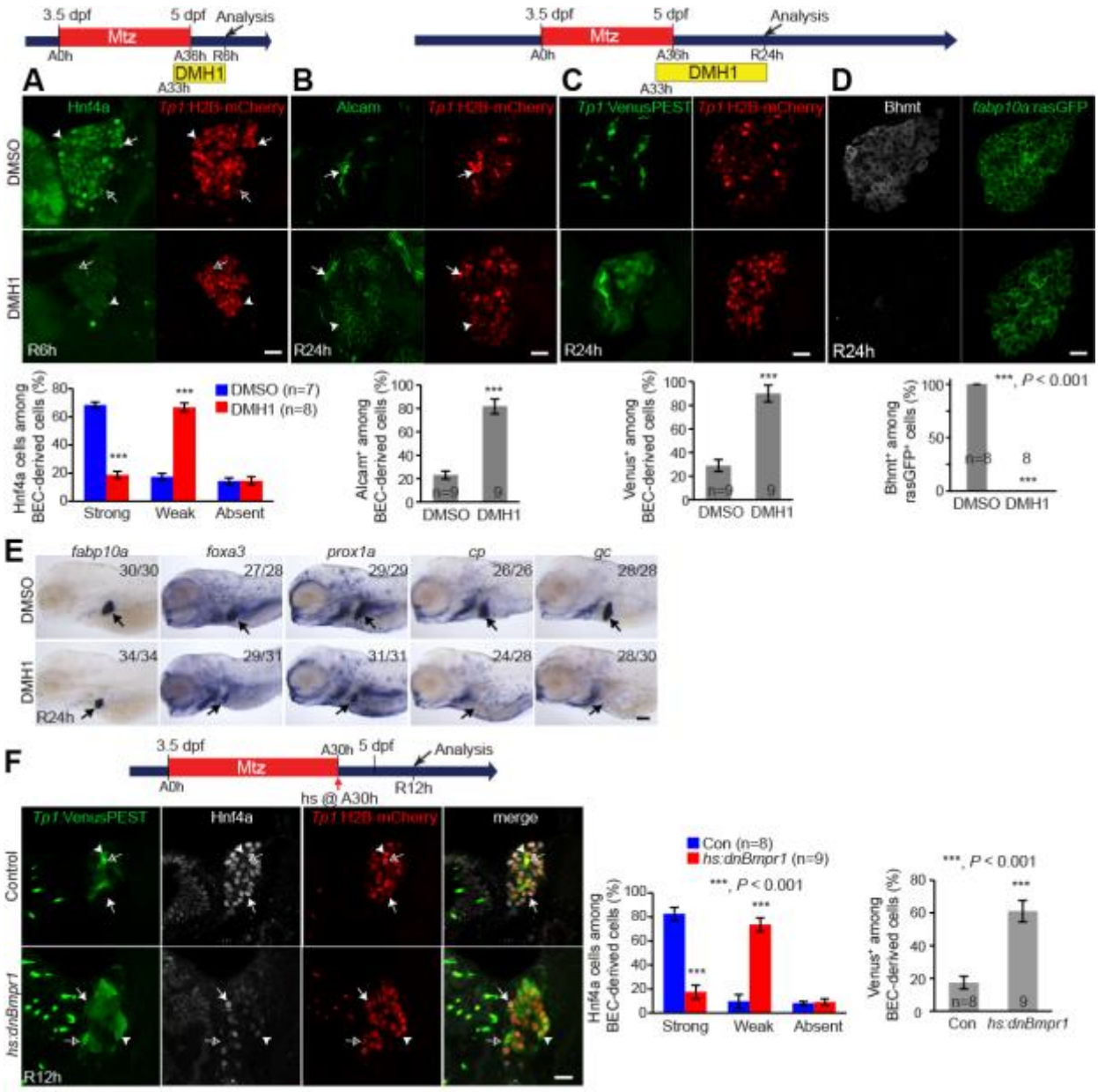

Figure 15: Bmp inhibition blocks HB-LC differentiation into hepatocytes

(A) Single-optical section images showing Hnf4a and *Tp1:*H2B-mCherry expression in regenerating livers. To quantify Hnf4a expression, BEC-derived H2B-mCherry^{+} cells were divided into three cases: Hnf4a^{strong} (arrows), Hnf4a^{weak} (arrowheads), and Hnf4a^{absent} (open arrows). Quantification of the

percentage of these three cell types among H2B-mCherry^{+} cells. **(B)** Single-optical section images showing Alcam and *Tp1:*H2B-mCherry expression in regenerating livers. In DMH1-treated regenerating livers, Alcam was expressed in both H2B-mCherry^{strong} (arrows) and H2B-mCherry^{weak} cells (arrowheads), whereas in control regenerating livers, Alcam was expressed only in H2B-mCherry^{strong} cells. Quantification of the percentage of Alcam^{+} cells among H2B-mCherry^{+} cells. **(C)** Single-optical section images showing the expression of *Tp1:*VenusPEST and *Tp1:*H2B-mCherry in regenerating livers. Quantification of the percentage of VenusPEST^{+} cells among H2B-mCherry^{+} cells. **(D)** Single-optical section images showing Bhmt and *fabp10a:*rasGFP expression in regenerating livers. Quantification of the percentage of Bhmt^{+} cells among BEC-derived *fabp10a:*rasGFP^{+} cells. **(E)** WISH images showing the expression of *fabp10a*, *foxa3*, *prox1a*, *cp* and *gc* in regenerating livers (arrows). **(F)** Single-optical section images showing Hnf4a, *Tp1:*VenusPEST, and *Tp1:*H2B-mCherry expression in regenerating livers. The *Tg(hs:dnBmpr1-GFP)* line was used to block Bmp signaling via a single heat-shock at A30h. Quantification of the percentage of Hnf4a^{strong} (arrows), Hnf4a^{weak} (arrowheads), and Hnf4a^{absent} (open arrows) cells and of VenusPEST^{+} cells among H2B-mCherry^{+} cells. Scale bars: 20 (A-D, F), 150 (E) μm; error bars: ±SEM.

3.2.3 Inhibition of BMP Signaling Maintains HB-LCs in their Undifferentiated State

Based on sustained Notch activity and Alcam expression in A33h DMH1-treated regenerating livers, we hypothesized that HB-LCs that failed to differentiate into hepatocytes remained as undifferentiated HB-LCs in DMH1-treated regenerating livers. To test this hypothesis, we used Cre/loxP-mediated lineage tracing and determined the lineages of HB-LCs. To label HB-LCs, we used two Cre lines, *Tg(Tp1:CreERT2)* that expresses CreERT2 under the *Tp1* promoter and *Tg(fabp10a:CreERT2)* that expresses CreERT2 under the *fabp10a* promoter [20]. Since Notch activity is strong in BECs but weak in HB-LCs, the former line labels most BECs but a few HB-LCs. Likewise, since *fabp10a* expression is strong in hepatocytes but weak in HB-LCs, the latter

line labels most hepatocytes but a few HB-LCs. When *Tp1:*CreERT2 and *fabp10a:*CreERT2 were activated by tamoxifen (4-OHT) treatment from A33h to R6h, 95% of BECs and 96% of hepatocytes, respectively, were labeled at R54h (Figure 16B). However, few hepatocytes were labeled by the *Tp1:*CreERT2 activation (Figure 16C) and few BECs were labeled by the *fabp10a:*CreERT2 activation (Figure 16D), indicating that few HB-LCs were labeled in these Cre activation settings. This low efficiency of HB-LC labeling can be explained by the weak Notch activity and weak *fabp10a* expression in HB-LCs and the short duration of HB-LCs in the zebrafish liver injury model. If the HB-LCs fail to differentiate and remain in a progenitor-like state, more HB-LCs will be labeled in the Cre activation settings, thereby more hepatocytes and BECs were labeled by *Tp1:*CreERT2 and *fabp10a:*CreERT2, respectively. We observed these phenomena in regenerating livers treated with DMH1 from A33h to R6h (Figures 16C and 16D), strongly suggesting that Bmp inhibition maintains HB-LCs in their undifferentiated state.

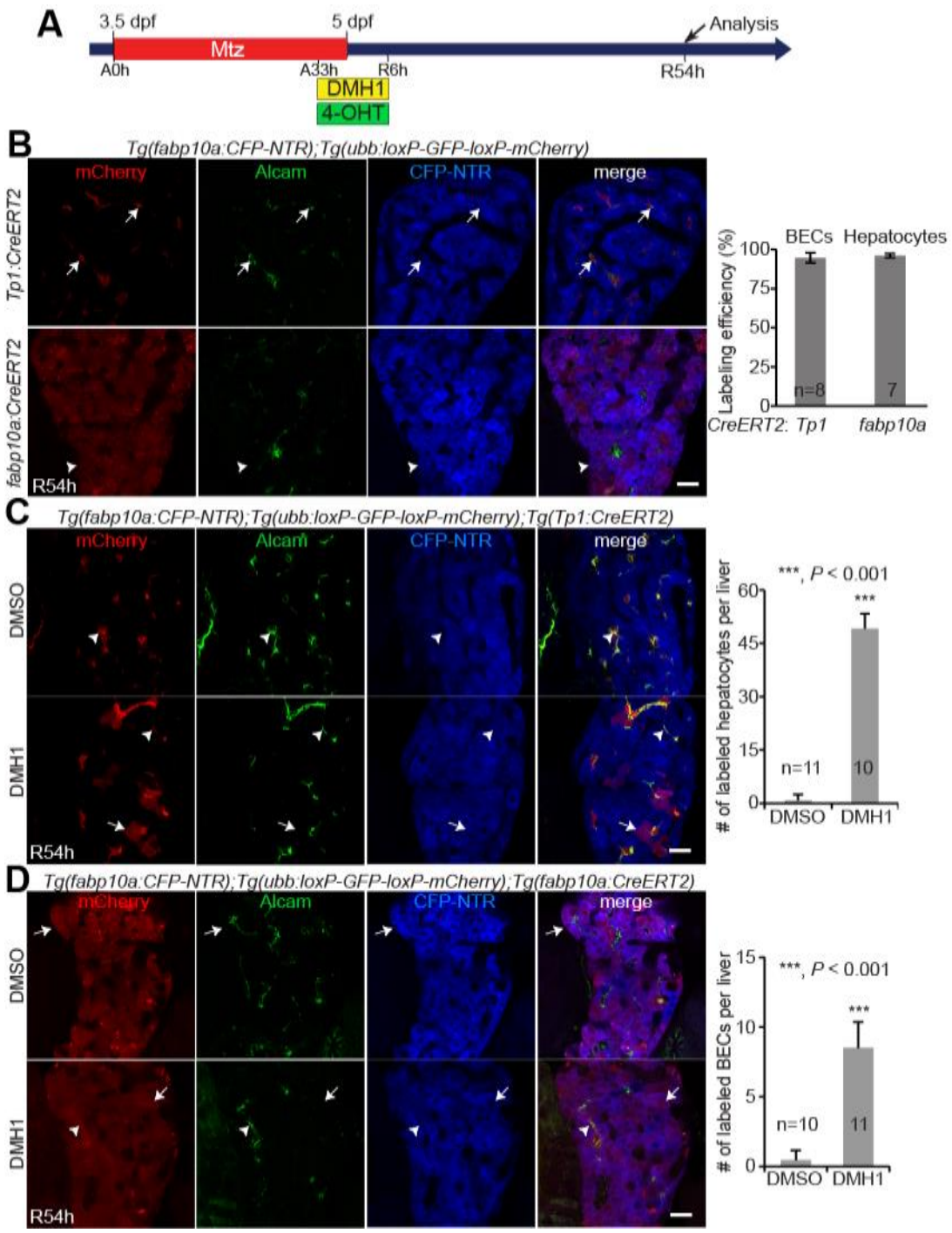

Figure 16: Bmp inhibition maintains HB-LCs in an undifferentiated state

(A) Experimental scheme illustrating the stages of Mtz, DMH1, and 4-OHT treatment. **(B)** Labeling efficiency of the lineage tracing with the *Tg(Tp1:CreERT2)* and *Tg(fabp10a:CreERT2)* lines. Arrows point to $CFP^-/mCherry^+/Alcam^+$ cells (Cre-labeled BECs); arrowheads point to $CFP^+/mCherry^+/Alcam^-$ cells (Cre-labeled hepatocytes). Quantification of the percentage of the labeled BECs and hepatocytes.

(C, D) Single-optical section images showing the expression of mCherry, Alcam, and *fabp10a:*CFP-NTR in regenerating livers at R54h. A Cre reporter line, *Tg(ubb:loxP-GFP-loxP-mCherry)*, was used together with the *Tg(Tp1:CreERT2)* (C) or the *Tg(fabp10a:CreERT2)* (D) line. Arrows point to $CFP^{+}/mCherry^{+}/Alcam^{-}$ hepatocytes; arrowheads point to $CFP^{-}/mCherry^{+}/Alcam^{+}$ BECs. Quantification of the numbers of $CFP^{+}/mCherry^{+}/Alcam^{-}$ hepatocytes and $CFP^{-}/mCherry^{+}/Alcam^{+}$ BECs per liver. Scale bars: 20 μm; error bars: ±SEM.

3.2.4 Inhibition of BMP Signaling After Hepatocyte Ablation Increases BEC Number in Regenerating Livers via Proliferation

Unlike its treatment from A33h, DMH1 treatment from R0h did not affect HB-LC differentiation into hepatocytes, as assessed by *cp* and *gc* expression (Figure 17).

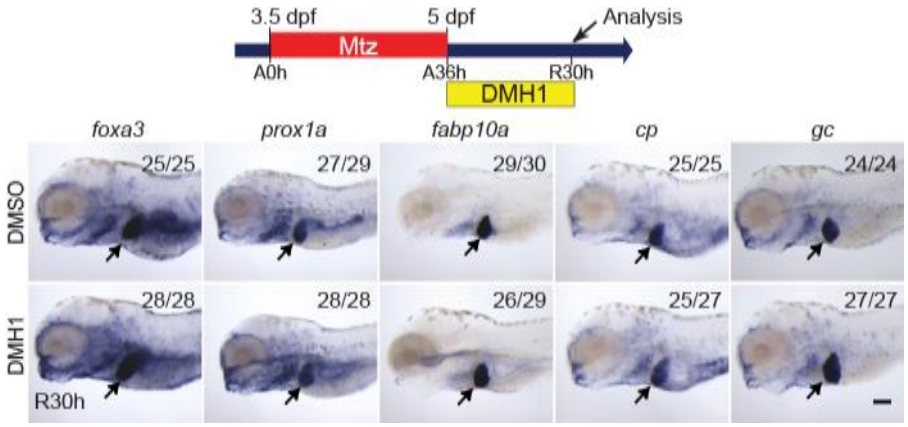

Figure 17: Inhibition of Bmp signaling after hepatocyte ablation does not affect HB-LC differentiation into hepatocytes

WISH images showing the expression of *foxa3*, *prox1a*, *fabp10a*, *cp* and *gc* in regenerating livers (arrows) at R30h. Numbers in the upper right corner indicate the proportion of larvae exhibiting the representative expression shown. Scale bar, 150 μm.

Given the increased number of BECs upon DMH1 treatment from R0h (Figure 13E), we determined the latest time point from which DMH1 treatment still increased BEC number. We found that DMH1 treatment from R12h, but not R24h, significantly increased BEC number (Figure 18A). Using a cell-cycle reporter line, *Tg(Tp1:mAGFP-gmnn)*, which reveals BECs in the S/G2/M (but not G0/G1) phases of the cell cycle, we observed that BEC proliferation was significantly increased in DMH1-treated regenerating livers at R30h compared with their controls (Figure 18B). In addition to the chemical inhibition of Bmp signaling, the overexpression of dnBmpr1 via a single heat-shock at R8h increased BEC proliferation in regenerating livers at R30h (Figures 18C and 18D). Altogether, these data indicate that Bmp signaling controls the number of BECs in regenerating livers by temporarily suppressing their proliferation.

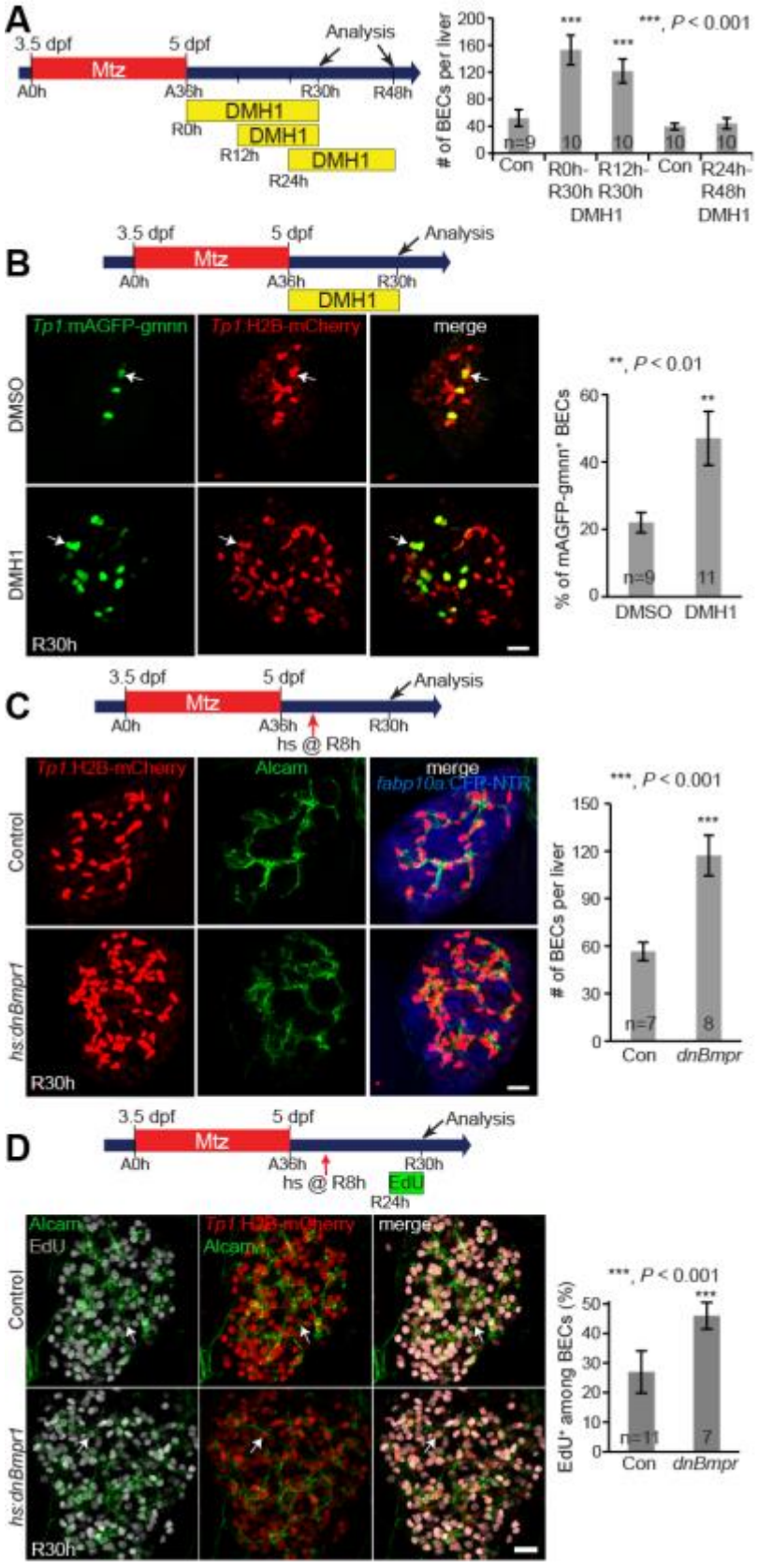
A
3.5 dpf
5 dpf
Analysis
Mtz
A0h
A36h
R30h
R48h
DMH1
R0h
R12h
R24h
# of BECs per liver
***, P < 0.001
Con
R0h-R30h DMH1
R12h-R30h DMH1
R24h-R48h DMH1
B
Tp1:mAGFP-gmnn
Tp1:H2B-mCherry
merge
DMSO
DMH1
R30h
**, P < 0.01
% of mAGFP-gmnn+ BECs
C
hs @ R8h
Alcam
fabp10a:CFP-NTR
Control
hs:dnBmpr1
D
EdU
EdU+ among BECs (%)

Figure 18: Bmp inhibition after hepatocyte ablation increases BEC number in regenerating livers via proliferation

(A) Experimental scheme illustrating the stages of Mtz and DMH1 treatment. Quantification of the total numbers of BECs in regenerating livers treated with DMH1 for three different time-windows. **(B)** Confocal projection images showing *Tp1:*H2B-mCherry and *Tp1:*mAGFP-gmnn expression in regenerating livers. Arrows point to mCherry/mAGFP-gmnn double-positive cells. Quantification of the percentage of mAGFP-gmnn^{+} cells among H2B-mCherry^{+} BECs. **(C)** Confocal projection images showing the expression of Alcam, *Tp1:*H2B-mCherry, and *fabp10a:*CFP-NTR in regenerating livers at R30h. Quantification of the total numbers of BECs (H2B-mCherry^{+}/Alcam^{+}) per liver. **(D)** Confocal projection images showing EdU labeling and Alcam and *Tp1:*H2B-mCherry expression in regenerating livers. Arrows point to EdU^{+} BECs. Quantification of the percentage of EdU^{+} cells among BECs. Scale bars: 20 μm; error bars: ±SEM.

3.2.5 *smad5* Mutants Exhibit a Defect in HB-LC Differentiation into Hepatocytes

Given the upregulation of genes implicated in Bmp signaling, such as *smad5, tbx2b*, and *id2a*, in regenerating livers (Figures 13A-13C), we determined if DMH1 treatment suppressed this upregulation. Indeed, quantitative RT-PCR (qPCR) and WISH showed a reduction of the hepatic expression of *smad5, tbx2b*, and *id2a* in DMH1-treated regenerating livers at R6h compared with their controls (Figure 19A), suggesting a potential role for these genes in mediating Bmp signaling during BEC-driven liver regeneration. To test this possibility, we examined BEC-driven liver regeneration in *smad5* mutants. Smad5, together with Smad1 and Smad9, known as receptor-regulated Smads (R-Smads), relays Bmp signaling from the cell surface to the nucleus [272]. Zebrafish *smad5*$^{-/-}$ mutants started to die from 3 dpf but *smad5* mRNA injection into one-cell-stage embryos increased their survival time [273], allowing for our liver regeneration assay. Although the mRNA-injected mutants had a smaller liver than their siblings, liver development occurred, as

observed by their liver growth (Figure 19B) and the branching of the intrahepatic biliary structure (Figure 19C).

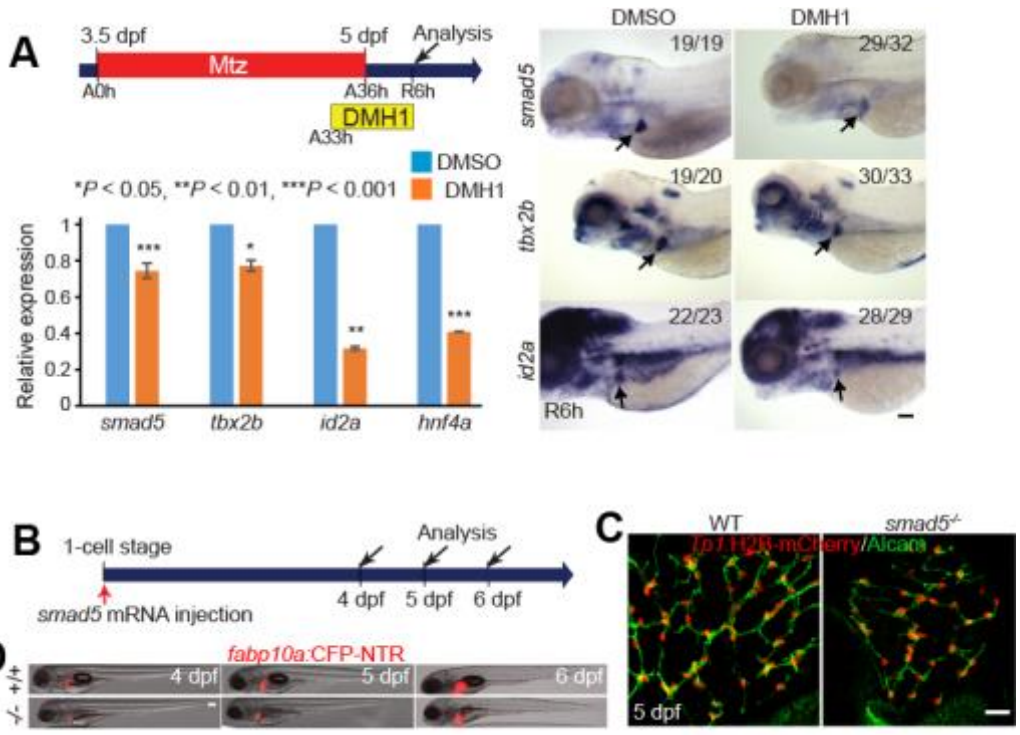

Figure 19: mRNA injection rescues survival of *smad5* mutants

(A) qPCR data showing the relative expression levels of *smad5*, *tbx2b*, *id2a* and *hnf4a* between DMSO- and DMH1-treated regenerating livers at R6h; WISH images showing the expression of *smad5*, *tbx2b* and *id2a* in regenerating livers (arrows). **(B)** Experimental scheme illustrating the stages of *smad5* mRNA injection (red arrow) and analysis (arrows) for C and D. **(C)** Single-optical section images showing *Tp1*:VenusPEST and *Tp1*:H2B-mCherry expression in the livers of *smad5*$^{-/-}$ mutants and wild-type siblings at 5 dpf. **(D)** Epifluorescence images showing hepatic *fabp10a:*CFP-NTR expression (red) in *smad5*$^{-/-}$ mutants and wild-type siblings at 4, 5, and 6 dpf. Scale bars: 150 (A, D), 20 (C) µm.

Since liver size was smaller in the mRNA-injected mutants than in wild-type, we applied Mtz from 5 dpf, when the mutant liver size is similar to that of 3.5-dpf wild-type livers. In this

rescue setting, the *smad5*$^{-/-}$ mutants exhibited sustained Notch activity and Alcam expression throughout regenerating livers (Figures 20B-20C) and no *cp*, but faint *gc*, expression (Figure 20D) at R24h, recapitulating the HB-LC differentiation defects observed in A33h DMH1-treated regenerating livers. The expression of *tbx2b* and *id2a* in regenerating livers also appeared to be reduced in the *smad5*$^{-/-}$ mutants compared with their siblings (Figure 20D), further supporting that Bmp signaling regulates *tbx2b* and *id2a* expression in regenerating livers.

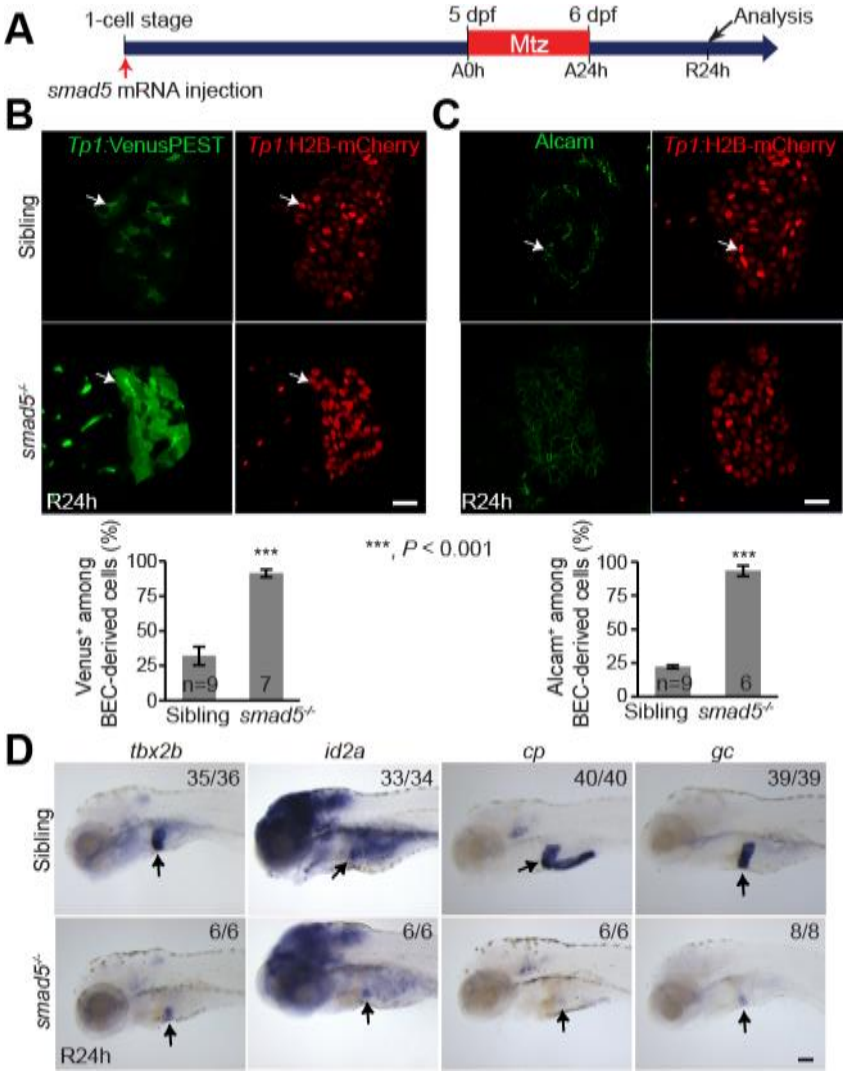

Figure 20: *smad5* mutants exhibit a defect in HB-LC differentiation into hepatocytes

(A) Experimental scheme illustrating the stages of *smad5* mRNA injection (red arrow) and Mtz treatment for B-D. **(B)** Single-optical section images showing *Tp1:*VenusPEST and *Tp1:*H2B-mCherry expression in regenerating livers. Quantification of the percentage of VenusPEST^{+} cells among BEC-derived H2B-mCherry^{+} cells. **(C)** Single-optical section images showing Alcam and *Tp1:*H2B-mCherry expression in regenerating livers. Quantification of the percentage of Alcam^{+} cells among BEC-derived H2B-mCherry^{+} cells. **(D)** WISH images showing the expression of *tbx2b*, *id2a*, *cp* and *gc* in regenerating livers (arrows). Scale bars: 150 (D), 20 (B, C) µm; error bars: ±SEM.

When examined at R48h, continuous DMH1 treatment from A33h was fatal for the zebrafish larvae recovering from severe liver injury, preventing the analysis of BEC-driven liver regeneration at later stages. However, the *smad5*$^{-/-}$ mutants recovered at R48h from the initial regeneration defects, as displayed by the rapid growth of their regenerating livers (Figure 21B), normal Notch activity (Figure 21C), and recovered *cp* and *gc* expression (Figure 21D). Altogether, data from *smad5* mutant analyses indicate the role of *smad5* in BEC-driven liver regeneration.

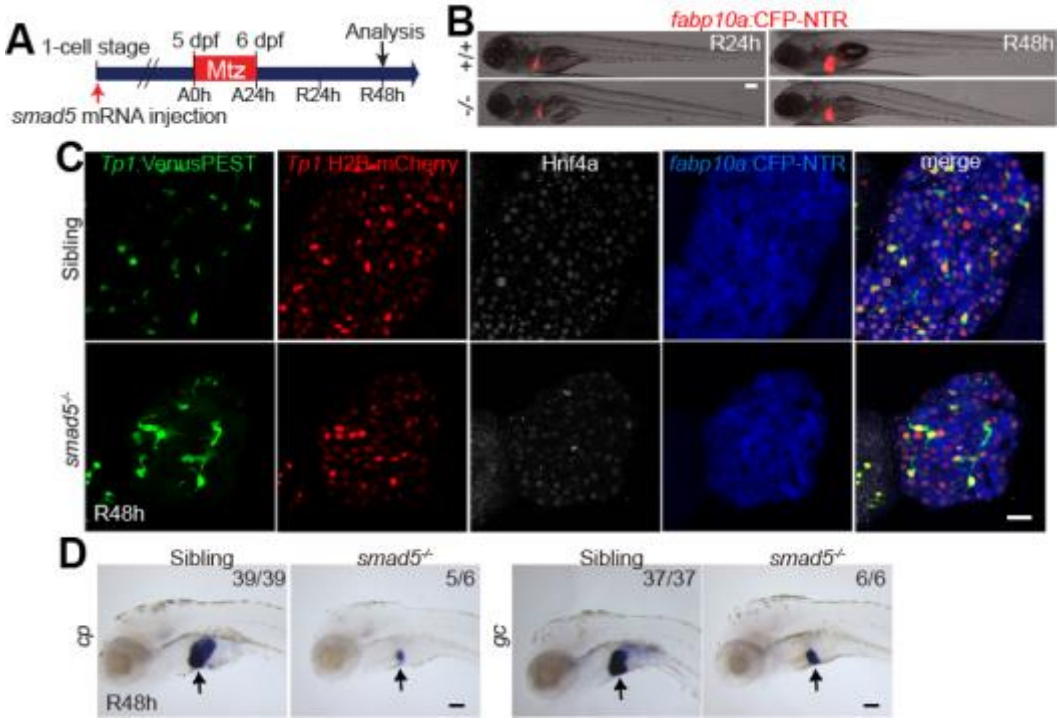

Figure 21: HB-LC differentiation defect observed in *smad5* mutants at R24h recovers at R48h

(A) Experimental scheme illustrating the stages of *smad5* mRNA injection and Mtz treatment and analysis for E-G. **(B)** Epifluorescence images showing *fabp10a:*CFP-NTR expression (red) in the regenerating livers of *smad5*$^{-/-}$ mutants and wild-type siblings at R24h and R48h. **(C)** Single-optical section images showing the expression of Hnf4a (gray), *Tp1:*H2B-mCherry (red), *Tp1:*VenusPEST (green), and *fabp10a:*CFP-NTR (blue) in the regenerating livers of *smad5*$^{-/-}$ mutants and wild-type siblings at R48h. **(D)** WISH images showing *cp* and *gc* expression in the regenerating livers (arrows) of *smad5*$^{-/-}$ mutants and wild-type siblings at R48h. Scale bars: 150 (B), 20 (C, D) μm.

3.2.6 *tbx2b* Mutants Exhibit a Defect in HB-LC Differentiation into Hepatocytes

TBX3, a T-box transcription factor, promotes hepatoblast proliferation and maintains the expression of HNF4A and CEBPA, two key transcription factors regulating hepatocyte differentiation, in hepatoblasts [274]. TBX2, a close homolog of TBX3, is required for the development of the heart, pharyngeal arch, and optic cup; importantly, its expression in these tissues is regulated by Bmp signaling [275]. Thus, to determine if *tbx2b* was required for BEC-driven liver regeneration, we used zebrafish *tbx2b* mutants because they develop with normal body morphology (Figure 22A) and survive long enough for our liver regeneration assay [276]. Despite the absence of liver developmental defects (Figure 22B), *tbx2b*$^{-/-}$ mutants exhibited a defect in HB-LC differentiation into hepatocytes during BEC-driven liver regeneration.

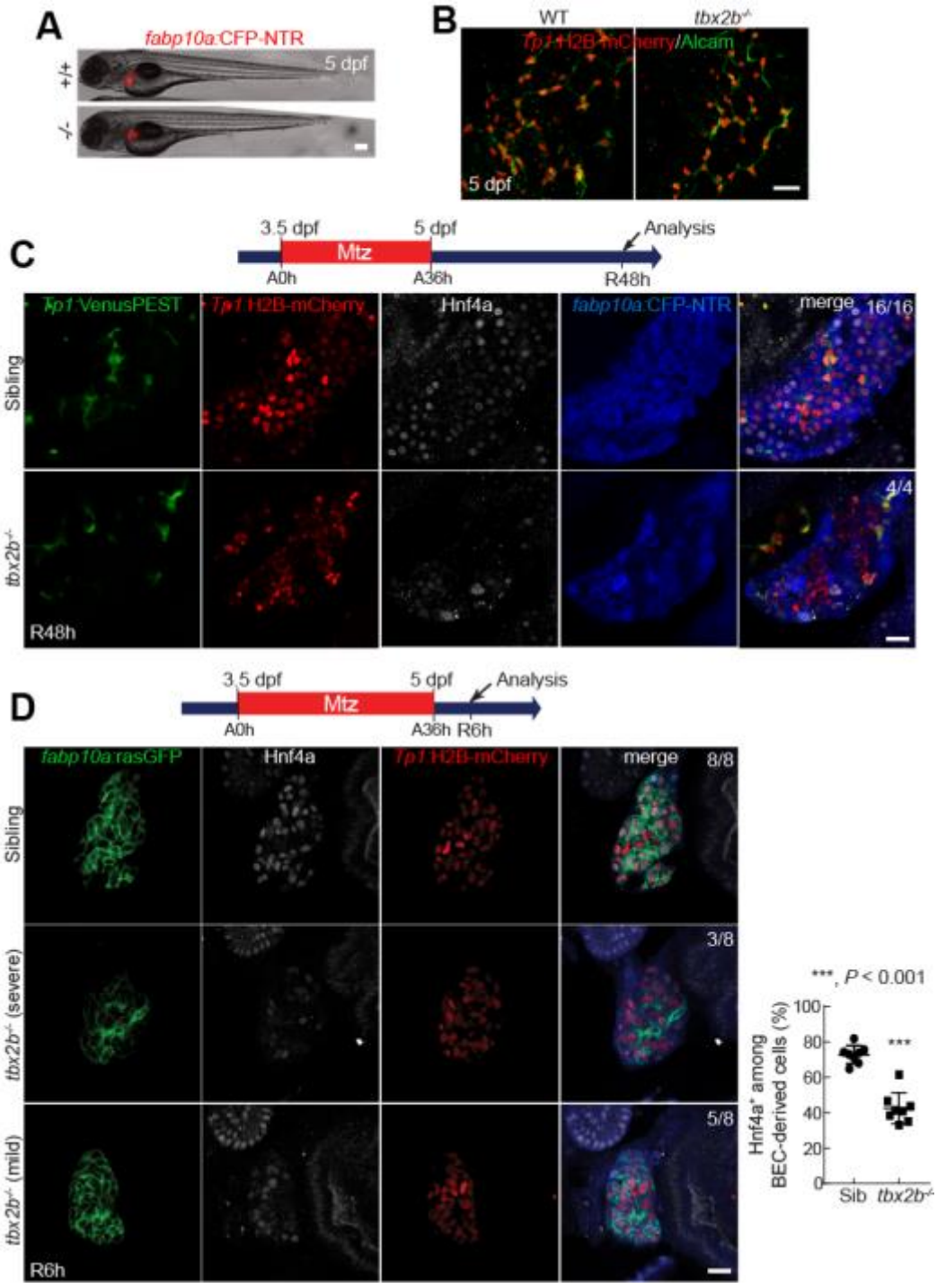

Figure 22: *tbx2b* mutants still exhibit a defect in HB-LC differentiation into hepatocytes at R48h

(A) Epifluorescence images showing hepatic *fabp10a:*CFP-NTR expression (red) in *tbx2b*$^{-/-}$ mutants and wild-type siblings at 5 dpf. **(B)** Confocal projection images showing Alcam (green) and *Tp1:*H2B-mCherry (red) expression in the uninjured liver of *tbx2b*$^{-/-}$ mutants and wild-type siblings at 5 dpf. **(C)**

Single-optical section images showing the expression of *Tp1:*VenusPEST (green), *Tp1:*H2B-mCherry (red), *fabp10a:*CFP-NTR (blue), and Hnf4a (gray) in the regenerating livers of *tbx2b*$^{-/-}$ mutants and their siblings at R48h. **(D)** Single-optical section images showing the expression of *fabp10a:*rasGFP (green), *Tp1:*H2B-mCherry (red), and Hnf4a (gray) in the regenerating livers of *tbx2b*$^{-/-}$ mutants and their siblings at R6h. Quantification of the percentage of Hnf4a^{+} cells among H2B-mCherry^{+} BEC-derived cells is shown. Numbers in the upper right corner indicate the proportion of larvae exhibiting the representative phenotype shown. Scale bars: 150 (A), 20 (B-D) μm.

In control regenerating livers, all *Tp1:*VenusPEST^{-}/*Tp1*:H2B-mCherry^{+} cells expressed Hnf4a and Bhmt at R24h, indicating that they are hepatocytes derived from BECs. However, in *tbx2b*$^{-/-}$ regenerating livers, many *Tp1:*VenusPEST^{-}/Tp1:H2B-mCherry^{+} cells not only failed to express Hnf4a and Bhmt (Figures 23A-23C), but also showed sustained Alcam expression at R24h (Figure 23D). This phenotype was severe in ~40% of the mutants, having few Bhmt^{+} hepatocytes, but mild in the rest of them, having a significant number of the hepatocytes (Figures 23B-23D). To determine whether the observed phenotype at R24h later recovered, we examined regenerating livers at R48h. All mutants at R48h still contained a significant number of *Tp1:*VenusPEST^{-}/Tp1:H2B-mCherry^{+} cells negative for Hnf4a (Figure 22C), suggesting that in the absence of Tbx2b, BEC-derived cells that failed to differentiate into hepatocytes at R24h do not recover at a later time point. We next examined if BEC dedifferentiation was affected in *tbx2b*$^{-/-}$ mutants. Although Hnf4a expression in regenerating livers at R6h was reduced in the mutants compared with their siblings, *fabp10a:*rasGFP expression appeared to be unaffected in the mutants (Figure 22D), suggesting that BECs normally dedifferentiate into HB-LCs in the absence of Tbx2b. Altogether, data from *tbx2b* mutant analyses indicate the crucial role of *tbx2b* in BEC-driven liver regeneration, in particular, HB-LC differentiation into hepatocytes.

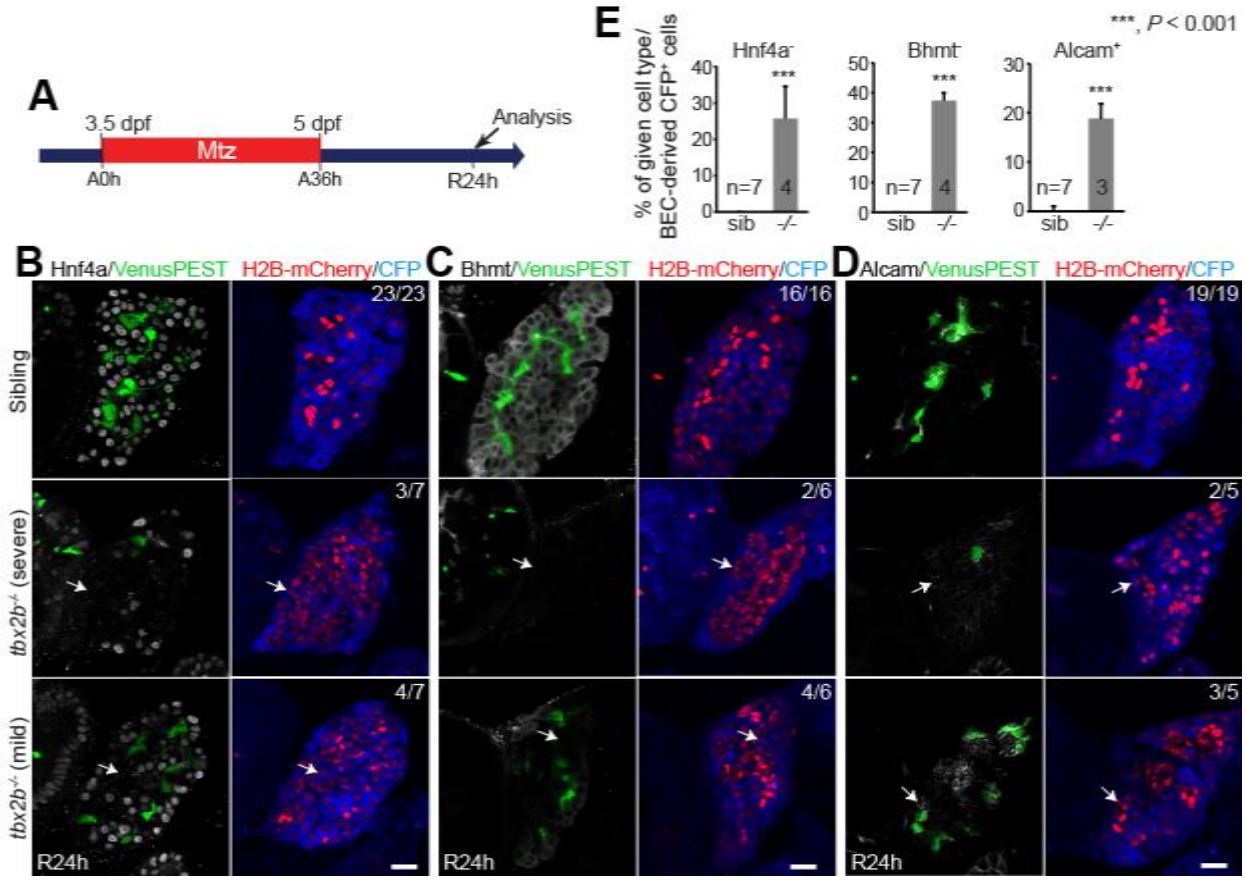

Figure 23: *tbx2b* mutants exhibit a defect in HB-LC differentiation into hepatocytes

(A) Experimental scheme illustrating the stage of Mtz treatment and analysis. **(B-D)** Single-optical section images showing the expression of *fabp10a:*CFP-NTR, *Tp1:*VenusPEST, *Tp1:*H2B-mCherry, and Hnf4a (B), Bhmt (C) or Alcam (D) in regenerating livers. **(E)** Quantification of the percentage of Hnf4a^{-}, Bhmt^{-}, or Alcam^{+} cells (arrows) among CFP-NTR^{+}/H2B-mCherry^{+} cells as shown in B-D. The mild cases were used for quantification. Scale bars: 20 μm; error bars: ±SEM.

3.2.7 *id2a* Mutants Temporarily Display an Excess of BECs in Regenerating Livers

Id2 is a well-known downstream target gene of Bmp signaling in many tissues, including pancreatic epithelia [226]; the mouse *Id2* promoter contains BMP-responsive elements [277]. *id2a*, the zebrafish orthologue of mouse *Id2*, is also regulated by Bmp signaling in cranial neural

crest cells [278]. Not only are *Id2* and *id2a* the direct targets of Bmp signaling, but they also mediate the effect of Bmp signaling in these tissues. Given its BEC-specific expression in the developing liver [279] and its regulation by Bmp signaling in regenerating livers (Figure 20A), we hypothesized that *id2a* served as a mediator of Bmp signaling in BEC-driven liver regeneration. Using transcription activator-like effector nuclease (TALEN) genome editing technology, we generated *id2a* mutants containing a 22-bp deletion in its first exon. The mutant larvae did not exhibit any liver developmental defects (Figures 24A and 24B) and grew normally to adults.

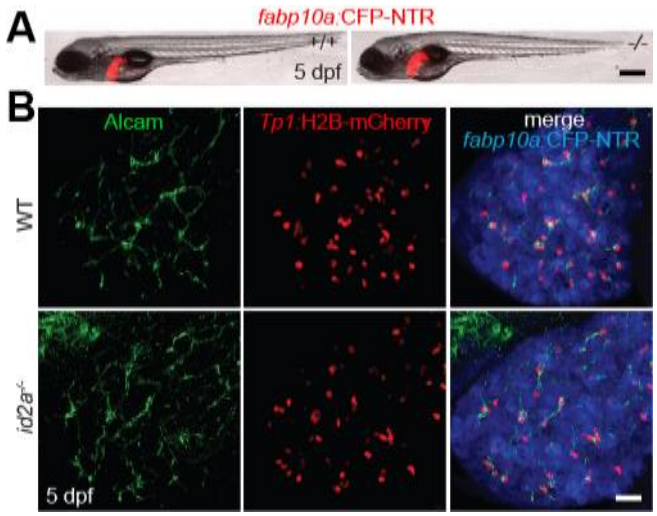

Figure 24: Liver development and BEC number are unaffected in *id2a* mutants

(A) Epifluorescence images showing *fabp10a:*CFP-NTR expression (red) in the uninjured livers of *id2a*$^{-/-}$ mutants and wild-type siblings at 5 dpf. **(B)** Confocal projection images showing the expression of *fabp10a:*CFP-NTR (blue), Alcam (green), and *Tp1:*H2B-mCherry (red) in the uninjured livers of *id2a*$^{-/-}$ mutants and wild-type siblings at 5 dpf. Scale bars: 300 (A), 20 (B) µm.

BEC-driven liver regeneration appeared to occur normally in *id2a*$^{-/-}$ mutants, as assessed by Hnf4a expression at R6h (Figure 25B) and *gc* expression at R24h (Figure 25C); however, the mutant regenerating livers had significantly more BECs than controls at R30h (Figure 25D),

resembling the excessive BEC phenotype seen in regenerating livers treated with DMH1 from R0h. This increased BEC number was due to increased proliferation, as revealed by EdU labeling (Figure 25E). However, this BEC phenotype was temporary because there was no difference in BEC number between wild-type and *id2a*$^{-/-}$ mutant regenerating livers at R72h (Figure 25F). Altogether, data from *id2a* mutant analyses suggest that *id2a* mediates, in part, the effect of Bmp signaling on BEC proliferation during BEC-driven liver regeneration.

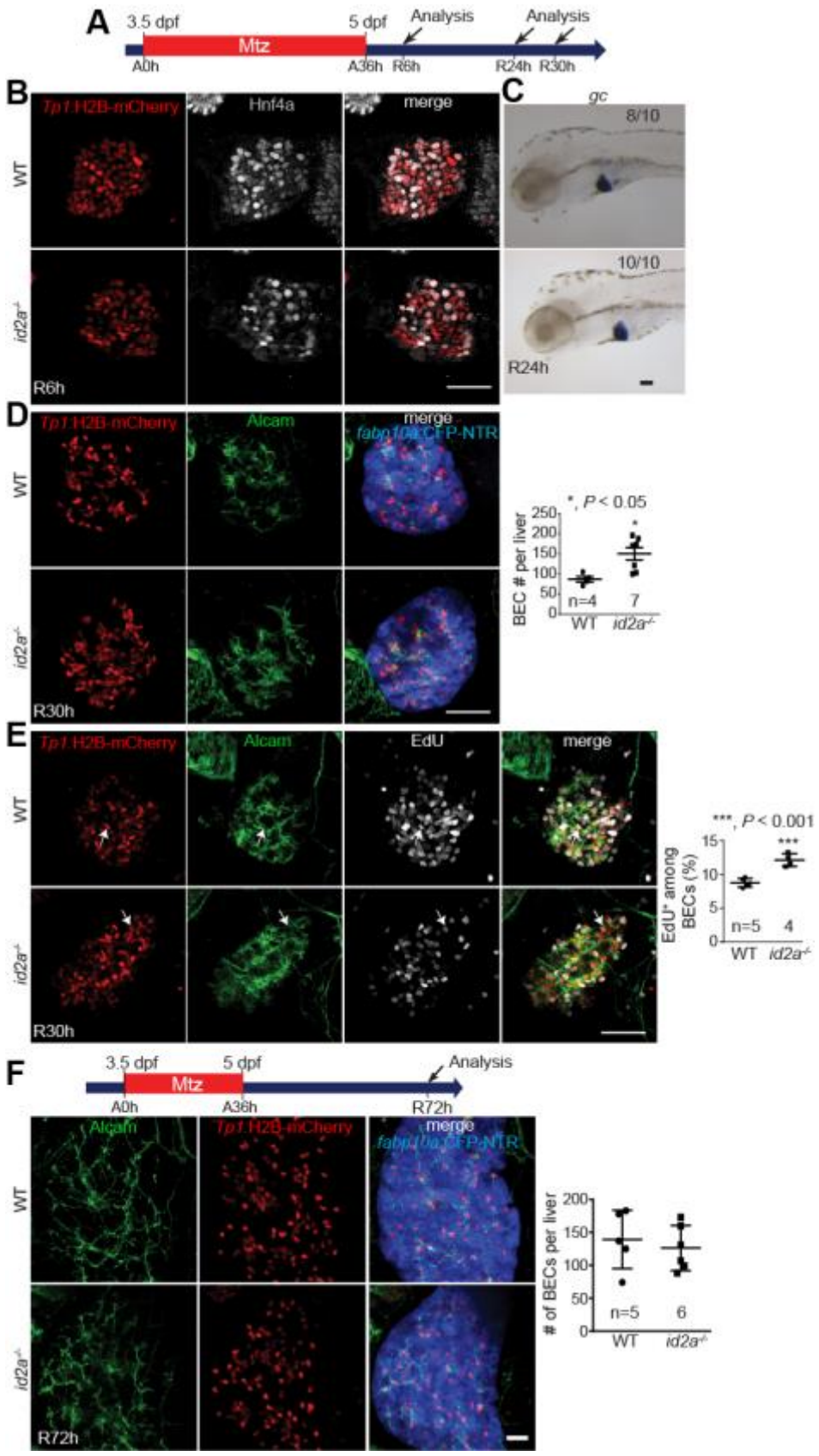
A
3.5 dpf
Mtz
5 dpf
Analysis
Analysis
A0h
A36h
R6h
R24h
R30h
B
Tp1:H2B-mCherry
Hnf4a
merge
WT
id2a-/-
R6h
C
gc
8/10
10/10
R24h
D
Tp1:H2B-mCherry
Alcam
merge
fabp10a:CFP-NTR
WT
id2a-/-
R30h
*, P < 0.05
BEC # per liver
250
200
150
100
50
0
n=4
7
WT
id2a-/-
E
Tp1:H2B-mCherry
Alcam
EdU
merge
WT
id2a-/-
R30h
***, P < 0.001
EdU+ among BECs (%)
15
10
5
0
***
n=5
4
WT
id2a-/-
F
3.5 dpf
Mtz
5 dpf
Analysis
A0h
A36h
R72h
Alcam
Tp1:H2B-mCherry
merge
fabp10a:CFP-NTR
WT
id2a-/-
R72h
# of BECs per liver
200
150
100
50
0
n=5
6
WT
id2a-/-

Figure 25: *id2a* mutants have excessive BECs in regenerating livers at R30 but recover by R72h

(A) Experimental scheme illustrating the stages of Mtz treatment and analysis. **(B)** Single-optical section images showing Hnf4a and *Tp1:*H2B-mCherry expression in regenerating livers. **(C)** WISH images showing *gc* expression in regenerating livers. **(D)** Confocal projection images showing the expression of Alcam, *Tp1:*H2B-mCherry, and *fabp10a:*CFP-NTR in regenerating livers. Quantification of the total numbers of BECs ($Alcam^+/H2B\text{-}mCherry^+$) per liver. **(E)** Confocal projection images showing EdU labeling and Alcam and *Tp1:*H2B-mCherry expression in regenerating livers. EdU was treated from R24h for 6 hours. Arrows point to EdU^+ BECs. Quantification of the percentage of EdU^+ cells among BECs. **(F)** Confocal projection images showing the expression of Alcam (green), *Tp1:*H2B-mCherry (red), and *fabp10a:*CFP-NTR (blue) in the regenerating livers of $id2a^{-/-}$ mutants and wild-type siblings at R72h. Quantification of the total numbers of BECs ($Alcam^+/H2B\text{-}mCherry^+$) per liver is shown. Scale bars: 50 (B, C, D, E), 20 (F) μm; error bars: ±SEM.

3.2.8 BMP2 Addition Promotes the Differentiation of a Murine Liver Progenitor Cell Line into Hepatocytes *in vitro*

To explore whether the findings from the zebrafish liver injury model can be translated to mammals, we used a murine liver progenitor cell line that was established from DDC-diet fed mice [116]. These cells can efficiently differentiate into either hepatocytes or BECs depending on culture conditions [116]. In the hepatocyte differentiation condition, addition of BMP2 significantly increased the expression of three hepatocyte markers, *G6pc*, *Tat* and *Tdo2* (Figure 26), consistent with findings from the zebrafish studies.

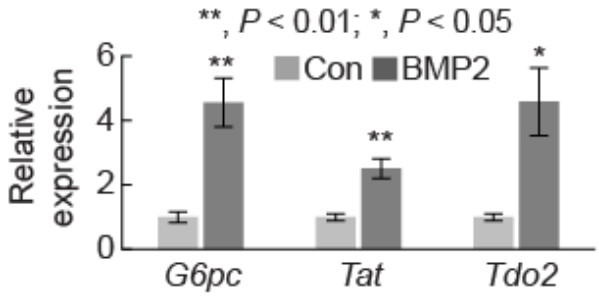

Figure 26: BMP2 treatment promotes the differentiation of a murine liver progenitor cell line into hepatocytes in vitro

qPCR data showing the relative expression levels of *G6pc, Tat,* and *Tdo2* between control and BMP2 treatment (n=4). Error bars: ±SEM.

3.3 METHODS

3.3.1 Zebrafish Lines

Experiments were performed with approval of the Institutional Animal Care and Use Committee at the University of Pittsburgh. We used *smad5*^{m169}, *tbx2b*^{c144}, and *id2a*^{pt661} mutant and the following transgenic lines: *Tg(fabp10a:rasGFP)*^{s942}, *Tg(Tp1:VenusPEST)*^{s940}, *Tg(Tp1:H2B-mCherry)*^{s939}, *Tg(ubb:loxP-EGFP-loxP-mCherry)*^{cz1701}, *Tg(Tp1:CreERT2)*^{s959}, *Tg(fabp10a:CFP-NTR)*^{s931}, *Tg(hs:dnBmpr1)*^{w30}, *Tg(fabp10a:CreERT2)*^{pt602}, *Tg(WRE:d2GFP)*^{kyu1}, and *Tg(Tp1:mAGFP-gmnn)*^{s707}. Their full names and references are listed in Table 1 (see Appendix A).

3.3.2 Hepatocyte Ablation and Chemical Treatment

Hepatocyte ablation was performed by treating *Tg(fabp10a:CFP-NTR)* larvae with 10 mM Mtz in egg water supplemented with 0.2% DMSO and 0.2 mM 1-phenyl-2-thiourea, as previously described [149]. To suppress Bmp signaling and Notch signaling, 10 μM DMH1 (Tocris, Bristol, UK) and 5 μM LY411575 (Cayman Chemical, Ann Arbor, MI), respectively, were prepared in 100% DMSO.

3.3.3 RNAseq Analysis

Over 100 livers were manually dissected for each condition (three non-ablating controls at 4.25, 5.25, and 6 days post-fertilization (dpf) and four regenerating livers at A18h, R6h, R12h, and R24h); total RNA was extracted from the dissected livers using the RNeasy Mini Kit (Qiagen, Valencia, CA). This RNA preparation was repeated three times and three-replicate RNA samples were mixed. These mixed samples were processed for single-end deep-transcriptome sequencing using the Illumina HiSeq 2000 platform, of which service was provided from Tufts University Core Facility. Galaxy was used to analyze the sequencing reads.

3.3.4 Generation of *Tg(Tp1:mAGFP-gmnn)* and *id2a* Mutant Lines

The *Tp1:mAGFP-gmnn* construct was generated by first replacing the *EF1* promoter in the *pT2KXIGΔin* vector [280] with the *Tp1* module (multiple RBP-Jκ-binding sites in front of a minimal promoter) and then placing *mAGFP-gmnn* [281] downstream of the *Tp1* element and a 5' beta-globin intron. The final construct together with *Tol2* mRNA was injected into one-cell stage

embryos as previously described [282]. The left (TAL3100, Plasmid #41274) and the right (TAL3101, Plasmid #41275) TALEN constructs of *id2a* were obtained from Addgene. The *id2a* target sequences are in the first exon, upstream of the helix-loop-helix domain; the spacer region contains a *TfiI* restriction enzyme site. After linearization with *SmaI* digestion, the TALEN mRNA was synthesized using the Ambion mMESSAGE mMACHINE T7 Ultra Transcription Kit (Thermo Fischer Scientific, Waltham, MA). *id2a* TALEN mRNAs were mixed at a 1:1 ratio to a final concentration of 200 ng/ul and subsequently injected into one-cell-stage embryos. Either the adult zebrafish' tail fin or whole embryo at 1-2 dpf was used to obtain genomic DNA for PCR-mediated genotyping. PCR products were sequenced to identify a frameshift mutation. F1 fish containing a 22-bp deletion was selected to establish the *id2a* mutant line.

3.3.5 Generation of *tbx2b*, *smad5* and *id2a* Mutants

For *id2a* genotyping, genomic DNA was amplified with the forward (5'-TCCTGCTGTCAACATGAAGGCA -3') and reverse (5'-AGTCGAGCGCGATCTGCAGG-3') primers, followed by digestion with *TfiI*. The wild-type allele generates two bands of 179 and 87 bp, whereas the *id2a* mutant allele generates a band of 244 bp. *tbx2b* [276] and *smad5* [273] genotyping were performed as previously described.

3.3.6 Heat-shock Condition

Tg(hs:dnBmpr1) larvae were heat-shocked at A30h or R8h by transferring them into egg water pre-warmed to 39°C and kept at this temperature for 20 minutes as previously described [70].

3.3.7 Cre/loxP-mediated Lineage Tracing

Fish carrying the *Tp1:CreERT2* or *fabp10a:CreERT2* transgene were crossed to the reporter line, *Tg(ubb:loxP-GFP-loxP-mCherry)*. Larvae from the crosses were treated with Mtz from 3.5 to 5 dpf and additionally treated with both 5 μM 4-OHT and 10 μM DMH1 (Tocris, Bristol, UK) from A33h to R6h for 9 hours. At R54h, 48 hours after 4-OHT and DMH1 washout, the larvae were harvested and processed for immunostaining to reveal lineage-traced mCherry^{+} cells as previously described [20].

3.3.8 EdU Labeling

EdU labeling was performed according to the protocol outlined in the Click-iT EdU Alexa Fluor 647 Imaging Kit (Life Technologies, Grand Island, NY). Larvae were treated with egg water containing 10 mM EdU and 5% DMSO. After a 6-hour EdU treatment, the larvae were harvested for subsequent analysis.

3.3.9 Whole-mount *In Situ* Hybridization (WISH) and Immunostaining

WISH was performed as previously described [242]. cDNA from livers at 5 dpf or R6h was used as a template for PCR to amplify genes-of-interest; PCR products were used to make in situ probes. The primers used for the probe synthesis are listed in Table 2 (see Appendix A). Whole-mount immunostaining was performed as previously described [149], using the following antibodies: rabbit anti-Prox1 (GTX128354, GeneTex, Irvine, CA), goat anti-Hnf4a (Santa Cruz, Dallas, TX), chicken anti-GFP (Aves Labs, Tigard, OR), mouse anti-Bhmt (1:500; a gift from J. Peng, Zhejiang

University, China), mouse anti-Alcam (ZIRC, Eugene, OR), rat anti-mCherry (Allele Biotechnology, San Diego, CA), and Alexa Fluor 488-, 568-, and 647-conjugated secondary antibodies (Life Technologies, Grand Island, NY).

3.3.10 Quantitative RT-PCR (qPCR)

Total RNA was extracted from 100 dissected livers using the RNeasy Mini Kit (Qiagen, Valencia, CA); cDNA was synthesized from the RNA using the SuperScript® III First-Strand Synthesis SuperMix (Life Technologies, Grand Island, NY) according to the kit protocols. qPCR was performed as previously described [283], using the Bio-Rad iQ5 qPCR machine with the iQ™ SYBR Green Supermix (Bio-Rad, Hercules, CA). *eef1b2* was used for normalization. At least three independent experiments were performed. The primers used for qPCR are listed in Table 3.

3.3.11 Mouse LPC Cell Line and Culture Condition

The LPC cell line, HSCE1, used in this study was established and maintained as described previously [284]. For their differentiation into hepatocytes, HSCE1 cells were cultured in the presence of 1% DMSO and 20 ng/mL mouse Oncostatin M with or without 500 ng/mL recombinant human BMP2 (Peprotech, Rocky Hill, NJ) (n = 4). After 5 days of hepatocyte induction, the cultured cells were harvested for RNA preparation. HSCE1 cells before the induction were used as a negative control. TRIzol reagent (Invitrogen, Carlsbad, CA) was used to extract total RNA; PrimeScript RT reagent kit (Takara, Shiga, Japan) was used to synthesize cDNA, according to the kit protocols. qPCR was conducted with a LightCycler 480 system and Universal Probe Library (Roche Diagnostics, Indianapolis, IN). The Universal Probe Library

Mouse *Actb* Gene Assay was used for normalization. The primers used for qPCR are listed in Table 3.

3.3.12 Image Acquisition, Processing and Statistical Analysis

Zeiss LSM700 confocal and Leica M205 FA epifluorescence microscopes were used to obtain image data. Confocal stacks were analyzed using the Zen 2009 software. All Figures, labels, arrows, scale bars, and outlines were assembled or drawn using the Adobe Illustrator software. Unpaired two-tailed Student's t-test was used for statistical analysis; $P<0.05$ was considered statistically significant. Quantitative data were shown as means ±SEM.

3.4 DISCUSSION

Using the zebrafish hepatocyte ablation model, we elucidate two distinct roles of Bmp signaling in BEC-driven liver regeneration: (1) initially, Bmp signaling regulates HB-LC differentiation into hepatocytes; (2) later, Bmp signaling controls the proliferation of newly-generated BECs. By analyzing the mutants of *smad5*, *tbx2b*, and *id2a*, genes involved in the Bmp signaling pathway, we discovered that Smad5 is the main receptor-regulated Smad during BEC-driven liver regeneration and that Tbx2b and Id2a mediate its effect on HB-LC differentiation into hepatocytes and on BEC proliferation, respectively. In addition, no difference in cell apoptosis was observed between DMSO- or DMH1-treated regenerating livers (Figure 27).

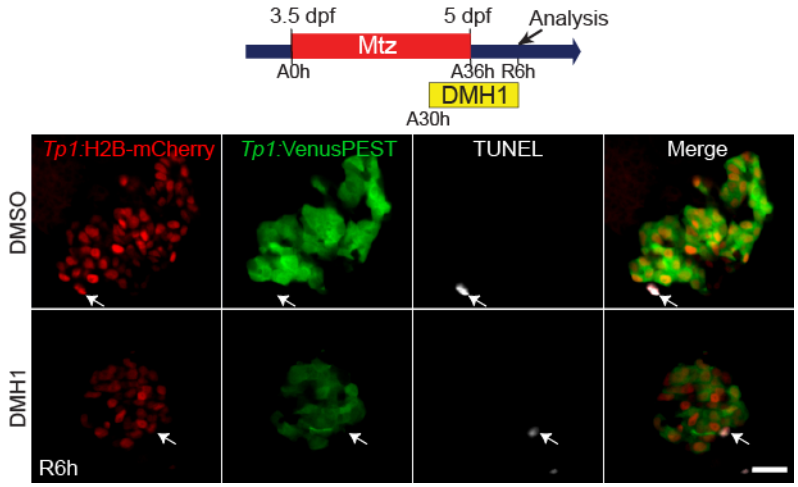

Figure 27: Inhibition of Bmp signaling does not affect cell death in regenerating livers at R6h

Single-optical section images showing *Tp1:*H2B-mCherry (red), *Tp1*:VenusPEST (green) expression and TUNEL^{+} cells (gray) in DMSO- and DMH1-treated regenerating livers at R6h. Arrows point to cells positive for both TUNEL and H2B-mCherry. Scale bar: 20 μm.

Bmp [70, 76], Fgf [69, 70], and Wnt/β-catenin signaling [28] are implicated in hepatoblast specification and proliferation during liver development. Given that regeneration often recapitulates development and key developmental factors are re-utilized during regeneration, these signaling pathways may also regulate liver regeneration. During hepatocyte-driven liver regeneration, both Wnt/β-catenin [285] and Fgf signaling [286] promote hepatocyte proliferation. During BEC-driven liver regeneration, Wnt/β-catenin signaling promotes oval cell proliferation [287] and Fgf signaling induces oval cell activation [139]. In contrast to Wnt/β-catenin and Fgf signaling, the influence of Bmp signaling on hepatocyte proliferation during hepatocyte-driven liver regeneration is ligand-dependent: BMP4 signaling through Alk3 represses hepatocyte proliferation, whereas BMP7 signaling through Alk2 promotes hepatocyte proliferation [169]. Previous *in vitro* studies have reported on the role of BMP signaling in the differentiation of LPCs into hepatocytes: BMP4 treatment induced the differentiation of rat

hepatic progenitor cells [288] and CD133^{+} hepatic cancer stem cells [289] into hepatocytes. Our *in vitro* and *in vivo* data support these findings and further reveal the crucial role of Bmp signaling in BEC-driven liver regeneration, specifically during the differentiation phase of LPCs into hepatocytes.

To further elucidate the mechanisms by which Bmp signaling controls BEC-driven liver regeneration, we analyzed *tbx2b* and *id2a* mutants. Our RNAseq data revealed that at R6h, both *tbx2b* (among the T-box transcription factor genes) and *id2a* (among the Id family genes) were highly upregulated in regenerating livers compared with the other *tbx* and *id* genes (Figure 28A and 28B), suggesting their importance in BEC-driven liver regeneration. As expected, both *tbx2b* and *id2a* expression decreased in both DMH1-treated and *smad5*$^{-/-}$ regenerating livers. Importantly, *tbx2b*$^{-/-}$ mutants exhibited a defect in HB-LC differentiation into hepatocytes and *id2a* mutants exhibited excessive BECs in regenerating livers at R30h, revealing *tbx2b* and *id2a* as the key downstream mediators of Bmp signaling that regulates BEC-driven liver regeneration.

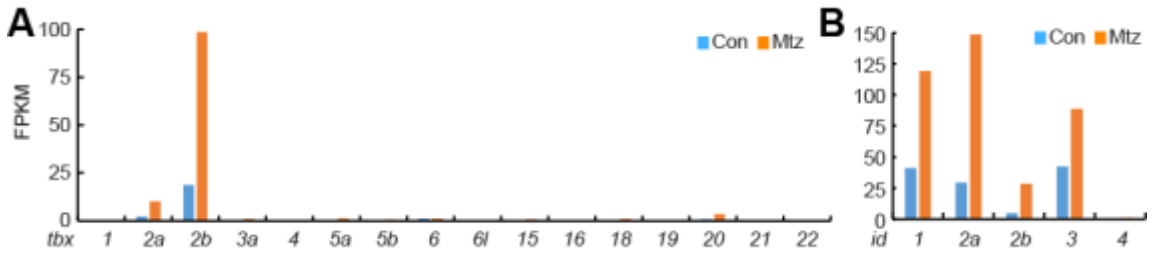

Figure 28: Expression levels of *tbx* and *id* genes in regenerating livers at R6h

(A, B) Graphs showing the expression levels of 16 *tbx* (A) and 5 *id* (B) genes in control and regenerating livers at R6h. FPKM stands for fragments per kilobase of exon per million fragments mapped.

Using a morpholino-mediated knockdown approach, we previously reported that during liver development, Id2a positively regulates hepatic outgrowth through hepatoblast proliferation and survival [279]. However, we found that during BEC-driven liver regeneration, Id2a

negatively regulates the proliferation of newly-generated BECs. Although we did not detect any developmental defects in the *id2a*$^{-/-}$ mutants, inconsistent with the morpholino results, this discrepancy might be explained by the genetic compensations that can occur in mutants but not in morphants [290]. Previous rodent studies have highlighted the role of *Id1* and *Id2* in hepatocyte-driven liver regeneration. Following partial hepatectomy, not only *Id1* was upregulated in liver sinusoidal endothelial cells (LSECs), but *Id1*$^{-/-}$ mice displayed abnormal liver function and impaired liver regeneration [291]. In fact, following acute liver injury, *Id1* was induced downstream of LSEC-specific upregulation of CXCR4/CXCR7 [292]. As a result, ID1 promotes the secretion of pro-regenerative angiocrine factors, such as Wnt2 and HGF, to aid in hepatocyte proliferation after liver injury [291, 292]. Similar to *Id1*, *Id2* levels also increased after partial hepatectomy and bile duct ligation in rats [259], but its role in liver regeneration has not yet been reported.

While Wnt/β-catenin signaling promotes LPC differentiation into hepatocytes, Notch signaling represses the process [141, 293]. Here, we presented Bmp signaling as another regulator of this differentiation process. Since we did not observe any changes in Wnt activity between DMSO- and DMH1-treated regenerating livers (Figure 29), it appears that Bmp signaling does not affect Wnt/β-catenin signaling.

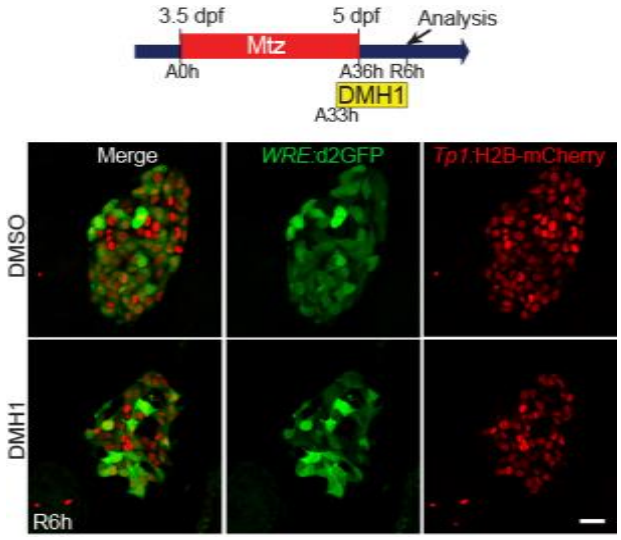

Figure 29: Inhibition of Bmp signaling does not affect Wnt activity in regenerating livers at R6h

Single-optical section images showing *WRE:*d2GFP (green) and *Tp1:*H2B-mCherry (red) expression in regenerating livers at R6h. The Wnt reporter line, *Tg(WRE:d2GFP)*, was used to reveal hepatic Wnt activity. Scale bar: 20 µm.

However, sustained, weak Notch activity observed in DMH1-treated regenerating livers suggests that Bmp signaling may suppress Notch signaling. Although it was reported that repression of Notch signaling promotes LPC differentiation into hepatocytes [141, 293], the hepatocyte differentiation defects observed in DMH1-treated livers were not rescued by inhibiting Notch signaling globally (Figure 30). Thus, it is unlikely that Bmp signaling controls LPC differentiation through Wnt/β-catenin or Notch signaling. However, we do not exclude the possibility that Wnt/β-catenin and Notch signaling control LPC differentiation through Bmp signaling.

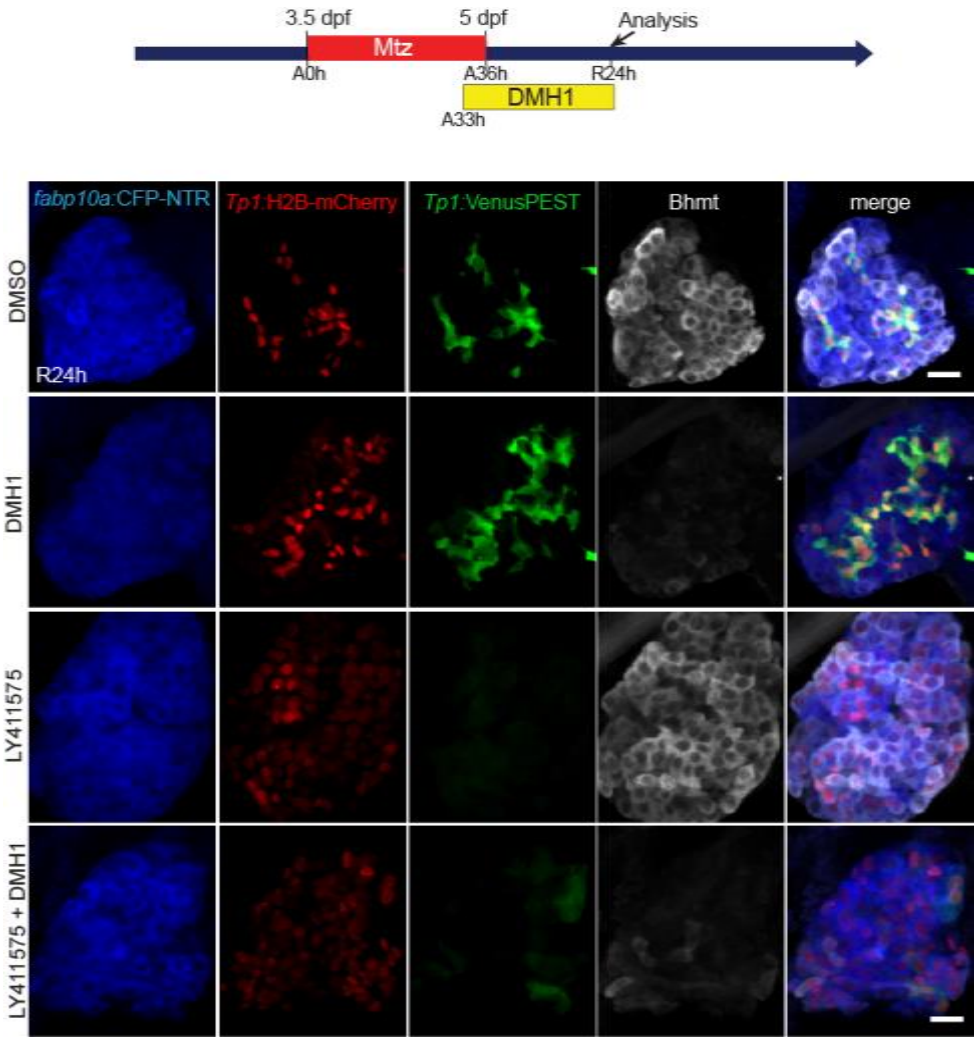

Figure 30: Hepatocyte differentiation defect observed in DMH1-treated larvae is not rescued by the global inhibition of Notch signaling

Confocal projection images showing the expression of *fabp10a:*CFP-NTR (blue), *Tp1:*H2B-mCherry (red), *Tp1:*VenusPEST (green) and Bhmt (gray) in regenerating livers treated with DMSO, DMH1, LY411575 (Notch inhibitor) and DMH1+LY411575 at R24h. Scale bar: 20 µm.

The zebrafish hepatocyte ablation model has contributed significantly to a better understanding of BEC- or LPC-driven liver regeneration. We previously reported that Wnt/β-catenin signaling via Wnt2bb regulates the proliferation of newly-generated hepatocytes [20] and that BET proteins regulate BEC dedifferentiation and the proliferation and maturation of newly-

generated hepatocytes [266]. Using the same model, others also reported on the involvement of Notch signaling in BEC-driven liver regeneration [294]. Here, we provide the gene expression profiles of regenerating livers at four distinct stages, A18h, R6h, R12h, and R24h. Although we focus on Bmp signaling and its downstream target genes in this study, these expression profiles will be useful for identifying other crucial genes involved in regulating BEC-driven liver regeneration.

In summary, we discovered that Bmp signaling regulates HB-LC differentiation into hepatocytes, partly, via Tbx2b and controls the proliferation of newly-generated BECs via Id2a. Liver biopsies of human patients suffering from chronic liver diseases display an abundance of oval cells, also known as HB-LCs. To promote the differentiation of these oval cells into hepatocytes in these patients, one possible therapy may involve enhancing hepatic Bmp signaling.

3.5 ACKNOWLEDGEMENTS

This chapter was adapted and modified from the following submitted work:
Choi T.Y., Khaliq M.K., Tsurusaki S., Ninov N., Stainier D.Y.R., Tanaka M., and Shin D. (In Revision) Bmp Signaling Governs Biliary-driven Liver Regeneration in Zebrafish via Tbx2b and Id2a.

We thank the Joung and Peterson labs for *id2a* TALEN constructs, which were created as part of an effort funded by an NIH grant (GM088040). We also thank Joshua Gamse for *tbx2b* and Mary Mullins for *smad5* mutant fish, and Neil Hukriede and Michael Tsang for discussions. The work was supported by grants from the NIH to D.S. (DK101426) and D.Y.R.S. (DK60322), from the

Packard foundation to D.Y.R.S., from the NIH to M.K. (F31DK105714-03), and from the Japan Society for the Promotion of Science to M.T. (2611007).

4.0 STAT3 SIGNALING REGUALTES BILIARY-DRIVEN LIVER REGENERAITON IN ZEBRAFISH

4.1 BACKGROUND

With the story of an eagle picking at Prometheus' liver daily, the Ancient Greeks first eluded to the remarkable ability of the liver to regenerate. To date, no true stem cell population has been identified in the liver. Instead, extensive studies have revealed two main methods of liver regeneration depending on the severity of the liver injury: (1) hepatocyte-driven or (2) biliary epithelial cell (BEC)-driven. Typically following liver injury, hepatocytes proliferate to restore the lost liver mass [112, 295]. However, if hepatocyte proliferation is blocked, then the BECs undergo dedifferentiation into hepatoblast-like cells (HB-LCs), also termed liver progenitor cells (LPCs) [261]. LPCs are bipotent [116], facultative resident stem progenitor cells that express both hepatocyte and BEC markers and can differentiate into mature hepatocytes and BECs to restore the lost liver mass [116, 117, 131].

Moreover, LPCs observed in our zebrafish model of liver regeneration share similar characteristics with the BEC-derived oval cells or ductular reactions observed in both rodents and human severe acute or chronic liver injury conditions [132, 144, 149]. Currently, chronic liver disease and cirrhosis are the 12th leading cause of death in the United States [296]. Although liver transplantation offers an effective therapy, more than 50% of patients on the transplant waiting list never receive a donor liver transplant [2]. Due to this shortage, an essential step in treating liver disease and augmenting the innate regenerative process is understanding the underlying mediators

and mechanisms of LPC-driven liver regeneration, including LPC activation, proliferation and differentiation.

With that goal in mind, our lab and others have previously reported on a zebrafish model in which following complete hepatocyte ablation, BECs extensively contribute to hepatocyte regeneration [132, 149]. This phenomenon is not zebrafish exclusive, however, as the BEC-to-hepatocyte-mediated regeneration was similarly observed in a hepatocyte-specific $Mdm2^{-/-}$ mouse model of liver injury [131].

One of the hallmarks of a LPC activation is the infiltration of inflammatory cells, including macrophages and leukocytes, into the injured liver [136]. These inflammatory cells then secrete specific cytokines, which can contribute to LPC/oval cell activation and proliferation [297-300]. One mouse model of oval cell activation is the choline-deficient, ethionine-supplemented (CDE) diet; mice on a CDE diet display an increased release of cytokines, such as IL-6, after liver injury. Once IL-6 binds to its cognate receptor and co-receptor, gp130-associated Janus tyrosine kinases (JAKs) are autophosphorylated and subsequently activated. JAKs can then phosphorylate transcription factors, such as signal transducer and activator (STAT) 3, which dimerize and translocate to the nucleus to affect downstream target genes [301, 302].

Previous reports have highlighted the involvement of Stat3 in hepatocyte-driven and oval cell-mediated liver regeneration [303, 304]. In the partial hepatectomy model of liver injury, *Stat3* deficiency led to an increased mortality rate and decreased DNA synthesis. In the CDE-diet model of liver injury, *Stat3* was found to be upregulated in the oval cell population with high proliferative potential. In addition, mice with a hepatocyte-specific knock out of Suppressor of cytokine signaling 3 (Socs3), a negative regulator of STAT3, display STAT3 hyperactivation after PH, which results in enhanced proliferation during regeneration [208]. Given the involvement of *Stat3*

in hepatocyte survival and proliferation after liver injury, we hypothesized that Stat3 signaling may also influence zebrafish LPC-driven liver regeneration.

Here, using the zebrafish hepatocyte ablation liver injury model, we report on the role of Stat3 in LPC proliferation and differentiation into hepatocytes. We investigated the role of Stat3 in LPC-driven liver regeneration by two methods: (1) utilizing a JAK-specific inhibitor to block Stat3 activation downstream and (2) utilizing zebrafish Stat3 mutants generated by TALEN mutagenesis. Our findings show that Stat3 plays a role in LPC differentiation into hepatocytes by regulating LPC proliferation.

4.2 RESULTS

4.2.1 Stat3 Inhibition Results in A Decreased Liver Size during Liver Regeneration

We, and others, have previously characterized a zebrafish BEC-driven liver regeneration model where upon extensive hepatocyte ablation, BECs contribute to the repopulation of the liver [132, 149]. We utilized the *Tg(fap10a:CFP-NTR)* transgenic fish, which express the bacterial nitroreductase (NTR) enzyme fused with the cyan fluorescent protein (CFP) from the hepatocyte-specific, *fabp10a*, promoter [149]. Upon treatment of a nontoxic prodrug, metronidazole (Mtz), cells expressing NTR metabolize Mtz into a cytotoxic agent [147]. As a result, only hepatocytes expressing NTR will undergo near-complete, genetic-based ablation, causing BECs to actively contribute to the liver regeneration process through a well-defined mechanism. Initially, the BECs dedifferentiate into hepatoblast-like cells (HB-LCs), also termed liver progenitor cells (LPCs). Next, these LPCs differentiate into hepatocytes and BECs, concluding with the proliferation of the

newly-generated hepatocytes and BECs and the restoration of the liver mass. Using this model, we explored the implications of inflammatory signaling, specifically focusing on Stat3, in BEC-driven liver regeneration.

To induce hepatocyte ablation, *fabp10a*:CFP^{+} larvae were treated with Mtz from 3.5-5 days post fertilization (dpf). Following this 36-hour period (ablation; A36h), Mtz washout was considered as the initiation of regeneration (R0h). Based on our RNAseq analysis (unpublished data), we found *stat3* and its negative feedback regulator, *socs3a*, were upregulated in regenerating livers at R6h compared to non-ablated controls (Figure 31; also see Appendix B). To elucidate the role of Stat3 in BEC-driven liver regeneration, we utilized a JAK-specific kinase inhibitor, JSI-124, that blocks Stat3 activation. JSI-124 has previously been used in zebrafish to block Stat3 signaling [305, 306]. We assessed the effect of Stat3 inhibition on (1) liver size and morphology; (2) BEC dedifferentiation into LPCs; and (3) LPC proliferation and LPC-to-hepatocyte/BEC differentiation during BEC-driven liver regeneration.

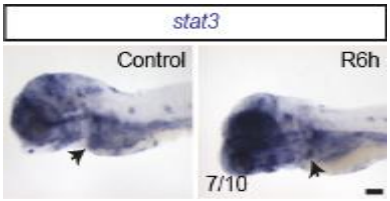

Figure 31: Expression of *stat3* is upregulated in regenerating livers during BEC-driven liver regeneration

WISH images showing *stat3* expression in control, non-ablated livers and Mtz-treated regenerating livers at R6h. At R6h, most of liver is composed of BEC-derived progenitor cells, termed LPCs. Numbers indicate the proportion of larvae exhibiting the representative expression shown. Arrows point to the liver. Scale bar: 100 µm.

To visualize the liver size in our regeneration setting, we utilized the *Tg(fabp10a:DsRed)* transgenic zebrafish larvae; these larvae express DsRed specifically in the hepatocytes. During the

Mtz treatment, Stat3 was inhibited from either A0h (at the start of Mtz treatment), A18h (to block Stat3 at time point when macrophages infiltrate into the injured liver and prior to BEC dedifferentiation) or R0h (to block Satat3 at later phases of liver regeneration, such as LPC proliferation and/or differentiation). Following Mtz washout, the liver size was examined at R24h and R48h. JSI-124 treatment significantly reduced the liver size at R24h from both the A0h and A18h treatment (Figure 32A-C). However, at R48h, only the A0h treatment resulted in a significant reduction of the liver size (Figure 32D-E).

Furthermore, we validated the effect of blocking Stat3 from A18h-R24h and A18h-R48h by using a different inhibitor, S3I-201, which blocks Stat3 dimerization and subsequent downstream translocation into the nucleus. Similar to the JSI-124 liver phenotype, S3I-201-treated larvae also exhibited a significantly smaller liver size at R24h during BEC-driven liver regeneration. Unlike JSI-124, however, continuous treatment of S3I-201 from A18h-R48h still caused a significant reduction of the liver size at R48h (Figure 32F-G). Altogether, these data suggest Stat3 signaling plays an important role in BEC-driven liver regeneration.

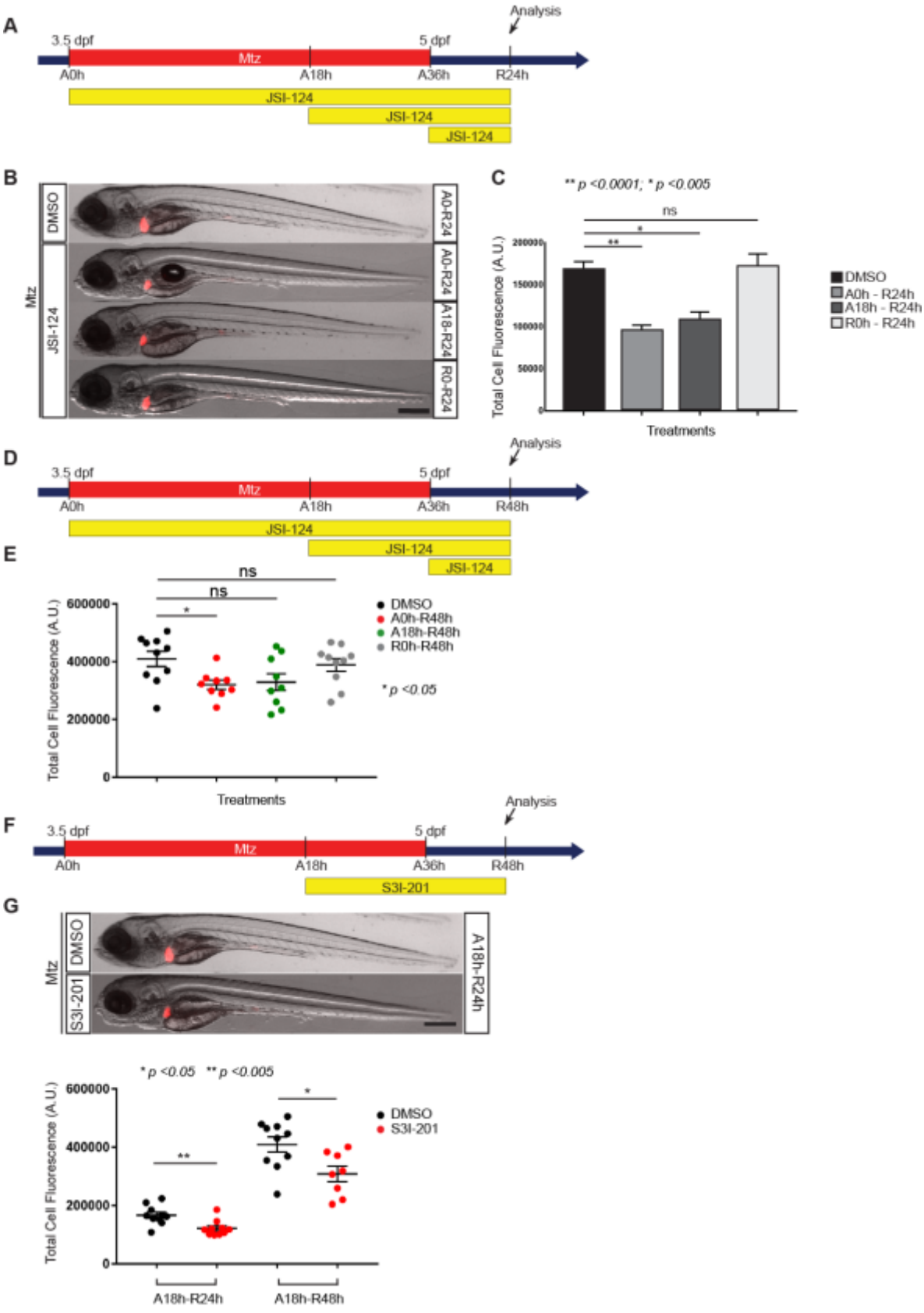
A
3.5 dpf
Mtz
5 dpf
Analysis
A0h
A18h
A36h
R24h
JSI-124
JSI-124
JSI-124
B
DMSO
JSI-124
Mtz
A0-R24
A0-R24
A18-R24
R0-R24
C
** p <0.0001; * p <0.005
ns
*
**
Total Cell Fluorescence (A.U.)
200000
150000
100000
50000
0
Treatments
DMSO
A0h - R24h
A18h - R24h
R0h - R24h
D
3.5 dpf
Mtz
5 dpf
Analysis
A0h
A18h
A36h
R48h
JSI-124
JSI-124
JSI-124
E
ns
ns
*
Total Cell Fluorescence (A.U.)
600000
400000
200000
0
Treatments
DMSO
A0h-R48h
A18h-R48h
R0h-R48h
* p <0.05
F
3.5 dpf
Mtz
5 dpf
Analysis
A0h
A18h
A36h
R48h
S3I-201
G
Mtz
DMSO
S3I-201
A18h-R24h
* p <0.05 ** p <0.005
*
**
Total Cell Fluorescence (A.U.)
600000
400000
200000
0
DMSO
S3I-201
A18h-R24h
A18h-R48h

Figure 32: Stat3 inhibition decreases size of regenerating livers during BEC-driven liver regeneration

(A) Scheme illustrating the Mtz treatment period (A, ablation), JSI-124 treatment and liver regeneration (R, regeneration). Arrows indicate analysis stages at R24h. **(B)** Epifluorescence images showing *fabp10a*:DsRed in the regenerating livers treated with DMSO or JSI-124 at the indicated time points. **(C)** Quantification of *fabp10a*:DsRed expression and area of the regenerating livers treated with JSI-124 at three different time points, from A0h-R24h, A18h-R24h and R0h-R24h. Total cell fluorescence (AU: arbitrary units) considers both area of the liver and fluorescence intensity. **(D)** Scheme illustrating the Mtz treatment period (A, ablation), JSI-124 treatment and liver regeneration (R, regeneration). Arrows indicate analysis stage at R48h. **(E)** Quantification of *fabp10a*:DsRed expression and area of the regenerating livers treated with JSI-124 at three different time points, from A0h-R48h, A18h-R48h and R0h-R48h. Total cell fluorescence (AU: arbitrary units) considers both area of the liver and fluorescence intensity. Scale bar: 250 μm; error bars: ±SEM.

Next, we sought to determine which step of BEC-driven liver regeneration was regulated by Stat3. To address this question we examined (1) BEC dedifferentiation and (2) LPC proliferation and/or differentiation into hepatocytes/BECs. First, to inspect BEC dedifferentiation into LPCs, we examined the induction of hepatoblast/hepatocyte marker, hepatocyte nuclear factor 4 alpha (Hnf4a), in *Tp1*:H2B-mCherry^{+} cells (BECs), indicative of dedifferentiated BECs. We used the *Tg(Tp1: H2B-mCherry)* transgenic line in which the H2B-mCherry fusion protein is driven by the Notch response element to mark BECs/BEC-derived cells [271]. Interestingly, in A0h-R6h JSI-124-treated larvae, the induction of Hnf4a in *Tp1*:H2B-mCherry^{+} cells was comparable to DMSO-treated control livers (Figure 33). Altogether, these data reveal Stat3 inhibition decreases the size of regenerating livers during BEC-driven liver regeneration. However, this phenotype is not due to a defect in BEC dedifferentiation. Next, we examined whether the smaller liver size was due to a LPC proliferation or a hepatocyte differentiation defect.

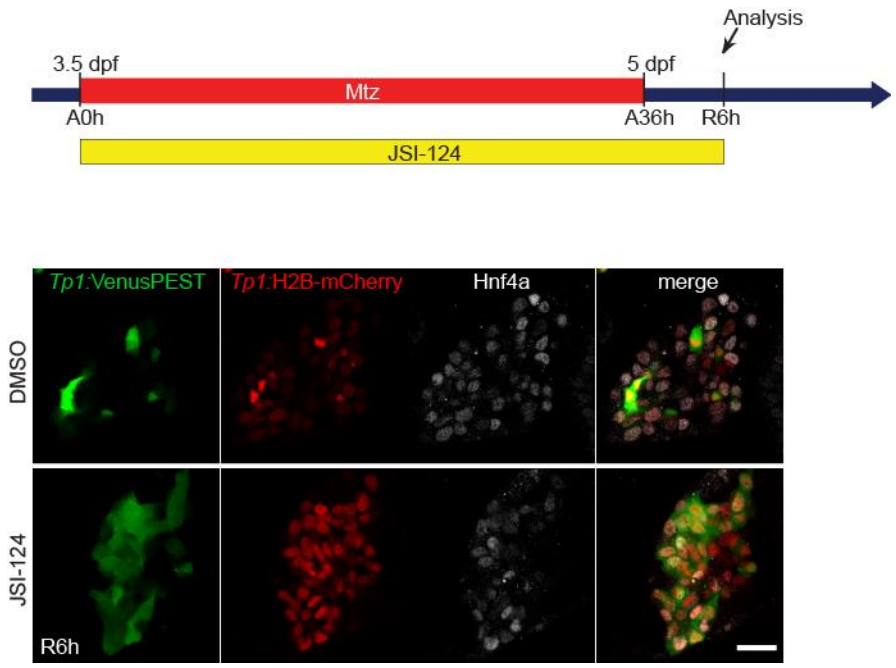

Figure 33: Stat3 inhibition does not affect the BEC dedifferentiation into LPCs during BEC-driven liver regeneration

Scheme illustrating the Mtz treatment period (A, ablation), JSI-124 treatment and liver regeneration (R, regeneration). Arrow indicates analysis stage at R6h. Single-optical section image showing *Tp1*:VenusPEST (green), *Tp1*:H2B-mCherry (red) expression and Hnf4a staining (gray) in regenerating livers at R6h. Scale bar: 20 µm.

4.2.2 Stat3 Inhibition Temporarily Delays LPC-to-hepatocyte Differentiation and Decreases BEC number during Liver Regeneration

Since BEC dedifferentiation into LPCs was unaffected in Stat3-inhibited regenerating livers, we next examined the effect of blocking Stat3 on LPC-to-hepatocyte differentiation at later stages of regeneration. We used the Betaine-homocysteine S-methyltransferase (Bhmt) to mark newly-generated hepatocytes. At R6h, upon Stat3 inhibition, Bhmt expression was visibly reduced in 75% of the regenerating livers, indicative of a LPC-to-hepatocyte differentiation defect (Figure

34). Interestingly, this LPC-to-hepatocyte differentiation defect was temporary, as at a later stage, such as R24h, Bhmt expression in both DMSO- or JSI-124-treated livers was comparable (Figure 34). In addition, when BECs dedifferentiate, Alcam, a marker of BECs in zebrafish [270], is expressed in BEC-derived LPCs. Later, when LPCs differentiate into hepatocytes, Alcam expression disappeared from mature hepatocytes. JSI-124 treatment from A0h resulted in sustained Alcam expression at R24h in mCherry-positive cells, providing further evidence for a hepatocyte differentiation defect (Figure 35A). In addition to the delayed hepatocyte differentiation in Stat3-inhibited regenerating livers, JSI-124 treatment significantly decreased the BEC number at R24h (Figure 35A). Unlike the hepatocyte differentiation defect, which was temporary, the BEC number remained low even at later time points (Figure 36A). Importantly, JSI-124 treatment in non-ablated control livers had no effect on liver morphology or on BEC number (Figure 35B).

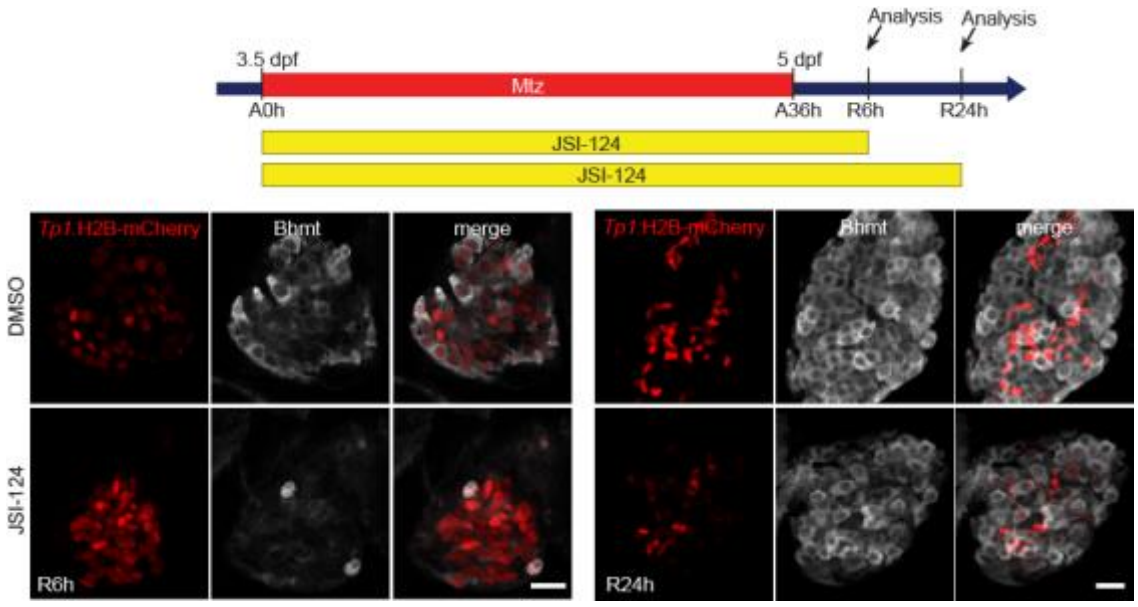

Figure 34: Stat3 inhibition delays LPC-to-hepatocyte differentiation during BEC-driven liver regeneration

Scheme illustrating the Mtz treatment period (A, ablation), JSI-124 treatment and liver regeneration (R, regeneration). Arrows indicate analysis stage at R6h and R24h. Confocal projection images showing *Tp1:*H2B-mCherry expression and Bhmt staining (gray) in regenerating livers treated with DMSO and JSI-124 at R6h and R24h. Scale bars: 20 µm.

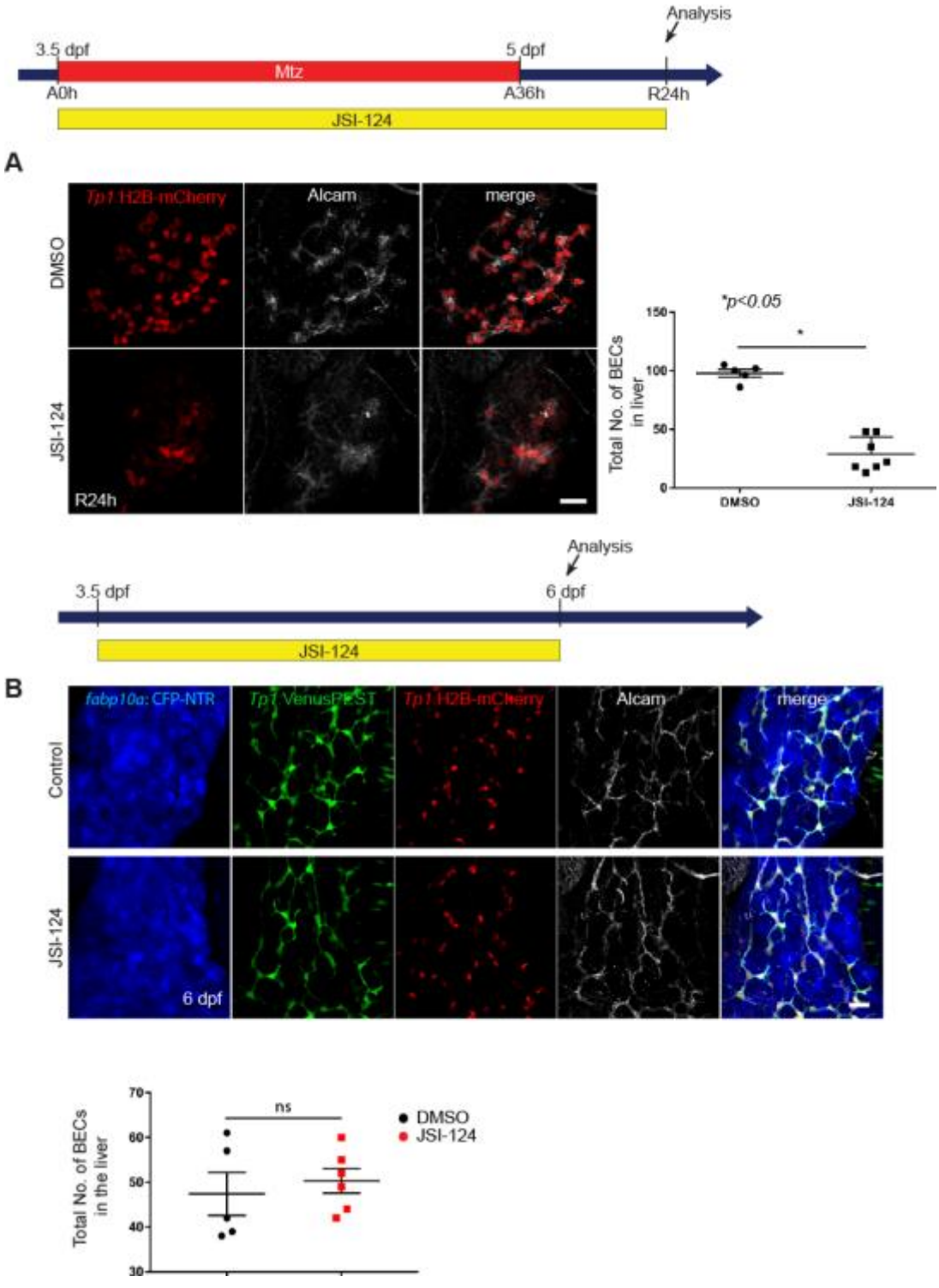

Figure 35: Stat3 inhibition decreases BEC number during BEC-driven liver regeneration and has no effect on non-ablated livers

(A) Confocal projection images showing *Tp1:*H2B-mCherry (red) expression and Alcam (gray) staining in regenerating livers at R24h. Quantification of the total numbers of BECs ($Alcam^+/H2B\text{-}mCherry^+$) per liver. **(B)** Confocal projection images showing *Tp1:*H2B-mCherry (red), *Tp1*:VenusPEST (green), *fabp10a*:CFP-NTR (blue) expression and Alcam (gray) staining in regenerating livers treated with DMSO and JSI-124 at 6 dpf. Quantification of the total numbers of BECs ($Alcam^+/H2B\text{-}mCherry^+$) per liver. Scale bars: 20 μm; error bars: ±SEM.

We further examined the impact of delayed LPC-to-hepatocyte differentiation and reduced BEC number by investigating hepatocyte polarity and biliary morphogenesis. Typically expressed on the apical side of the hepatocyte membrane, the bile salt export pump marker, ATP binding cassette subfamily B member 11 (Abcb11) marks the bile canaliculi in hepatocytes [66, 307]. The number of $Abcb11^+$ cells per liver area was significantly decreased in JSI-124-treated livers as compared to DMSO-treated controls (Figure 36A). We confirmed the Abcb11-phenotype with the BODIPY C5 Analog Assay, which allowed us to visualize the intrahepatic biliary conduits and processing of C5 lipid analog as it passed through the biliary network [308]. Compared to the DMSO-treated control livers, which had thin and elongated bile canaliculi, JSI-124-treated livers had a reduced number of biliary conduits as well as short or absent bile canaliculi (Figure 36B).

Altogether, these data implicate Stat3 as an important regulator in the timing for LPC-to-hepatocyte differentiation and in the establishment of proper BEC population during BEC-driven liver regeneration.

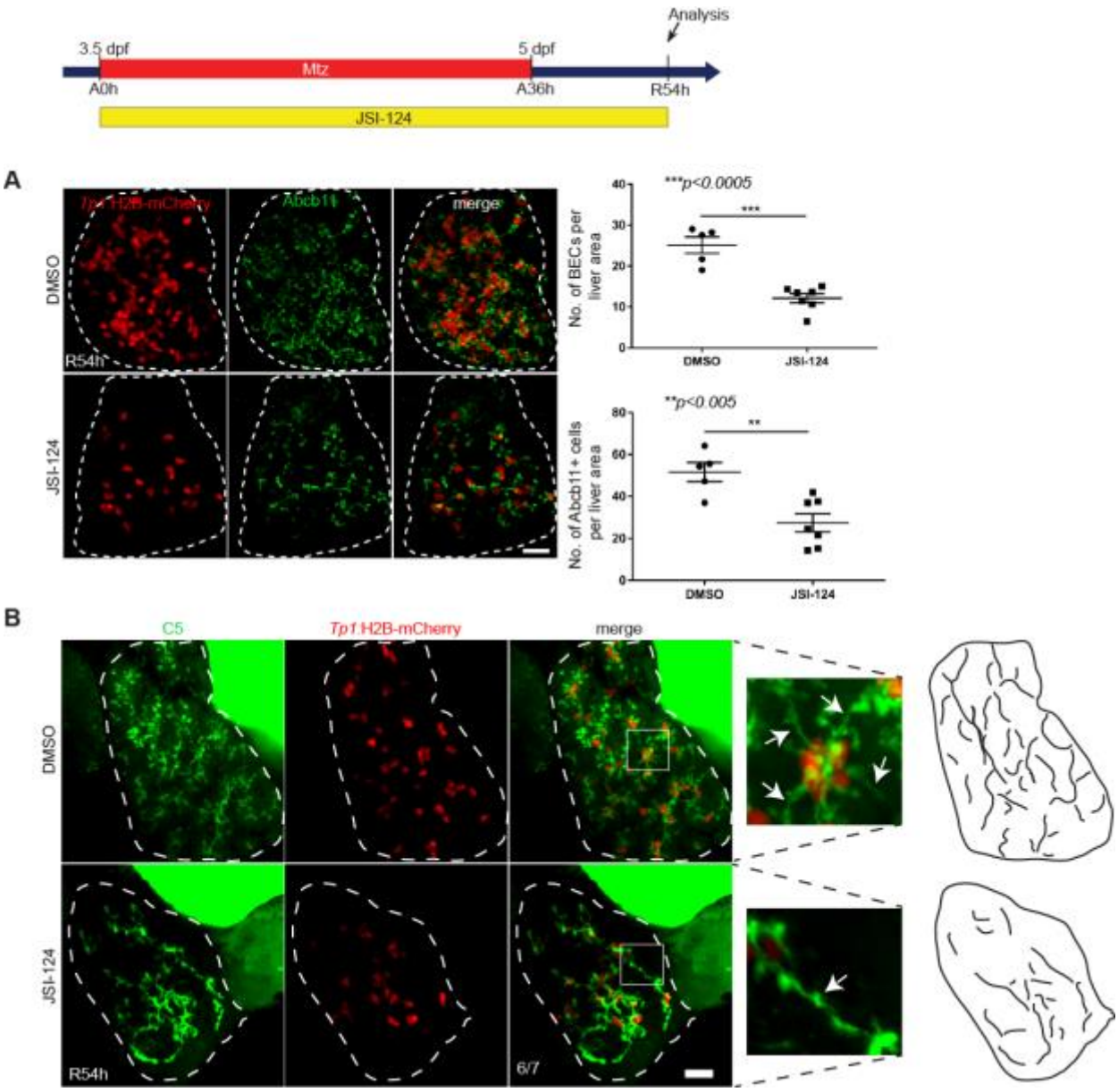

Figure 36: Stat3-inhibited livers maintain low BEC numbers and display aberrant intrahepatic biliary morphogenesis

(A) Confocal projection images showing *Tp1:*H2B-mCherry (red) expression and Abcb11 (green) staining in regenerating livers at R54h. Quantification of the total number of BECs (H2B-mCherry^{+} cells) and bile canaliculi (Abcb11^{+} cells) per liver area. **(B)** Confocal projection images showing BODIPY C5 staining (green) and *Tp1*:H2B-mCherry (red) expression at R54h. Inset boxes show a magnified image of the selected area. Arrows point to bile ductules. Right: Scheme of bile ductules and

bile canaliculi in DMSO- and JSI-124-treated regenerating livers at R54h. Scale bars: 20 μm; error bars: ±SEM.

4.2.3 Stat3 inhibition Reduces the Regenerating Liver Size and BEC number due to a Proliferation Defect

Given the smaller liver size and reduced number of BECs observed in JSI-124-treated livers, we investigated whether the observed phenotypes were due to cell death or a proliferation defect. To assess cell proliferation, we used the 5-ethynyl-2'-deoxyuridine (EdU) labeling and the cell cycle reporter line, *Tg(fabp10a:mAGFP-gmnn)* [143]. Based on the cell cycle oscillator phenomenon with Cdt1 and Geminin proteins, this transgenic line only labels hepatocytes in the S/G2/M phases of the cell cycle [309]. Since we observed a gross phenotype (i.e., smaller liver size) at R24h, we hypothesized that any proliferation or cell death defect would occur prior to R24h. At R24h, we expected no change in EdU labeling of hepatocytes since at R48h, we observed no significant difference in the size of regenerating livers (Figure 32E). Following this logic, we conducted our EdU and transgenic cell cycle assays at R6h and R24h. Since the *fabp10a*:mAGFP-gmnn labels proliferating LPCs at R6h, we found that compared to the DMSO-control livers, JSI-124-treated regenerating livers displayed a significant decrease in LPC proliferation at R6h (Figures 37A-B). As expected, however, this proliferation defect was temporary as at R24h, the JSI-124-treated livers recovered and proliferation was unaffected (data not shown).

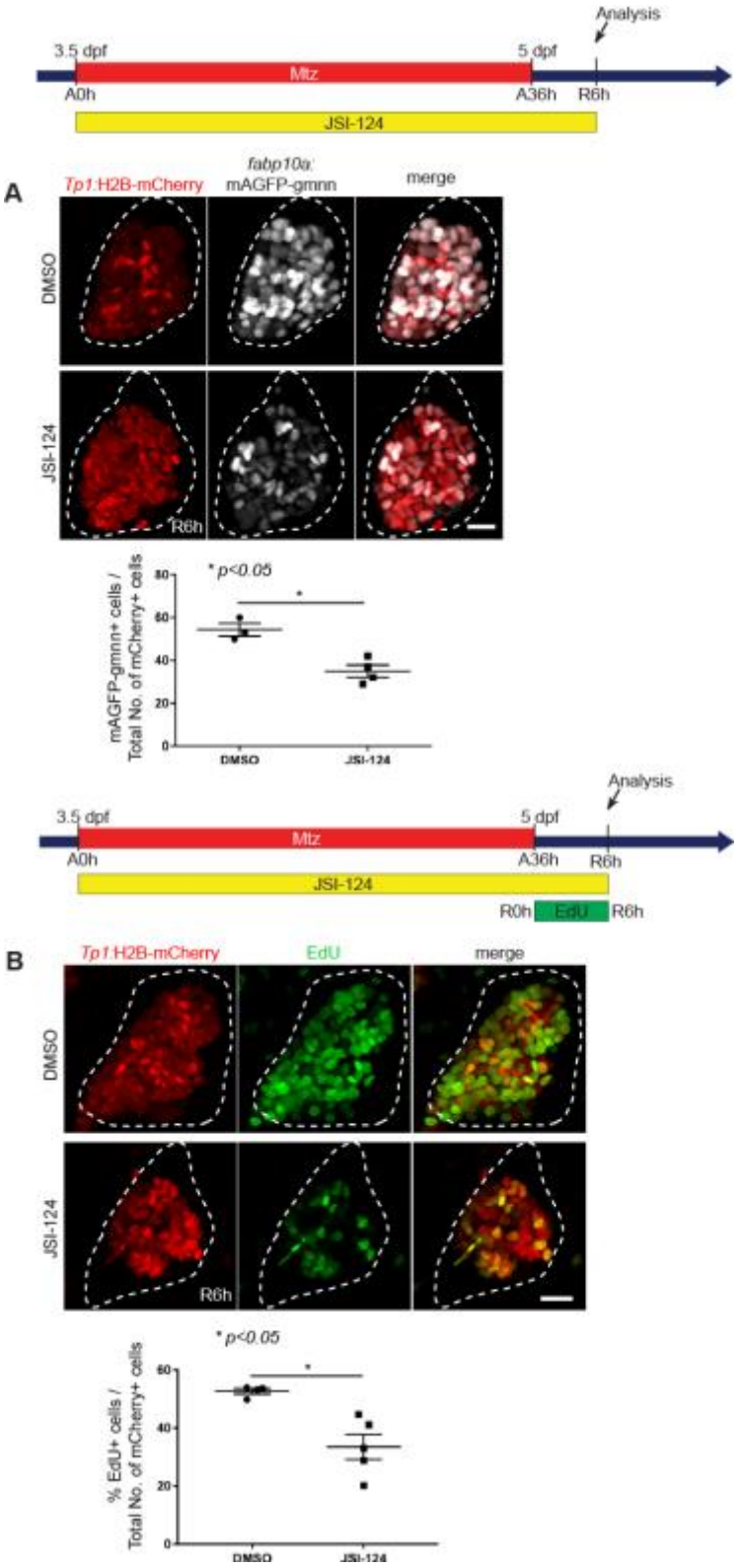

Figure 37: Stat3 inhibition reduces the regenerating liver size and BEC number due to a proliferation defect

(A) Confocal projection images showing *Tp1:*H2B-mCherry (red) and *fabp10a*:mAGFP-gmnn (gray) expression in regenerating livers at R6h. Quantification of the percent fucci^{+} cells per total number of BECs (H2B-mCherry^{+} cells) in the liver. **(B)** Confocal projection images showing *Tp1:*H2B-mCherry (red) expression and EdU staining (green) in regenerating livers at R6h. Quantification of the percent EdU^{+} cells per total number of BECs (H2B-mCherry^{+} cells) in the liver. Scale bars: 20 μm; error bars: ±SEM.

To assess cell death, we used the Terminal deoxynucleotidyl transferase dUTP nick end labeling (TUNEL) assay to label dying cells in the DMSO- and JSI-124-treated regenerating livers at A18h and R6h. At A18h, extensive hepatocyte death and macrophage infiltration is typically observed in BEC-driven liver regeneration. Again, the gross decrease of liver size at R24h points to the after-effect of an earlier defect in either proliferation and/or cell death. Since we observed a proliferation defect at R6h, we also anticipated any difference in cell death to occur at R6h. However, at both A18h and R6h, we observed no significant difference in TUNEL/*Tp1*:H2B-mCherry-double positive cells between DMSO- or JSI-124-treated regenerating livers (Figures 38A-B).

Altogether, these data provide evidence that the smaller liver size and decreased BEC number is not due to an increase in cell death, but rather a proliferation defect. In addition to its role in the timing of LPC-to-hepatocyte differentiation and BEC number maintenance, Stat3 signaling also appears to mediate LPC proliferation.

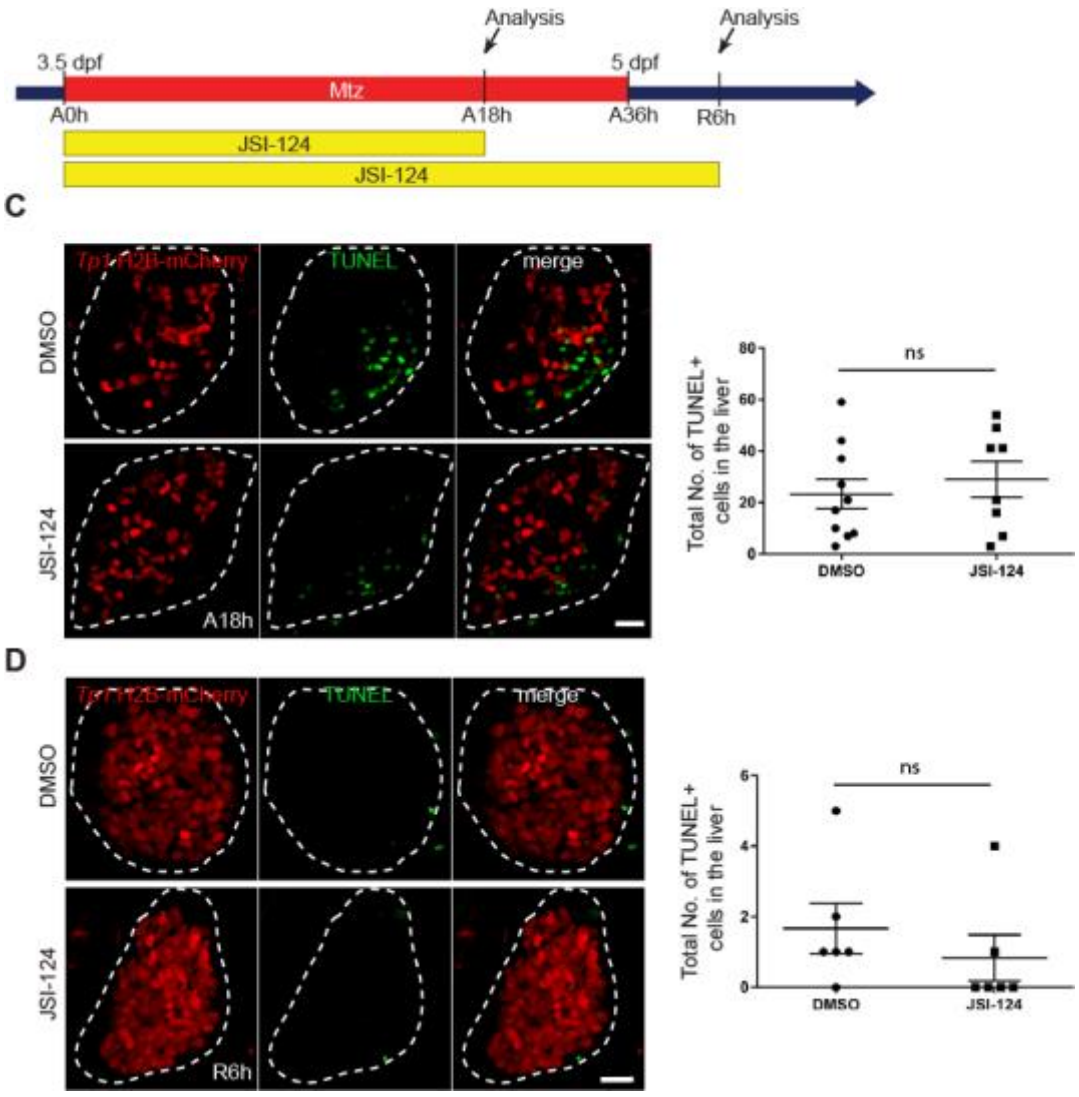

Figure 38: Stat3 inhibition has no effect on cell death in regenerating livers

(A) Confocal projection images showing *Tp1:*H2B-mCherry (red) expression and TUNEL^{+} (green) at A18h. Quantification of the total number of TUNEL^{+} cells per liver area at A18h. **(B)** Confocal projection images showing *Tp1:*H2B-mCherry (red) expression and TUNEL^{+} (green) at R6h. Quantification of the total number of TUNEL^{+} cells per liver area at R6h. Scale bars: 20 µm; error bars: ±SEM.

4.3 METHODS

4.3.1 Zebrafish Maintenance

Embryos and adult zebrafish (*Danio rerio*) were raised and maintained under standard laboratory conditions [239] with protocols approved by the University of Pittsburgh Institutional Animal Care and Use Committee. We used *stat3*^{sa15744} mutants [310] and the following transgenic lines: *Tg*(*fabp10a*:*DsRed,ela31*:*GFP*)^{gz12} [39] [referred to as *Tg*(*fabp10a*:*dsRed*)], *Tg(EPV.Tp1-Mmu.Hbb:Venus-Mmu.Odc1)*^{s940} [311] [referred to as *Tg(Tp1:VenusPEST)*], *Tg(EPV.Tp1-Mmu.Hbb:hist2h21-mCherry)*^{s939} [311] [referred to as *Tg(Tp1:H2B-mCherry)*], *Tg(fabp10a:CFP-NTR)*^{s931} [20] [referred to as *Tg(fabp10a:CFP-NTR)*], and *Tg(fabp10a:mAGFP-gmnn)*^{pt608} [143] [referred to as *Tg(fabp10a:mAGFP-gmnn)*].

4.3.2 Hepatocyte Ablation and Chemical Inhibitor Treatments

To ablate hepatocytes, *Tg(fabp10a:CFP-NTR)* or *Tg(fabp10a:CFP-NTR; fabp10a:dsRed)* double transgenic larvae were treated with 10 mM metronidazole (Mtz) in egg water supplemented with 0.2% dimethyl sulfoxide (DMSO) and 0.2 mM 1-phenyl-2-thiourea (PTU) as previously described [149]. For Stat3 inhibitor experiments, larvae were treated with 7 uM JSI-124 (also known as Cucurbitacin I, Cayman Chemical, Ann Arbor, MI, USA) or 300 uM S3I-201 (Sigma-Aldrich, St. Louis, MO, USA). Larvae were treated with JSI-124 or S3I-201 from A0h to R24h or from A18h to R24h followed by the examination of *fabp10a*:DsRed expression and liver size at R24h or R48h using the Leica M205 FA microscope.

4.3.3 Zebrafish Whole-mount *In Situ* Hybridization (WISH) and Immunostaining

Whole-mount in situ was performed as previously described [242]. Whole-mount immunostaining was performed as previously described [29], using the following antibodies: goat anti-Hnf4a (1:35; Santa Cruz, Dallas, TX), mouse monoclonal anti-Bhmt (1:100; a gift from J. Peng, Zhejiang University, China), mouse monoclonal anti-Alcam (1:10; ZIRC, Eugene, OR) and rabbit polyclonal anti-Abcb11 (1:100; PC-064, Kamiya Biomedical, Seattle, WA), and Alexa Fluor 488-, 568-, and 647-conjugated secondary antibodies (1:300; Life Technologies, Grand Island, NY).

4.3.4 TUNEL and EdU Assays

Apoptotic cell death was analyzed according to the protocol of the *In Situ* Cell Death Detection Kit, TMR Red (Roche, Switzerland). Following whole-mount immunostaining, TUNEL labeling was applied. Cell Proliferation was performed using the protocol outlined in the Click-iT EdU Alexa Fluor 647 Imaging Kit (Life Technologies, Grand Island, NY, USA). Larvae were treated with egg water supplemented with 0.2 mM PTU containing 50 mM EdU and 5% DMSO at R0h or R18h. After a 6-hour treatment window, larvae were harvested at either R6h or R24h, respectively, and fixed in fresh 3% formaldehyde overnight at 4°C. After fixation, samples were prepared for subsequent imaging and statistical analysis.

4.3.5 Image Acquisition, Processing and Statistical Analysis

Zeiss LSM700 and Leica M205 FA were used for confocal microscopy and epifluorescence microscopy, respectively. ZEN 2009 software was used to assemble and analyze confocal stacks.

Leica MZ16 stereomicroscope was used to obtain *in situ* images. Adobe Illustrator, Photoshop and Microsoft Powerpoint were used for assembling figures, tables, schematics and labels. GraphPad Prism 7 software was used to create and assemble quantitative data. Quantification for liver size, fluorescence, and cell counting was performed using the NIH ImageJ software. Unpaired two-tailed Student's t-tests were used for statistical analyses; $p < 0.05$ was considered statistically significant. Quantitative data are shown as means ± standard error of the mean (SEM).

4.3.6 BODIPY C5 Lipid Analog Assay

A 2-hour treatment of 0.5 uM BODIPY C5 (Life Technologies, Grand Island, NY) [308] was used to assess ductal morphology and morphogenesis in DMSO- vs. JSI-124-treated regenerating livers. Following BODIPY treatment, larvae were rinsed briefly and anesthetized with 0.016% Tricaine in egg water supplemented with 0.2 mM PTU and mounted in 1% low-melting agarose for confocal imaging.

4.4 DISCUSSION

The signaling pathways regulating LPC proliferation and differentiation into hepatocytes and BECs during BEC-driven liver regeneration remain poorly understood. In this study, we sought to determine the role of Stat3 in BEC-driven liver regeneration. We blocked Stat3 signaling with the JAK-inhibitor, JSI-124, which reduced the size of regenerating livers at R24h. To further elucidate the exact process of liver regeneration being affected by JSI-124, we examined (1) BEC dedifferentiation and (2) LPC proliferation and differentiation into hepatocytes/BECs. First, by

Hnf4a staining, we found BEC dedifferentiation was unaffected in JSI-124-treated livers, as compared to DMSO-controls. We further noted that Stat3 deficiency decreased the number of mature BECs in regenerating livers at R24h and this decrease was still maintained later at R54h. Lastly, our data revealed that Stat3 inhibited-livers exhibited a decrease in LPC proliferation at R6h (but not at R24h) during liver regeneration, which helps to explain the decreased liver size at R24h and subsequent recovery later on at R48h.

Using our zebrafish BEC-driven liver regeneration model, our RNAseq analysis (unpublished) and WISH analysis highlighted the upregulation of *stat3* in the initial phases of liver regeneration (Figure 31). It was also reported that in the 2-AAF/PHx rat model of oval cell activation, *Stat3* was highly upregulated in the oval cell population that corresponded with the highest proliferative potential [303]. This supports our finding that inhibition of Stat3 resulted in a proliferation defect in LPCs at R6h (Figure 37). Therefore, we can speculate that the smaller liver size at R24h is a result of the lower number of LPCs established at R6h, resulting in subsequent lower number of LPCs available for differentiation and expansion.

Several mouse studies have also examined the role of Stat3 in liver regeneration. For example, following partial hepatectomy in liver-specific *Stat3* conditional knockout (L- *Stat3*$^{-/-}$) mice, the mortality rate was significantly increased during liver regeneration [304]. This increase was speculated to be due to a defect in the Stat3-dependent acute-phase response; this response is activated following liver injury and involves the induction of survival-related proteins [312, 313]. In a separate model of liver injury (i.e., CCl_4), although liver-specific *Stat3* knockout mice had slight decrease in DNA synthesis, they displayed no difference in survival or necrosis compared to wild-type littermates [304].

In our BEC-driven liver regeneration model, we discovered an absence of Bhmt staining in 75% of JSI-124-treated regenerating livers at R6h, which indicated a LPC-to-hepatocyte differentiation defect. However, at R24h, no difference was observed in Bhmt staining between DMSO-control and JSI-124-inhibited regenerating livers, indicating a delay in hepatocyte differentiation rather than a complete blockage. One explanation for the delay is that Stat3 is one of several proteins implicated in hepatocyte differentiation and upon Stat3 inhibition, other compensatory mechanisms are instead activated to counteract the deficiency. Such a phenomenon was detected in liver-specific *Stat3* knockout mice, which displayed STAT1 activation in liver extracts compared to control mice [314].

Depending on the cell type and injury-stimulus, Stat3 plays a critical role in several biological processes, including proliferation, apoptosis and inflammation. Previous studies have implicated Stat3 in the regulation of myogenic differentiation in skeletal muscle [315, 316]. *Stat3* activation in satellite cells during muscle repair drove these multipotent cells to choose differentiation over self-renewal, which predictably led to a smaller satellite cell pool. In contrast, ablation of *Stat3* in satellite cells promoted the precursor, satellite cells to self-renew instead, leading to enhanced repair [317]. Similarly, in our liver regeneration studies, Stat3 inhibition also led to a transient hepatocyte differentiation defect, indicating that Stat3 regulates the decision of LPCs to either commit to a hepatocyte fate or proliferate. Although Stat3-inhibited livers displayed a proliferation defect, we did not observe any difference in cell death between JSI-treated and DMSO-treated regenerating livers.

Although we did not address the upstream activators or downstream mediators of the Stat3 signaling pathway, future studies can focus on identifying these factors and their role in LPC proliferation and differentiation. Factors such as the interleukin (IL) cytokines may be important

activators of Stat3 pathway during BEC-driven liver regeneration. In particular, IL-6 treatment caused a decrease in the number of LPCs in CDE diet-fed mice [214]. Findings from current and future studies can provide insight into developing novel therapies for patients suffering from chronic liver diseases.

4.5 ACKNOWLEDGEMENTS

We thank Lila Solnica-Krezel for providing *stat3* mutant fish. We also thank Ken Poss for the *stat3 in situ* probe. The work was supported by grants from the NIH to D.S. (DK101426) and M.K. (F31DK105714).

5.0 CONCLUDING REMARKS AND FUTURE DIRECTIONS

Altogether, these findings establish the power of zebrafish in two ways: (1) in the study of liver development and (2) in using the complete hepatocyte-specific ablation injury model to reveal underlying mechanisms in LPC/BEC-driven liver regeneration. We have shown that Id2a, a HLH factor downstream of the BMP signaling pathway, is an important regulator of hepatic outgrowth during hepatogenesis. In fact, *id2a* knockdown results in a smaller liver during liver development. This failure of the liver bud to expand is caused by decreased hepatoblast proliferation and increased hepatoblast cell death during liver development.

We also concluded that BMP signaling pathway is important for regulating LPC-to-hepatocyte differentiation and BEC proliferation. BMP-deficient livers failed to establish mature hepatocytes after LPC induction and displayed increased number of BECs. These phenotypes were mediated by factors Tbx2b and Id2a, respectively.

During liver development, the finding that Id2a knockdown resulted in a smaller liver size raised an important question about the type of bHLH factor that was negatively regulated by Id2a. As mentioned earlier, the main function of Id2a is to dimerize with bHLH (or ETS factors) and negatively regulate their activity by preventing them from binding DNA. Since the liver size was decreased after Id2a knockdown, we speculated the unknown bHLH factor to function as a repressor of hepatic outgrowth during liver development. To identify the potential bHLH factor, we conducted a literature search of bHLH factors that were either expressed in the liver or important in developmental processes. Next, from a narrowed list of 50 candidates, we completed an *in situ* analysis of bHLH factors during liver development, especially focusing on stages of hepatoblast specification and BEC differentiation. Findings from the in situ screen are presented

in Appendix B. Future studies can focus on knocking down bHLH factors specifically expressed in the hepatoblasts and BECs and examining effect on hepatic outgrowth. Finally, we can confirm the binding target of Id2a by conducting biochemical studies using Co-immunoprecipitation assay/Western blotting or the yeast-2-hybrid system. Since the *id2a* mutants also exhibit a transient BEC phenotype during BEC-driven liver regeneration, we speculate that Id2a binds a biliary-specific bHLH factor that regulates BEC proliferation. Since during development Id2a is expressed in a subset of the BECs, future experiments can examine whether all proliferating BECs (EdU^+) observed in regenerating livers are also Id2a-negative.

In addition to the BMP signaling pathway, the Stat3 signaling pathway is also necessary for proper BEC-driven liver regeneration. By chemically inhibiting Stat3 via the JAK-specific inhibitor, JSI-124, we observed a reduced liver size and BEC number in regenerating livers. Additionally, the LPC-to-hepatocyte differentiation, which can begin as early as R6h, was delayed until R24h. Future studies can focus on elucidating the upstream activators and downstream mediators of Stat3 signaling pathway in BEC-driven liver regeneration. One approach to reveal the downstream factors is to conduct a qPCR analysis by dissecting livers from both DMSO- and JSI-124-treated larvae at R6h (for LPC proliferation and LPC-to-hepatocyte differentiation defect). Based on our liver regeneration phenotypes, we expect hepatocyte-specific genes (such as *fabp10a*, *bhmt*) and proliferation-related genes (*cyclinD1*, *myc*) to be downregulated in JSI-124-treated livers. Additional, known downstream target genes of Stat3 can also be examined, such as *socs3a*, *zip6*, *mcl-1a, mcl-1b*, *bax1* and *bcl-2*.

In addition to Stat3, previous studies have highlighted the cross-talk between Stat3 and NF-κB pathways (reviewed in [318]). Hence, we hypothesized that in addition to Stat3 signaling, NF-κB pathway was also important for BEC-driven liver regeneration. Using the *Tg(6xHsa.NF-*

κB:eGFP) line [319], we showed NF-κB activation in the regenerating livers (see Appendix C; Figure 43). To elucidate the role of NF-κB in BEC-driven liver regeneration, future experiments can focus on finding a reliable method of blocking and/or enhancing NF-κB signaling in regenerating livers (see Appendix C; Figure 44).

APPENDIX A

CHAPTER 3 TABLES

Table 1: Transgenic and mutant lines used in Chapter 3

Names used in this study	Official names (ZFIN database)	Allele #	Ref
Tg(Tp1:VenusPEST)	*Tg(EPV.Tp1-Mmu.Hbb:Venus-Mmu.Odc1)*	*s940*	[320]
Tg(Tp1:H2B-mCherry)	*Tg(EPV.Tp1-Mmu.Hbb:hist2h2l-mCherry)*	*s939*	[320]
Tg(ubb:loxP-GFP-loxP-mCherry)	*Tg(-3.5ubb:LOXP-EGFP-LOXP-mCherry)*	*cz1701*	[321]
Tg(Tp1:CreERT2)	*Tg(EPV.Tp1-Mmu.Hbb:Cre-ERT2,cryaa:mCherry)*	*s959*	[322]
Tg(fabp10a:CreERT2)	*Tg(fabp10a:Cre-ERT2,cryaa:ECFP)*	*pt602*	[20]
Tg(fabp10a:rasGFP)	*Tg(-2.8fabp10a:CAAX-EGFP)*	*s942*	[323]
Tg(fabp10a:CFP-NTR)	*Tg(fabp10a:CFP-NTR)*	*s931*	[20]
Tg(hs:dnBmpr1)	*Tg(hsp70l:dnXla.Bmpr1a-GFP)*	*w30*	[324]
Tg(Tp1:mAGFP-gmnn)	*Tg(EPV.Tp1-Mmu.Hbb:mAGFP-gmnn)*	*s707*	this study
Tg(WRE:d2GFP)	*Tg(OTM:d2EGFP)*	*kyu1*	[325]
smad5	*smad5*	*m169*	[273]
tbx2b	*tbx2b*	*c144*	[276]
id2a	*id2a*	*pt661*	this study

Table 2: Sequences of primers used for *in situ* probe synthesis

Gene	Primer	Nucleotide sequence (5' to 3')
pprc1	forward	CTAGCATTGTTATCAAGACCGTTG
pprc1	reverse	GCCTTTTTGTATCCTCACTGCTAT
tfpia	forward	CAGGTTTTACTTTGACATCGACAC
tfpia	reverse	TCTTTATCCGTATTTGCTTTCTCC
hmgb3a	forward	GCTTATGCCTATTTCGTTCAGACT
hmgb3a	reverse	CTATTCGTCGTCGTCATATTCGT
hmgb2b	forward	GGTGAAAGGAGACGTGAACAA
hmgb2b	reverse	TCTTCCTCATCATCTTCCTCGT
hmgb2a	forward	GTAAAGATCCAAATAAGCCCAGAG
hmgb2a	reverse	CTCATCATCGTCATCATCAGCTT
cbx3a	forward	CAGGCAAGTCAAAGAAGGAAGTT
cbx3a	reverse	GCTCATCCTCAGGACAAGAATG
cbx5	forward	ATGGGAAAGAAGAGCCAGAAC
cbx5	reverse	CTGTGGCACTCTTCTCCTTCTTG

brd3a	forward	TTTCAACACAATGTTCACAAACTG
brd3a	reverse	TTGACAGCATTTCTTTAAGGATGA
foxp4	forward	CCAGCCGTAGAGTGAAAGTAGAGT
foxp4	reverse	GTAGATTCAGAATGTGTTGCTGCT
foxp1a	forward	TAAAACTCAGACTCTCAACCACCA
foxp1a	reverse	TGTTCGAGTGAACCAGTTGTAGAT
tbx2b	forward	ATAAATATCAGCCCAGGTTCCATA
tbx2b	reverse	GGAGAGAAGCTGTCTTTACTACCG
id2a	forward	TCCTGCTGTCAACATGAAGGCA
id2a	reverse	TAATACGACTCACTATAGGGCCAGTTCCCAGGTCCTGTGTGT
mlf2	forward	TTTCGTTACTTGAATGATGTGGAT
mlf2	reverse	ATAATCTAAACTGCGGGCAGTAGG
irf6	forward	AGTATCAGGAAGGAGTGGATGAAC
irf6	reverse	GAACAGCTCCTCTTGGTTCACTAT
igf2a	forward	GGATGATTACCATGTATTCTGTGC
igf2a	reverse	GTTTGCTCCTCATCTTGGATTTT
akt2	forward	ACAGCAATTCTGAAAGAGAGGAGT
akt2	reverse	GCCAAAGTCTGTGATTTTAATGTG
sgk1	forward	ACAAGATGTGGAGCTAATGAACAG
sgk1	reverse	GCAGGCCATATAACATTTCATACA
plk3	forward	GAATCCACCTTTTGAAACCTTAGA
plk3	reverse	AAGACAAGCAGCTGTTAAGAACCT
mych	forward	GTATCTGAACTTTTAATGGAGGACAC
mych	reverse	TAATACGACTCACTATAGGGATCTGCAGACCTCGCTGGGAGT
max	forward	CAACGATGATATCG AGGTCGACAG
max	reverse	TAATACGACTCACTATAGGGTGAAACAGGCCATTGCTGTGACTC
mdm2	forward	TACAGATTCAGACTCTCGCTCATC
mdm2	reverse	GAGTTTCTTTTCGAAGGTTGTGTT
rbb4	forward	AATCATGAAGGAGAGGTTAACAGG
rbb4	reverse	GAACCTGGAAGATTTCATCTTTGT
rbb4l	forward	TGGATCAGTTAGTGGAAAGATTGA
rbb4l	reverse	GACCTGGAAGATTTCATCCTTATG
smad5	forward	AAACAGAAAGAAGTGTGCATCAAC
smad5	reverse	ACCTCTCCTCCAACATAGTACAGG
epcam	forward	CACAATGTGCTTGTAAAACAATGA
epcam	reverse	TAGATCAGGACATTCTCCATTGAA
mmp15b	forward	AGGTAATGATCTGTTCCTGGTAGC
mmp15b	reverse	GAAGAAGTAAGTGAAGCCAGAAGG
samd4	forward	ACCTTCAAAGTGCCCTCGT
samd4	reverse	GTCTAACGGTGTGGGGTCTG
smad1	forward	AAGGCCCTAGAGTGCTGTGA
smad1	reverse	GGACTCCTTTTCCGATGTGA
smad9	forward	GCACAGCTTCCCAAACTCTC
smad9	reverse	CCGTGCAGGTGGATTTCTAT

Underlined are T7 primer sequences.

Table 3: Sequences of primers used for qPCR

Gene	Forward primer sequence (5' to 3')	Reverse primer sequence (5' to 3')
pprc1	TGCTACGGTTGAGCTGATTG	AGGCAGTGGTCTTGCCTCTA
tfpia	CAAGGCAATGAAGGACAGGT	TTGGCTTCCTCTTCCTCTGA
hmgb3a	TTGAAGACATGGCCAAACAA	ACAGTTAGCCATTGGCATCC
hmgb2b	TATGCGTTCTTCGTGCAGAC	TCTTTGCTGCTCTGCTTTGA
hmgb2a	CCTCTTACGCCTTCTTCGTG	GGTGAAAGCTTGGACCACAT
cbx3a	AGGTAATGGACCAGCGAGTG	CGCTTCATCAGAGTCCTTCC
cbx5	AAGAAGAGCCAGAACCGTGA	TTTTTCCTCTTGCTGGTGCT
brd3a	GGGTGCGGAACAGTGTATCT	TTCTTTGGTTGCCTGTTTCC
foxp4	GGTTTTCCTGAGGGTCTTCC	CGTTGCTGTGTTTCTCCTGA
foxp1a	ACTGGCTCTCCTCTGGTGAA	TTGGTGTCTGGACTCTGCTG
tbx2b	GCCAAAGGCTTCAGAGACAC	TCGTCTTTCTTCTCCGCAAT
id2a	GAAGGCAATAAGCCCAGTGA	GTCAGGGGTGTTCTGGATGT
MLF2	ATGGATCCGTTTGCTCTCAC	ATCGTTTGACGCGTCTCTCT
irf6	GCTGGTCTGGCTGGATAGAG	CCGTCTCGTATGTGGGAACT
igf2a	GACTCTCTGTGGCGGAGAAC	GGTTTGCTCCTCATCTTGGA
akt2	AGAACACACGGCATCCTTTC	GTCTTCATGGTGGCCTCATT
sgk1	GTGCTTTGGGTTACCTGCAT	CTGCAGTGGCTTGTTCAAAA
plk3	CCGGGAGGTCGTACTGTAAA	GATGCCTTTGTTGTGGAGGT
mych	CTCCGACATAGACACGCAGA	TGCTGCTGGATTTCAAAGTG
max	TCGAGGTCGACAGTGATGAA	TTGGTGTACAGGCTGCTGTC
mdm2	CCTCCTCTTCCTCGACACTG	GGGTCTCTTCCTGACTGCTG
rbb4	GTTCATTCTGGCCACAGGTT	CCCATGGTTCATTTGGATTC
rbb4l	GTGTTGGGCACACACACTTC	TTCCAGGACAAACCATAGCC
smad5	CGGCTCCAAACAGAAAGAAG	GTCTTGCCCCATCTGTTCAT
epcam	CTTGTTTGTTGTGGCATTGG	TTGACGCACCAGCATACTTC
mmp15b	GAGCCGCAGATCAGGACTAC	TCAGAACCACATCCACCTCA
hnf4a	GCCGACACTACAGAGCATCA	TGGTAGGTTGAGGGATGGAG
eef1b2	CCCTCTCAGGCTGATATTGC	TAAGCTGCAAGCCTCTCCTC
G6pc	TCTGTCCCGGATCTACCTTG	GAAAGTTTCAGCCACAGCAA
Tdo2	GGGGATCCTCAGGCTATCAT	AATCCACAAAAACCTTGTACCTG
Tat	GGAGGAGGTCGCTTCCTATT	GCCACTCGTCAGAATGACATC

APPENDIX B

CHAPTER 4 EXPERIMENTS

To determine whether the Stat3 inhibitor phenotype would be recapitulated in the Stat3 homozygous mutants, we obtained the *stat*$^{+/-}$ zebrafish mutants [310]. In the *stat3*$^{-/-}$ mutants, we examined three main phenotypes that we also observed in the JSI-124 treatment case: (1) LPC-to-hepatocyte differentiation, as measured by Bhmt staining; (2) BEC number, as measured by *Tp1*:H2B-mCherry+ cells; and (3) proliferation defect, as measured by EdU staining. First, similar to the JSI-124-treated livers, the *stat3*$^{-/-}$ mutants also exhibited reduced Bhmt staining at R6h during BEC-driven liver regeneration (data not shown), indicative of an initial defect in LPC-to-hepatocyte differentiation. This defect was observed in only about 20% of the *stat3*$^{-/-}$ mutants, possibly due to an incomplete penetrance of the homozygous mutant phenotype. Moreover, as in the JSI-124-treated livers, hepatocyte differentiation is not blocked, but rather delayed as Bhmt staining at R24h showed no difference between wild-type and *stat3*$^{-/-}$ mutants (Figure 39A). Second, the number of BECs were significantly decreased in the *stat3*$^{-/-}$ mutants; again, this BEC decrease was observed in a subset of the *stat3*$^{-/-}$ mutants and was not as robust as we observed in the JSI-124-treated regenerating livers (Figure 39A). Lastly, unlike the chemical inhibitor experiments, *stat3*$^{-/-}$ mutants displayed no significant difference in the percentage of EdU^{+} cells/*Tp1*:H2B-mCherry^{+} cells at R6h (Figure 39B). Although we cannot identify a proliferation defect as the reason for the decreased BEC number, we cannot rule out the possibility that the decreased number of BECs at R24h is instead due to the maintenance of LPCs in a progenitor cell-like state. For future experiments, we will examine Hnf4a expression in *Tp1*:H2B-mCherry^{+} at

R6h and R24h in wild-type and *stat3*$^{-/-}$ mutants to determine if the lower BECs at R24h is caused by a retention of LPCs in their progenitor state.

In addition, we will also examine the *socs3a*$^{-/-}$ mutants closely to study the effect of Stat3 hyperactivation on BEC-driven liver regeneration. Initial experiments at R6h indicated a delay in LPC-to-hepatocyte differentiation, although similar to the *stat3*$^{-/-}$ mutants, this phenotype was not fully penetrant (less than 20% of the homozygous mutants displayed the phenotype). Moreover, as in the *stat3*$^{-/-}$ mutants, no difference in Bhmt staining at R24h between wild-type and *socs3a*$^{-/-}$ mutants was observed (data not shown).

Lastly, because Stat3 has been implicated in cell survival and macrophage infiltration in other regeneration settings [326], we also sought to determine the role of Stat3 in macrophage recruitment in our BEC-driven liver regeneration model. Compared to DMSO-treated livers, Stat3-inhibited livers had a significant increase in macrophage number during injury (A18h) and subsequent regeneration (R6h) (Figure 40). To determine whether Stat3 mediates its effect on BEC-driven liver regeneration through a macrophage-derived or -secreted factor(s), we can examine our liver injury model in *irf8* zebrafish mutants which completely lack macrophages during embryogenesis and instead have an increased number of neutrophils [327].

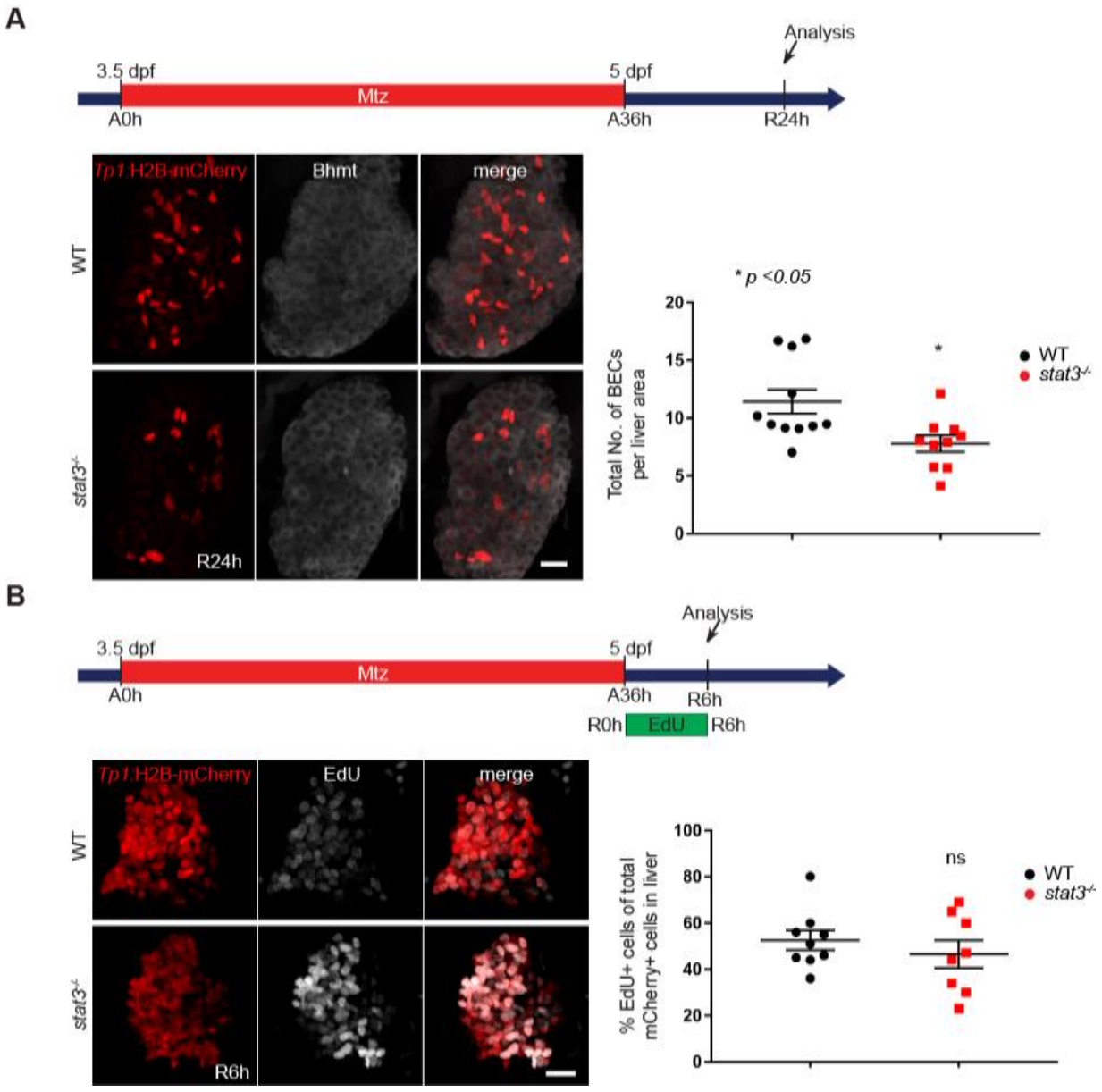

Figure 39: *stat3* homozygous mutants exhibit fewer BECs during BEC-driven liver regeneration

(A) Confocal projection images revealing *Tp1*:H2B-mCherry (BECs; red) expression and Bhmt (gray) staining in R24h regenerating livers. Quantification of the number of H2B-mCherry^{+} cells as shown in (A). Scale bars: 20 μm; error bars: ±SEM. (B) Confocal projection images showing *Tp1:*H2B-mCherry (red) expression and EdU staining (gray) in regenerating livers at R6h. Quantification of the percent EdU^{+} cells per total number of BECs (H2B-mCherry^{+} cells) in the liver. Scale bars: 20 μm; error bars: ±SEM.

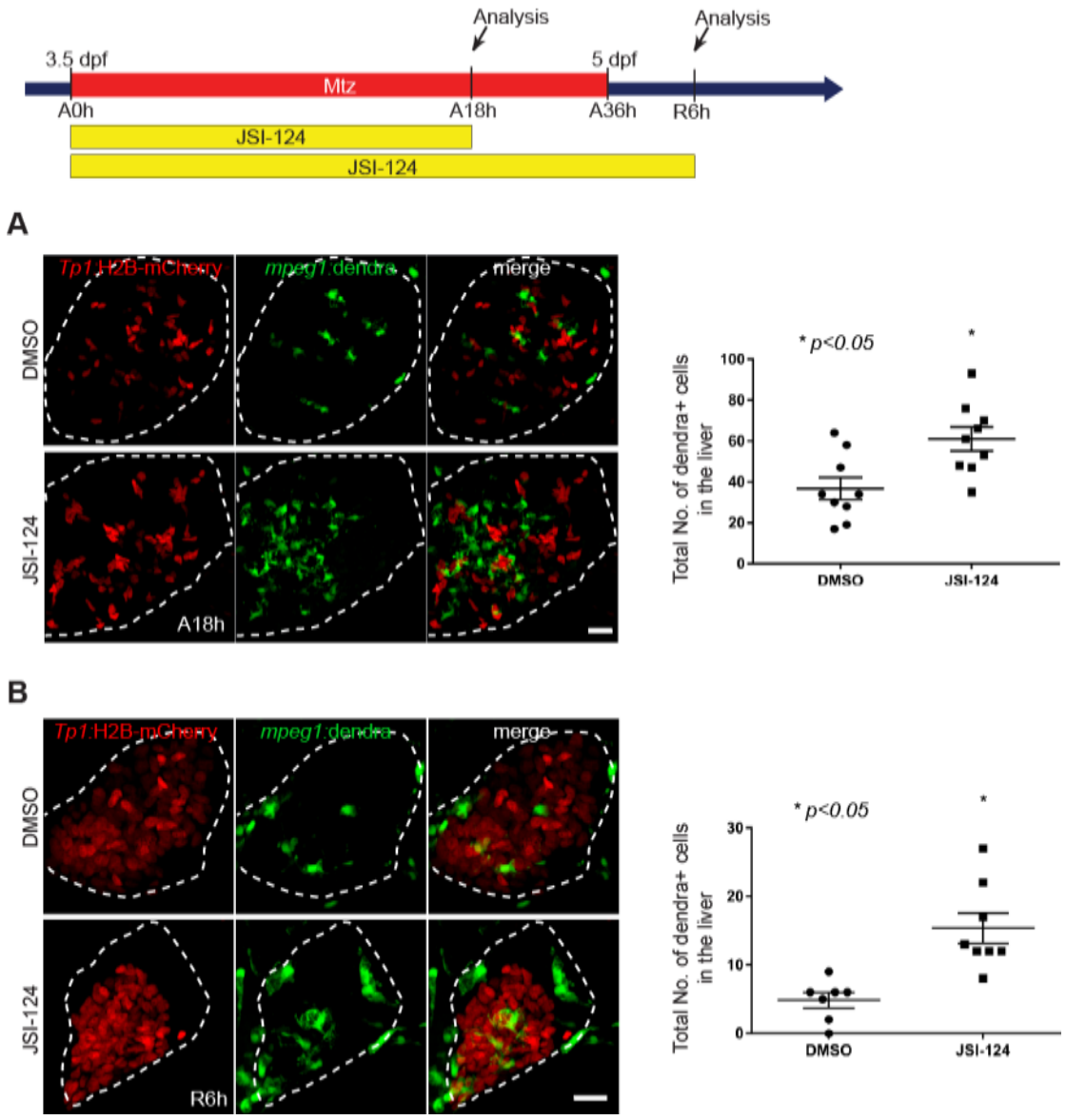

Figure 40: Stat3 inhibition increases macrophage number in the regenerating livers

(A) Confocal projection images revealing *fabp10a*:CFP-NTR (hepatocytes; blue), *Tp1*:H2B-mCherry (BECs; red) and *mpeg1*:dendra (macrophages; green) expression in A18h regenerating livers (n=8). Quantification of the number of dendra/mCherry double-positive cells in DMSO- and JSI-124-treated livers. Scale bars: 20 µm; error bars: ±SEM. **(B)** Confocal projection images revealing *fabp10a*:CFP-NTR (hepatocytes; blue), *Tp1*:H2B-mCherry (BECs; red) and *mpeg1*:dendra (macrophages; green) expression in R6h regenerating livers (n=8). Quantification of the number of dendra/mCherry double-positive cells in DMSO- and JSI-124-treated livers. Dotted lines outline the liver. Scale bars: 20 µm; error bars: ±SEM.

APPENDIX C

C.1 BHLH PROTEINS *IN SITU* SCREEN

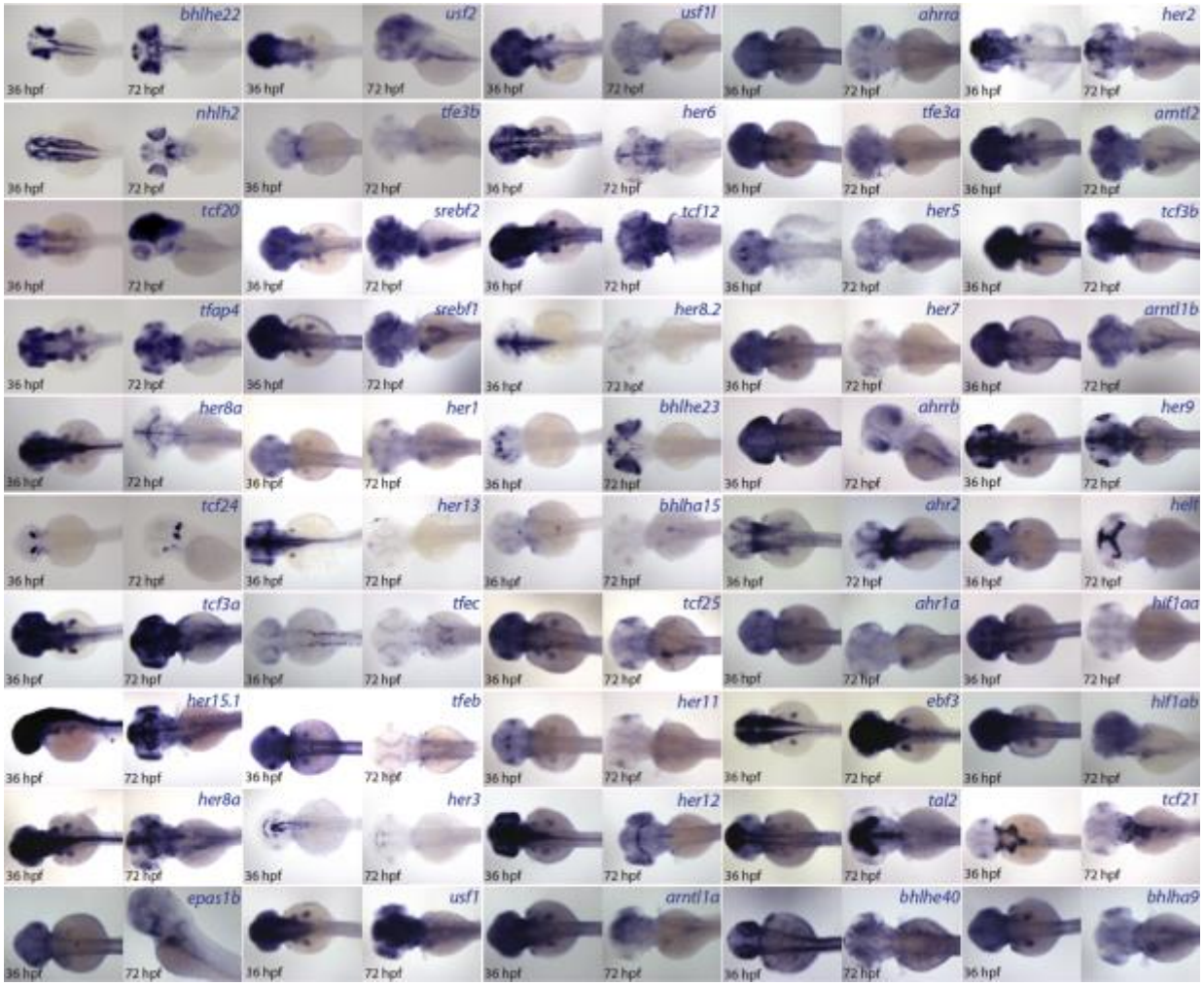

Figure 41: bHLH *in situ* screen to identify factors expressed in the liver during development

Wild-type embryos (n=10 for each stage) were processed for WISH analysis with 50 bHLH probes at 36 hpf and 72 hpf, after hepatoblast specification and differentiation stages, respectively. In addition, we also focused on bHLH factors specifically expressed in the liver BECs.

Table 4: Primer sequences for bHLH *in situ* probes

Probe	Forward Primer (5' to 3')	Reverse Primer (5' to 3')
her5	GCAAAAAGACATGAGAAGGGTCCC	GCTTAGGACTTGAAGTCATGGC
her12	CCTTTGACCATCTTCACTTCAGCG	TGTTAATACCACCGTCCCTCAGG
her11	GCACACCGACTTTCAACATGACG	GCAGGATGTGCTGGTAAAAGTGG
her1	CCGATTTTCAGCCATGGTTACTCC	GGCTCTCATGTGTCCAATCGATTG
her7	AACCTGAAACTTCTGCTCCTGC	CCAAGGTCTCCAAACAGTCTGG
her3	ATGGCTGCAGCATCCAACAG	AGTCATTAGCCTACCAAGGTCGC
her8a	GGTCCGGAGAAGAATTTCAACGC	AGAGCATGGGGCTGTAAGGAG
her6	TGTATCAGCGTACTTGACAGCG	CGGTGTTAACCCCTTCACATGTG
her13	GTGGAGAAAAAGAGACGAGCACG	GACCAGAAAACTCCAGTCCAGG
her1	TAGAGAAGAAACGGAGAGACCG	TGCAGGACAACTCTGGATTTGGG
her8.2	AGCAGATGGACATGACTGCTACC	TGGGCCTCTTACACAAGAAAGGAG
her15.1	CACAAATTGCGAAAGCCAGTGG	AGCACCATCTAGTGTTTGAGCG
her9	GACAGCATCACCTATTGCTGGTG	TCTGAAGGACTGAGTTTGGAACCC
her2	CGCATCAACAAATGCATCGAGC	GCAGAAACGTACTGAGGTGCC
helt	ATGCGCGAGCACTTTATAAGCG	GGGTCTGGTGAGATTGTGCCTAA
tfe3a	GTCAATCTCATCAGCGTTGAGCC	CGATCTCTTCTTTGTTGGACCCC
tfe3b	TGCAAACCCATCTGGAAAACCC	TCTCCTTCATGAAAGCTCTGGCC
tfeb	ATTACATGCAGCATCGCATGCC	CCTTCTCCTCCTTTCAATCAGG
tcf25	CTGATAGGAGAGGCTGATGTGG	TGGGTTGATCTGTAGGAGAACCAC
tcf12	GGGCAGCATGTATTACTACAACGG	GTTTGAGGGGAAACTACTGCTGG
tfap4	ATGGTACCAGCTCAGAAGGTGC	GAGCGCTCTTTATCCAGCTGC
tcf21	TTTCACGAATCTGAGCTGCTGG	TGAGTCTCAGGAAGCTGTAGTCC
tcf24	GGTTGGAAGACAGTCGATCCG	ACAGGATGTAAGTAGCCATCGC
tcf20	GTTGATGGCCCTTTAAACACCC	CTGGCTATAGCATTCTGGAAAGGC
tfec	ATCTGGAGAACTCCAAGTACCACC	TGTTCCCAGCTCCTTGATCCTG
tcf3a	TCAAACGGGAAAAGCAGAGGC	CAGACTGACCCCAATGATCTGG
tcf3b	GTGACCTGTTGGATTTCAGTGC	TACACAGAGCCAGGTTTGGAG
bhlhe23	CTGAAATCGATCAGCAACGACACC	CGGAGAACGAGTTGCATTTCTCC
bhlha15	CAGACTTTACGCTGGAAACAGAGC	GTGCAGTGTGTGTTAGCTGTCC
bhlhe22	GACTGCGGGTATTGATCTTTCCG	TGCTCGTATGCGCTTAAACCC
bhlhe40	GACATGCAAGGAATGGACTTTCCC	GTCCTTTGAATGACAGGCACACAG
bhlha9	ATATCCATGACTCCAGCGAGCG	CCCAACATCACCAATCCGTCCATA
srebf1	GCCCTTCTCAATGACATCGACG	GAGTCGGCCTTAATGAACTGCG
srebf2	GAGTTTATGGACACCATGGACCC	TGCGGAGACGTCATGATACTCTG
usf1	GTTCCAGTCATTGAAGAAGGGGC	GCTCAACTTCATTGTGCTGAGC
usf1l	GGGTTCTGATCCTGAAGATTCTCC	CCATTGGTTGATCTTGTCCCTCC
usf2	CTCGATCAGAGCTTGGACACC	TGTGTACGAGGAGCAATGGTCC
nhlh2	GGCAAGATAACATCCAGTGCAC	CTGTGCGTTTTCGATTTGATCG
tal2	CAGGAAGGTGTTCACTAACACACG	CCTGCAGTGTCTTGCCTTGATAC
ahrrb	TGTCTGTATGCTGGGAGAAAGAGG	GTCACAACATCCTCATCAGTGTCC
epas1b	GCAGACGGAGTAAAGAGACAGAGG	CCGTTACACACCTTTAGATGACCC
hif1ab	AGGTGTTCTACGAGTTAGCACACC	GGCTCACAGATGAGCACAAGGTA

hif1aa	TTATGAGCTGTCCAGAGAACTCCC	CCTTCTCAACACCATCTGCTGT
ebf3	GGAACCACTATGAAAGAGGAACCG	CGTCTCGTTCCTGTTTCCACAG
ahrra	GAGGAAGCCCATACAGAAGCAG	CCCTGGAACTGCATAGTCAGGAA
ahr1a	GCAAAAGGAGGAAACCTGTCCAG	GGACTGTAGCACGTCCTTGATG
ahr2	CAGAAAATACCCAAACCACCACCC	CCTGGTGATATCACTGCTGCTCT
arntl1a	AGCTCTGCAGATCTGATCAGCAG	CCAGTTTTGGCATCGATGAGTCTC
arntl1b	GATCGTGTCAGAAAGCCTCAGG	GCTCATCGTCTGATAAAAAGGCCG
arntl2	AAACACAGGAGATGTGCTGGAG	GTCCAATTAACTCCGTCCGACTGT

Note: T7 primer sequence was included in all reverse primers
(5'-3': TAATACGACTCACTATAGGG)

C.2 IN SITU SCREEN TO IDENTIFY GENES IMPORTANT IN BEC-DRIVEN LIVER REGENERATION

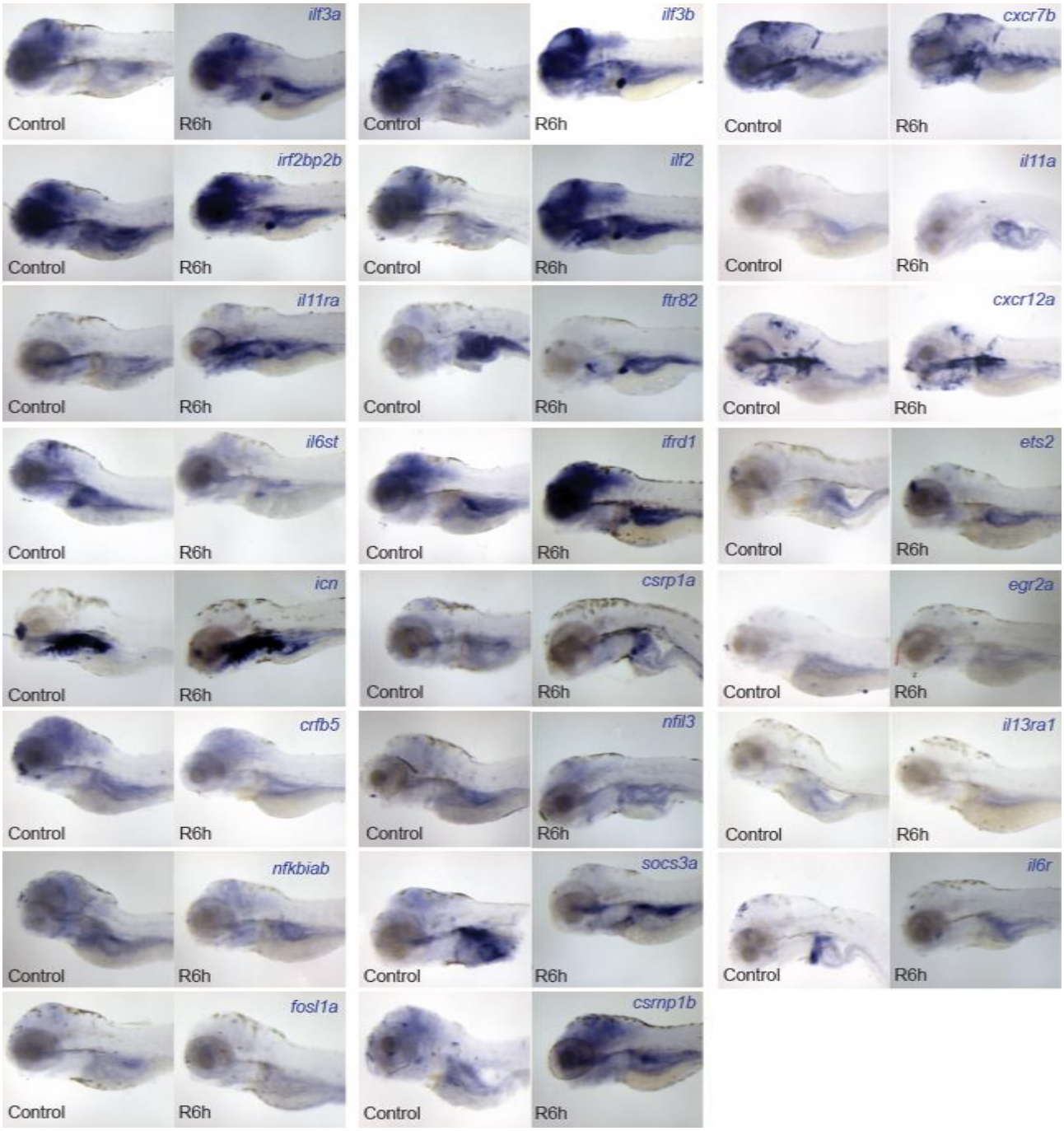

Figure 42: An *in situ* screen of factors involved in the inflammatory signaling pathways

5 dpf embryos treated with DMSO (Control) or ablated with Mtz and examined at R6h (R6h) processed for WISH analysis (n=10 for each stage/condition). In total, 24 probes were used. Zebrafish mutants of *il11ra*, *ftr82*, *ifrd1*, *ilf3a* and *ilf2* were obtained. None of these zebrafish mutants displayed any significant phenotype in our LPC/BEC-driven liver regeneration model.

Table 5: Primer sequences for R6h *in situ* probes in BEC-driven liver regeneration

Probe	Forward Primer	Reverse Primer
ilf2	TACGCAATGAGAGGAGATCGTG	GCTTCCAAGGTGGGCAGAATCTT
ilf3b	AACACTCGGCCATCTATCCC	GGTGAAGTCAGGTGAATGGTGA
ilf3a	AATCTCATGCAGGAGGGGTACC	GGTGAGCAGCACCAACTCTAA
il13ra	AAGCATGTCAGAGCTTCCTC	TGAAGATGGGAGGATGTGTC
crfb5	AACACCCAGTATGTGCTGCAC	GCTCTTTAGCCTGCCGAGTGT
irf2bp2b	TTTCAGGAGGGCAGATCACC	CCCTTCTGCGTCCACTCAT
il11ra	ATCCTCTTCTGTGAGCTCGTCAC	CGGTATCCTTCTGTTCACAGGGTT
fosl1a	AAGTACTCTGTGGCAGGATCAGG	GTCAGTTCTCGTCGACGGTTCCTA
socs3a	AAGACCTTCAGCTCCAAGGTG	GTGTGTCCGTTCACAGTCTTCCT
egr2a	TACTCGGCCCCAAAATCAACC	CATGCAGATGCGGCACTGAAA
csrp1a	TCATATCCACACACCTAGCAGG	GCACATTGCACATCGGAA
ifrd1	AACAGGGAAATGTCCAACCG	CGCAAGCTTGTCTGGCTTGAA
nfkiab	ATTGCTCTCAAACACCGACGAG	CCTTGTGTTAGGAGGCCGAA
ftr82	ATGGCTGAGCAAATGTCTCCAG	CTGACAGTACAGATGGCGCAA
ets2	ATGGAGTCGCTTTTACCTGG	CAGCTGCAGTCAGACACCTT
icn	ATCGTGACCACCAGAACCACC	CTCCTGAAAGTCCACAGAACCA
csrnp1b	TACTCAGAGTGGGACTCAGATGG	GGAAGGAGCCATCATCCACATT
nfil3	AAAGAGCCCCCATGCAGTGG	GGTGAGTGCTTGATGACCGAA
il6r	AATGTGTCGTTGGCTTCAGC	GCATGCACCTGTCTTCCAT

Note: T7 primer sequence was included in all reverse primers (5'-3': TAATACGACTCACTATAGGG). The plasmids for *cxcr7b* and *cxcr12a* were provided by Tatjana Piotrowski. The *gp130* (*il6st*) plasmid was provided by Dan Goldman. The *il11a* probe was provided by Ken Poss.

C.3 NF-KB IN BEC-DRIVEN LIVER REGENERATION

C.3.1 NF-κB Expression in BEC-driven Liver Regeneration

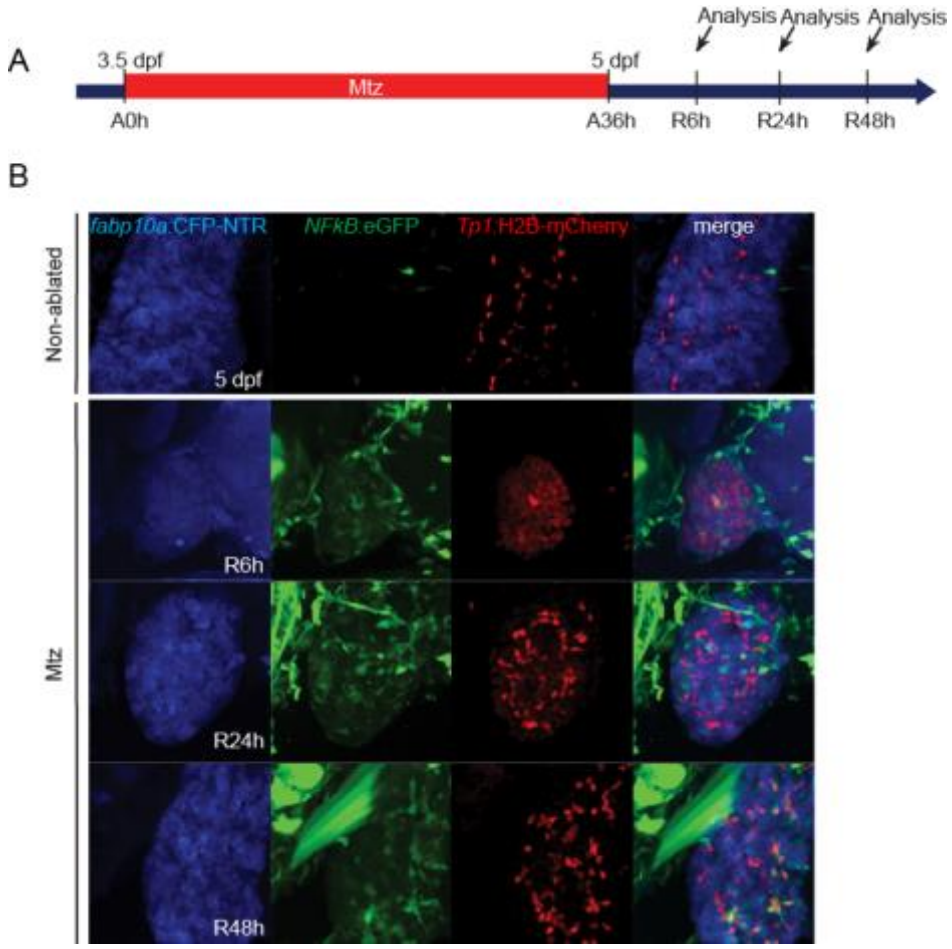

Figure 43: Expression of active NF-κB signaling in the liver during BEC-driven liver regeneration

(A) Scheme illustrating Mtz treatment (A, ablation) and liver regeneration (R, regeneration). **(B)** Confocal projection images revealing *fabp10a*:CFP-NTR (hepatocytes; blue), *Tp1*:H2B-mCherry (BECs; red) and *6xHsa.NF-κB*:eGFP (green) expression in non-ablated control embryos and at different stages of liver regeneration (R6h, R24h, R48h). NF-κB appears to be expressed in a subset of $mCherry^{+}$ cells during regeneration. In control embryos, NF-κB is mostly absent, only appearing in 1-2 endothelial cells (data not shown). At later stages, it appears to be maintained in mature BECs.

C.3.2 Inhibiting NF-κB in BEC-driven Liver Regeneration

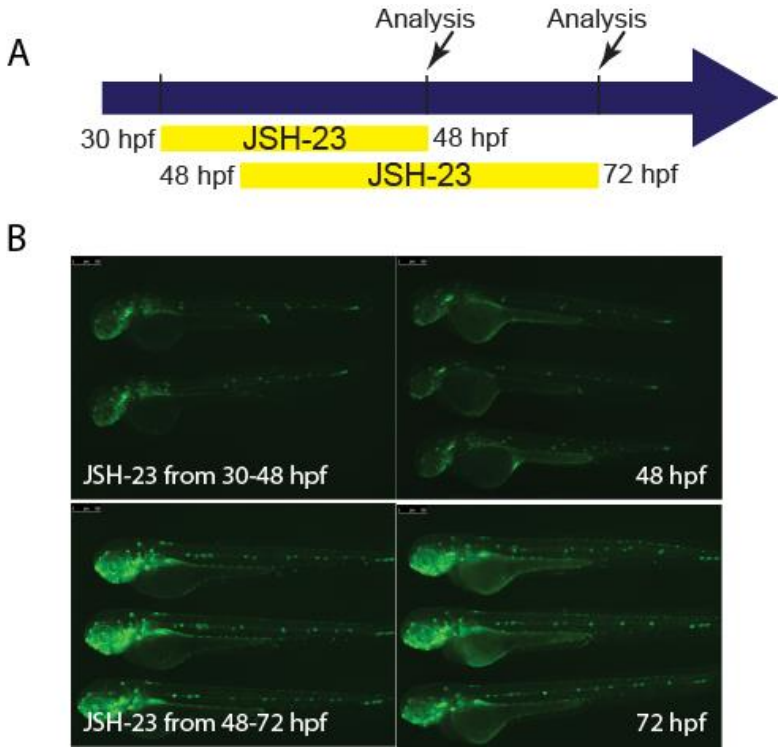

Figure 44: Inhibiting NF-κB signaling in zebrafish larvae during development

(A) Scheme illustrating the NF-κB inhibitor, JSH-23, treatment in non-injured, developing larvae. **(B)** Epifluorescence images of *6xHsa.NF-κB*:eGFP (green) expression at 48 hpf or 72 hpf in NF-κB-inhibited larvae. For 48 hpf and 72 hpf embryos, 400 μM JSH-23 was administered for either 18 hours (from 30 hpf to 48 hpf) or 24 hours (from 48 hpf to 72 hpf), respectively. Following washout, embryos were anesthetized and mounted in 3% methylcellulose for imaging. No difference in GFP activity was observed in either case. A better method of NF-κB inhibition is needed for further study.

BIBLIOGRAPHY

1. Mann, R.E., R.G. Smart, and R. Govoni, *The epidemiology of alcoholic liver disease.* Alcohol Res Health, 2003. **27**(3): p. 209-19.
2. Services, U.D.o.H.a.H., *Health Resources and Services Administration and Scientific Registry of Transplant Recipients*, in *OPTN & SRTR Annual Data Reccord 2011*. 2013, US Department of Health and Human Services.
3. Everhart, J.E. and C.E. Ruhl, *Burden of digestive diseases in the United States Part III: Liver, biliary tract, and pancreas.* Gastroenterology, 2009. **136**(4): p. 1134-44.
4. Jemal, A., et al., *Global cancer statistics.* CA Cancer J Clin, 2011. **61**(2): p. 69-90.
5. Ablain, J. and L.I. Zon, *Of fish and men: using zebrafish to fight human diseases.* Trends Cell Biol, 2013. **23**(12): p. 584-6.
6. Major, R.J. and K.D. Poss, *Zebrafish Heart Regeneration as a Model for Cardiac Tissue Repair*. Drug Discov Today Dis Models, 2007. **4**(4): p. 219-225.
7. Phillips, J.B. and M. Westerfield, *Zebrafish models in translational research: tipping the scales toward advancements in human health.* Dis Model Mech, 2014. **7**(7): p. 739-43.
8. Santoriello, C. and L.I. Zon, *Hooked! Modeling human disease in zebrafish.* J Clin Invest, 2012. **122**(7): p. 2337-43.
9. Wilkins, B.J. and M. Pack, *Zebrafish models of human liver development and disease.* Compr Physiol, 2013. **3**(3): p. 1213-30.
10. Peterson, R.T., et al., *Small molecule developmental screens reveal the logic and timing of vertebrate development.* Proc Natl Acad Sci U S A, 2000. **97**(24): p. 12965-9.
11. Rennekamp, A.J. and R.T. Peterson, *15 years of zebrafish chemical screening.* Curr Opin Chem Biol, 2015. **24**: p. 58-70.
12. Zhong, H. and S. Lin, *Chemical screening with zebrafish embryos.* Methods Mol Biol, 2011. **716**: p. 193-205.
13. North, T.E., et al., *Prostaglandin E2 regulates vertebrate haematopoietic stem cell homeostasis.* Nature, 2007. **447**(7147): p. 1007-11.
14. Nishiya, N., et al., *A zebrafish chemical suppressor screening identifies small molecule inhibitors of the Wnt/beta-catenin pathway.* Chem Biol, 2014. **21**(4): p. 530-40.
15. Cao, Y., et al., *Chemical modifier screen identifies HDAC inhibitors as suppressors of PKD models.* Proc Natl Acad Sci U S A, 2009. **106**(51): p. 21819-24.
16. North, T.E., et al., *PGE2-regulated wnt signaling and N-acetylcysteine are synergistically hepatoprotective in zebrafish acetaminophen injury*. Proc Natl Acad Sci U S A, 2010. **107**(40): p. 17315-20.
17. Seth, A., D.L. Stemple, and I. Barroso, *The emerging use of zebrafish to model metabolic disease.* Dis Model Mech, 2013. **6**(5): p. 1080-8.
18. Hoegg, S., et al., *Phylogenetic timing of the fish-specific genome duplication correlates with the diversification of teleost fish.* J Mol Evol, 2004. **59**(2): p. 190-203.
19. Howe, K., et al., *The zebrafish reference genome sequence and its relationship to the human genome.* Nature, 2013. **496**(7446): p. 498-503.

20. Choi, T.Y., et al., *Extensive conversion of hepatic biliary epithelial cells to hepatocytes after near total loss of hepatocytes in zebrafish.* Gastroenterology, 2014. **146**(3): p. 776-88.
21. Dorsky, R.I., L.C. Sheldahl, and R.T. Moon, *A transgenic Lef1/beta-catenin-dependent reporter is expressed in spatially restricted domains throughout zebrafish development.* Dev Biol, 2002. **241**(2): p. 229-37.
22. Huang, C.J., et al., *Germ-line transmission of a myocardium-specific GFP transgene reveals critical regulatory elements in the cardiac myosin light chain 2 promoter of zebrafish.* Dev Dyn, 2003. **228**(1): p. 30-40.
23. Lin, J.W., et al., *Differential requirement for ptf1a in endocrine and exocrine lineages of developing zebrafish pancreas.* Dev Biol, 2004. **270**(2): p. 474-86.
24. Parsons, M.J., et al., *Notch-responsive cells initiate the secondary transition in larval zebrafish pancreas.* Mech Dev, 2009. **126**(10): p. 898-912.
25. Schiavone, M., et al., *Zebrafish reporter lines reveal in vivo signaling pathway activities involved in pancreatic cancer.* Dis Model Mech, 2014. **7**(7): p. 883-94.
26. Pack, M., et al., *Mutations affecting development of zebrafish digestive organs.* Development, 1996. **123**: p. 321-8.
27. Sadler, K.C., et al., *Liver growth in the embryo and during liver regeneration in zebrafish requires the cell cycle regulator, uhrf1.* Proc Natl Acad Sci U S A, 2007. **104**(5): p. 1570-5.
28. Ober, E.A., et al., *Mesodermal Wnt2b signalling positively regulates liver specification.* Nature, 2006. **442**(7103): p. 688-91.
29. Dong, P.D., et al., *Fgf10 regulates hepatopancreatic ductal system patterning and differentiation.* Nat Genet, 2007. **39**(3): p. 397-402.
30. Bill, B.R., et al., *A primer for morpholino use in zebrafish.* Zebrafish, 2009. **6**(1): p. 69-77.
31. Rosen, J.N., M.F. Sweeney, and J.D. Mably, *Microinjection of zebrafish embryos to analyze gene function.* J Vis Exp, 2009(25).
32. Eisen, J.S. and J.C. Smith, *Controlling morpholino experiments: don't stop making antisense.* Development, 2008. **135**(10): p. 1735-43.
33. Huang, P., et al., *Heritable gene targeting in zebrafish using customized TALENs.* Nat Biotechnol, 2011. **29**(8): p. 699-700.
34. Hwang, W.Y., et al., *Efficient genome editing in zebrafish using a CRISPR-Cas system.* Nat Biotechnol, 2013. **31**(3): p. 227-9.
35. Boyer, J.L., *Bile formation and secretion.* Compr Physiol, 2013. **3**(3): p. 1035-78.
36. Carpentier, R., et al., *Embryonic ductal plate cells give rise to cholangiocytes, periportal hepatocytes, and adult liver progenitor cells.* Gastroenterology, 2011. **141**(4): p. 1432-8, 1438 e1-4.
37. Yin, C., et al., *Hand2 regulates extracellular matrix remodeling essential for gut-looping morphogenesis in zebrafish.* Dev Cell, 2010. **18**(6): p. 973-84.
38. Gebhardt, R. and M. Matz-Soja, *Liver zonation: Novel aspects of its regulation and its impact on homeostasis.* World J Gastroenterol, 2014. **20**(26): p. 8491-504.
39. Korzh, S., et al., *Requirement of vasculogenesis and blood circulation in late stages of liver growth in zebrafish.* BMC Dev Biol, 2008. **8**: p. 84.
40. McLin, V.A., S.A. Rankin, and A.M. Zorn, *Repression of Wnt/beta-catenin signaling in the anterior endoderm is essential for liver and pancreas development.* Development, 2007. **134**(12): p. 2207-17.

41. Zaret, K.S., *Regulatory phases of early liver development: paradigms of organogenesis.* Nat Rev Genet, 2002. **3**(7): p. 499-512.
42. Tremblay, K.D. and K.S. Zaret, *Distinct populations of endoderm cells converge to generate the embryonic liver bud and ventral foregut tissues.* Dev Biol, 2005. **280**(1): p. 87-99.
43. Zorn, A.M. and J.M. Wells, *Vertebrate endoderm development and organ formation.* Annu Rev Cell Dev Biol, 2009. **25**: p. 221-51.
44. Bossard, P. and K.S. Zaret, *GATA transcription factors as potentiators of gut endoderm differentiation.* Development, 1998. **125**(24): p. 4909-17.
45. Caravaca, J.M., et al., *Bookmarking by specific and nonspecific binding of FoxA1 pioneer factor to mitotic chromosomes.* Genes Dev, 2013. **27**(3): p. 251-60.
46. Cirillo, L.A., et al., *Opening of compacted chromatin by early developmental transcription factors HNF3 (FoxA) and GATA-4.* Mol Cell, 2002. **9**(2): p. 279-89.
47. Liu, J.K., Y. Bergman, and K.S. Zaret, *The mouse albumin promoter and a distal upstream site are simultaneously DNase I hypersensitive in liver chromatin and bind similar liver-abundant factors in vitro.* Genes Dev, 1988. **2**(5): p. 528-41.
48. Gao, X., et al., *Distinct functions are implicated for the GATA-4, -5, and -6 transcription factors in the regulation of intestine epithelial cell differentiation.* Mol Cell Biol, 1998. **18**(5): p. 2901-11.
49. Molkentin, J.D., *The zinc finger-containing transcription factors GATA-4, -5, and -6. Ubiquitously expressed regulators of tissue-specific gene expression.* J Biol Chem, 2000. **275**(50): p. 38949-52.
50. Reiter, J.F., Y. Kikuchi, and D.Y. Stainier, *Multiple roles for Gata5 in zebrafish endoderm formation.* Development, 2001. **128**(1): p. 125-35.
51. Kuo, C.T., et al., *GATA4 transcription factor is required for ventral morphogenesis and heart tube formation.* Genes Dev, 1997. **11**(8): p. 1048-60.
52. Molkentin, J.D., et al., *Requirement of the transcription factor GATA4 for heart tube formation and ventral morphogenesis.* Genes Dev, 1997. **11**(8): p. 1061-72.
53. Watt, A.J., et al., *Development of the mammalian liver and ventral pancreas is dependent on GATA4.* BMC Dev Biol, 2007. **7**: p. 37.
54. Zhao, R., et al., *GATA6 is essential for embryonic development of the liver but dispensable for early heart formation.* Mol Cell Biol, 2005. **25**(7): p. 2622-31.
55. Holtzinger, A. and T. Evans, *Gata4 regulates the formation of multiple organs.* Development, 2005. **132**(17): p. 4005-14.
56. Kaestner, K.H., et al., *Inactivation of the winged helix transcription factor HNF3alpha affects glucose homeostasis and islet glucagon gene expression in vivo.* Genes Dev, 1999. **13**(4): p. 495-504.
57. Shen, W., et al., *Foxa3 (hepatocyte nuclear factor 3gamma) is required for the regulation of hepatic GLUT2 expression and the maintenance of glucose homeostasis during a prolonged fast.* J Biol Chem, 2001. **276**(46): p. 42812-7.
58. Ang, S.L. and J. Rossant, *HNF-3 beta is essential for node and notochord formation in mouse development.* Cell, 1994. **78**(4): p. 561-74.
59. Weinstein, D.C., et al., *The winged-helix transcription factor HNF-3 beta is required for notochord development in the mouse embryo.* Cell, 1994. **78**(4): p. 575-88.
60. Lee, C.S., et al., *The initiation of liver development is dependent on Foxa transcription factors.* Nature, 2005. **435**(7044): p. 944-7.

61. Margagliotti, S., et al., *Role of metalloproteinases at the onset of liver development.* Dev Growth Differ, 2008. **50**(5): p. 331-8.
62. Wallace, K.N. and M. Pack, *Unique and conserved aspects of gut development in zebrafish.* Dev Biol, 2003. **255**(1): p. 12-29.
63. Wallace, K.N., et al., *Zebrafish hhex regulates liver development and digestive organ chirality.* Genesis, 2001. **30**(3): p. 141-3.
64. Korzh, S., A. Emelyanov, and V. Korzh, *Developmental analysis of ceruloplasmin gene and liver formation in zebrafish.* Mech Dev, 2001. **103**(1-2): p. 137-9.
65. Mudumana, S.P., et al., *Expression analyses of zebrafish transferrin, ifabp, and elastaseB mRNAs as differentiation markers for the three major endodermal organs: liver, intestine, and exocrine pancreas.* Dev Dyn, 2004. **230**(1): p. 165-73.
66. Lorent, K., et al., *Reiterative use of the notch signal during zebrafish intrahepatic biliary development.* Dev Dyn, 2010. **239**(3): p. 855-64.
67. Lorent, K., et al., *Inhibition of Jagged-mediated Notch signaling disrupts zebrafish biliary development and generates multi-organ defects compatible with an Alagille syndrome phenocopy.* Development, 2004. **131**(22): p. 5753-66.
68. Zhang, W., et al., *Regulation of Hex gene expression and initial stages of avian hepatogenesis by Bmp and Fgf signaling.* Dev Biol, 2004. **268**(2): p. 312-26.
69. Jung, J., et al., *Initiation of mammalian liver development from endoderm by fibroblast growth factors.* Science, 1999. **284**(5422): p. 1998-2003.
70. Shin, D., et al., *Bmp and Fgf signaling are essential for liver specification in zebrafish.* Development, 2007. **134**(11): p. 2041-50.
71. Berg, T., et al., *Fibroblast growth factor 10 is critical for liver growth during embryogenesis and controls hepatoblast survival via beta-catenin activation.* Hepatology, 2007. **46**(4): p. 1187-97.
72. Mavila, N., et al., *Fibroblast growth factor receptor-mediated activation of AKT-beta-catenin-CBP pathway regulates survival and proliferation of murine hepatoblasts and hepatic tumor initiating stem cells.* PLoS One, 2012. **7**(11): p. e50401.
73. Shin, D., et al., *Restriction of hepatic competence by Fgf signaling.* Development, 2011. **138**(7): p. 1339-48.
74. Zaret, K.S., *Genetic programming of liver and pancreas progenitors: lessons for stem-cell differentiation.* Nat Rev Genet, 2008. **9**(5): p. 329-40.
75. Serls, A.E., et al., *Different thresholds of fibroblast growth factors pattern the ventral foregut into liver and lung.* Development, 2005. **132**(1): p. 35-47.
76. Rossi, J.M., et al., *Distinct mesodermal signals, including BMPs from the septum transversum mesenchyme, are required in combination for hepatogenesis from the endoderm.* Genes Dev, 2001. **15**(15): p. 1998-2009.
77. Poulain, M. and E.A. Ober, *Interplay between Wnt2 and Wnt2bb controls multiple steps of early foregut-derived organ development.* Development, 2011. **138**(16): p. 3557-68.
78. Goss, A.M., et al., *Wnt2/2b and beta-catenin signaling are necessary and sufficient to specify lung progenitors in the foregut.* Dev Cell, 2009. **17**(2): p. 290-8.
79. Tsukiyama, T. and T.P. Yamaguchi, *Mice lacking Wnt2b are viable and display a postnatal olfactory bulb phenotype.* Neurosci Lett, 2012. **512**(1): p. 48-52.
80. Hurlstone, A.F., et al., *The Wnt/beta-catenin pathway regulates cardiac valve formation.* Nature, 2003. **425**(6958): p. 633-7.

81. Decaens, T., et al., *Stabilization of beta-catenin affects mouse embryonic liver growth and hepatoblast fate.* Hepatology, 2008. **47**(1): p. 247-58.
82. Goessling, W., et al., *APC mutant zebrafish uncover a changing temporal requirement for wnt signaling in liver development.* Dev Biol, 2008. **320**(1): p. 161-74.
83. Monga, S.P., et al., *Beta-catenin antisense studies in embryonic liver cultures: role in proliferation, apoptosis, and lineage specification.* Gastroenterology, 2003. **124**(1): p. 202-16.
84. Bogue, C.W., et al., *Hex expression suggests a role in the development and function of organs derived from foregut endoderm.* Dev Dyn, 2000. **219**(1): p. 84-9.
85. Bort, R., et al., *Hex homeobox gene-dependent tissue positioning is required for organogenesis of the ventral pancreas.* Development, 2004. **131**(4): p. 797-806.
86. Bort, R., et al., *Hex homeobox gene controls the transition of the endoderm to a pseudostratified, cell emergent epithelium for liver bud development.* Dev Biol, 2006. **290**(1): p. 44-56.
87. Martinez Barbera, J.P., et al., *The homeobox gene Hex is required in definitive endodermal tissues for normal forebrain, liver and thyroid formation.* Development, 2000. **127**(11): p. 2433-45.
88. Hunter, M.P., et al., *The homeobox gene Hhex is essential for proper hepatoblast differentiation and bile duct morphogenesis.* Dev Biol, 2007. **308**(2): p. 355-67.
89. Sosa-Pineda, B., J.T. Wigle, and G. Oliver, *Hepatocyte migration during liver development requires Prox1.* Nat Genet, 2000. **25**(3): p. 254-5.
90. Seth, A., et al., *Prox1 ablation in hepatic progenitors causes defective hepatocyte specification and increases biliary cell commitment.* Development, 2014. **141**(3): p. 538-47.
91. Tchorz, J.S., et al., *Notch2 signaling promotes biliary epithelial cell fate specification and tubulogenesis during bile duct development in mice.* Hepatology, 2009. **50**(3): p. 871-9.
92. Zong, Y., et al., *Notch signaling controls liver development by regulating biliary differentiation.* Development, 2009. **136**(10): p. 1727-39.
93. Ader, T., et al., *Transcriptional profiling implicates TGFbeta/BMP and Notch signaling pathways in ductular differentiation of fetal murine hepatoblasts.* Mech Dev, 2006. **123**(2): p. 177-94.
94. Li, L., et al., *Alagille syndrome is caused by mutations in human Jagged1, which encodes a ligand for Notch1.* Nat Genet, 1997. **16**(3): p. 243-51.
95. McDaniell, R., et al., *NOTCH2 mutations cause Alagille syndrome, a heterogeneous disorder of the notch signaling pathway.* Am J Hum Genet, 2006. **79**(1): p. 169-73.
96. Farber, E., *Similarities in the sequence of early histological changes induced in the liver of the rat by ethionine, 2-acetylamino-fluorene, and 3'-methyl-4-dimethylaminoazobenzene.* Cancer Res, 1956. **16**(2): p. 142-8.
97. Roskams, T.A., et al., *Nomenclature of the finer branches of the biliary tree: canals, ductules, and ductular reactions in human livers.* Hepatology, 2004. **39**(6): p. 1739-45.
98. Bucher, N.L.R. and R.A. Malt, *Regeneration of liver and kidney*. [1st ed. New England journal of medicine medical progress series. 1971, Boston,: Little. xiv, 278 p.
99. Duncan, A.W., C. Dorrell, and M. Grompe, *Stem cells and liver regeneration.* Gastroenterology, 2009. **137**(2): p. 466-81.
100. Zajicek, G., R. Oren, and M. Weinreb, Jr., *The streaming liver.* Liver, 1985. **5**(6): p. 293-300.

101. Furuyama, K., et al., *Continuous cell supply from a Sox9-expressing progenitor zone in adult liver, exocrine pancreas and intestine.* Nat Genet, 2011. **43**(1): p. 34-41.
102. Espanol-Suner, R., et al., *Liver progenitor cells yield functional hepatocytes in response to chronic liver injury in mice.* Gastroenterology, 2012. **143**(6): p. 1564-1575 e7.
103. Higgins GM, A.R., *Experimental pathology of the liver - Restoration of the liver of the white rat following partial surgical removal.* Arch Pathol, 1931. **12**: p. 186-202.
104. Bucher, N.L. and M.N. Swaffield, *Rate of incorporation of [6-14C]orotic acid into uridine 5'-triphosphate and cytidine 5'-triphosphate and nuclear ribonucleic acid in regenerating rat liver.* Biochim Biophys Acta, 1965. **108**(4): p. 551-67.
105. Grisham, J.W., *A morphologic study of deoxyribonucleic acid synthesis and cell proliferation in regenerating rat liver; autoradiography with thymidine-H3.* Cancer Res, 1962. **22**: p. 842-9.
106. Miyaoka, Y., et al., *Hypertrophy and unconventional cell division of hepatocytes underlie liver regeneration.* Curr Biol, 2012. **22**(13): p. 1166-75.
107. Lindroos, P.M., R. Zarnegar, and G.K. Michalopoulos, *Hepatocyte growth factor (hepatopoietin A) rapidly increases in plasma before DNA synthesis and liver regeneration stimulated by partial hepatectomy and carbon tetrachloride administration.* Hepatology, 1991. **13**(4): p. 743-50.
108. Stolz, D.B., et al., *Growth factor signal transduction immediately after two-thirds partial hepatectomy in the rat.* Cancer Res, 1999. **59**(16): p. 3954-60.
109. Blindenbacher, A., et al., *Interleukin 6 is important for survival after partial hepatectomy in mice.* Hepatology, 2003. **38**(3): p. 674-82.
110. Cressman, D.E., R.H. Diamond, and R. Taub, *Rapid activation of the Stat3 transcription complex in liver regeneration.* Hepatology, 1995. **21**(5): p. 1443-9.
111. Yamada, Y., et al., *Analysis of liver regeneration in mice lacking type 1 or type 2 tumor necrosis factor receptor: requirement for type 1 but not type 2 receptor.* Hepatology, 1998. **28**(4): p. 959-70.
112. Michalopoulos, G.K., *Liver regeneration.* J Cell Physiol, 2007. **213**(2): p. 286-300.
113. Block, G.D., et al., *Population expansion, clonal growth, and specific differentiation patterns in primary cultures of hepatocytes induced by HGF/SF, EGF and TGF alpha in a chemically defined (HGM) medium.* J Cell Biol, 1996. **132**(6): p. 1133-49.
114. Paranjpe, S., et al., *Combined systemic elimination of MET and epidermal growth factor receptor signaling completely abolishes liver regeneration and leads to liver decompensation.* Hepatology, 2016. **64**(5): p. 1711-1724.
115. Kan, N.G., D. Junghans, and J.C. Izpisua Belmonte, *Compensatory growth mechanisms regulated by BMP and FGF signaling mediate liver regeneration in zebrafish after partial hepatectomy.* FASEB J, 2009. **23**(10): p. 3516-25.
116. Okabe, M., et al., *Potential hepatic stem cells reside in EpCAM+ cells of normal and injured mouse liver.* Development, 2009. **136**(11): p. 1951-60.
117. Paku, S., et al., *Origin and structural evolution of the early proliferating oval cells in rat liver.* Am J Pathol, 2001. **158**(4): p. 1313-23.
118. Dorrell, C., et al., *Prospective isolation of a bipotential clonogenic liver progenitor cell in adult mice.* Genes Dev, 2011. **25**(11): p. 1193-203.
119. Huch, M., et al., *In vitro expansion of single Lgr5+ liver stem cells induced by Wnt-driven regeneration.* Nature, 2013. **494**(7436): p. 247-50.

120. Sackett, S.D., et al., *Foxl1 is a marker of bipotential hepatic progenitor cells in mice.* Hepatology, 2009. **49**(3): p. 920-9.
121. Suzuki, A., et al., *Flow cytometric isolation and clonal identification of self-renewing bipotent hepatic progenitor cells in adult mouse liver.* Hepatology, 2008. **48**(6): p. 1964-78.
122. Yovchev, M.I., et al., *Novel hepatic progenitor cell surface markers in the adult rat liver.* Hepatology, 2007. **45**(1): p. 139-49.
123. Dorrell, C., et al., *Surface markers for the murine oval cell response.* Hepatology, 2008. **48**(4): p. 1282-91.
124. Kamiya, A., et al., *Enrichment and clonal culture of progenitor cells during mouse postnatal liver development in mice.* Gastroenterology, 2009. **137**(3): p. 1114-26, 1126 e1-14.
125. Alison, M.R., M.H. Golding, and C.E. Sarraf, *Pluripotential liver stem cells: facultative stem cells located in the biliary tree.* Cell Prolif, 1996. **29**(7): p. 373-402.
126. Michalopoulos, G.K., L. Barua, and W.C. Bowen, *Transdifferentiation of rat hepatocytes into biliary cells after bile duct ligation and toxic biliary injury.* Hepatology, 2005. **41**(3): p. 535-44.
127. Nishikawa, Y., et al., *Transdifferentiation of mature rat hepatocytes into bile duct-like cells in vitro.* Am J Pathol, 2005. **166**(4): p. 1077-88.
128. Evarts, R.P., et al., *A precursor-product relationship exists between oval cells and hepatocytes in rat liver.* Carcinogenesis, 1987. **8**(11): p. 1737-40.
129. Akhurst, B., et al., *A modified choline-deficient, ethionine-supplemented diet protocol effectively induces oval cells in mouse liver.* Hepatology, 2001. **34**(3): p. 519-22.
130. Preisegger, K.H., et al., *Atypical ductular proliferation and its inhibition by transforming growth factor beta1 in the 3,5-diethoxycarbonyl-1,4-dihydrocollidine mouse model for chronic alcoholic liver disease.* Lab Invest, 1999. **79**(2): p. 103-9.
131. Lu, W.Y., et al., *Hepatic progenitor cells of biliary origin with liver repopulation capacity.* Nat Cell Biol, 2015. **17**(8): p. 971-83.
132. He, J., et al., *Regeneration of liver after extreme hepatocyte loss occurs mainly via biliary transdifferentiation in zebrafish.* Gastroenterology, 2014. **146**(3): p. 789-800 e8.
133. Ohlson, L.C., L. Koroxenidou, and I.P. Hallstrom, *Inhibition of in vivo rat liver regeneration by 2-acetylaminofluorene affects the regulation of cell cycle-related proteins.* Hepatology, 1998. **27**(3): p. 691-6.
134. Ochoa-Callejero, L., et al., *Maraviroc, a CCR5 antagonist, prevents development of hepatocellular carcinoma in a mouse model.* PLoS One, 2013. **8**(1): p. e53992.
135. Jelnes, P., et al., *Remarkable heterogeneity displayed by oval cells in rat and mouse models of stem cell-mediated liver regeneration.* Hepatology, 2007. **45**(6): p. 1462-70.
136. Bird, T.G., et al., *Bone marrow injection stimulates hepatic ductular reactions in the absence of injury via macrophage-mediated TWEAK signaling.* Proc Natl Acad Sci U S A, 2013. **110**(16): p. 6542-7.
137. Jakubowski, A., et al., *TWEAK induces liver progenitor cell proliferation.* J Clin Invest, 2005. **115**(9): p. 2330-40.
138. Tirnitz-Parker, J.E., et al., *Tumor necrosis factor-like weak inducer of apoptosis is a mitogen for liver progenitor cells.* Hepatology, 2010. **52**(1): p. 291-302.
139. Takase, H.M., et al., *FGF7 is a functional niche signal required for stimulation of adult liver progenitor cells that support liver regeneration.* Genes Dev, 2013. **27**(2): p. 169-81.

140. Ishikawa, T., et al., *Hepatocyte growth factor/c-met signaling is required for stem-cell-mediated liver regeneration in mice.* Hepatology, 2012. **55**(4): p. 1215-26.
141. Kitade, M., et al., *Specific fate decisions in adult hepatic progenitor cells driven by MET and EGFR signaling.* Genes Dev, 2013. **27**(15): p. 1706-17.
142. Boulter, L., et al., *Macrophage-derived Wnt opposes Notch signaling to specify hepatic progenitor cell fate in chronic liver disease.* Nat Med, 2012. **18**(4): p. 572-9.
143. Ko, S., et al., *Bromodomain and extraterminal (BET) proteins regulate biliary-driven liver regeneration.* J Hepatol, 2016. **64**(2): p. 316-25.
144. Stueck, A.E. and I.R. Wanless, *Hepatocyte buds derived from progenitor cells repopulate regions of parenchymal extinction in human cirrhosis.* Hepatology, 2015. **61**(5): p. 1696-707.
145. Curado, S., et al., *Conditional targeted cell ablation in zebrafish: a new tool for regeneration studies.* Dev Dyn, 2007. **236**(4): p. 1025-35.
146. Anlezark, G.M., et al., *The bioactivation of 5-(aziridin-1-yl)-2,4-dinitrobenzamide (CB1954)--I. Purification and properties of a nitroreductase enzyme from Escherichia coli--a potential enzyme for antibody-directed enzyme prodrug therapy (ADEPT).* Biochem Pharmacol, 1992. **44**(12): p. 2289-95.
147. Curado, S., D.Y. Stainier, and R.M. Anderson, *Nitroreductase-mediated cell/tissue ablation in zebrafish: a spatially and temporally controlled ablation method with applications in developmental and regeneration studies.* Nat Protoc, 2008. **3**(6): p. 948-54.
148. Lindmark, D.G. and M. Muller, *Antitrichomonad action, mutagenicity, and reduction of metronidazole and other nitroimidazoles.* Antimicrob Agents Chemother, 1976. **10**(3): p. 476-82.
149. Choi, T.Y., et al., *Hepatocyte-specific ablation in zebrafish to study biliary-driven liver regeneration.* J Vis Exp, 2015(99): p. e52785.
150. Urist, M.R., *Bone: formation by autoinduction.* Science, 1965. **150**(3698): p. 893-9.
151. Eblaghie, M.C., et al., *Evidence that autocrine signaling through Bmpr1a regulates the proliferation, survival and morphogenetic behavior of distal lung epithelial cells.* Dev Biol, 2006. **291**(1): p. 67-82.
152. Luo, G., et al., *BMP-7 is an inducer of nephrogenesis, and is also required for eye development and skeletal patterning.* Genes Dev, 1995. **9**(22): p. 2808-20.
153. Miyazaki, Y., et al., *Bone morphogenetic protein 4 regulates the budding site and elongation of the mouse ureter.* J Clin Invest, 2000. **105**(7): p. 863-73.
154. Solloway, M.J. and E.J. Robertson, *Early embryonic lethality in Bmp5;Bmp7 double mutant mice suggests functional redundancy within the 60A subgroup.* Development, 1999. **126**(8): p. 1753-68.
155. Miyazono, K. and K. Miyazawa, *Id: a target of BMP signaling.* Sci STKE, 2002. **2002**(151): p. pe40.
156. Yamada, M., et al., *Expression of chick Tbx-2, Tbx-3, and Tbx-5 genes during early heart development: evidence for BMP2 induction of Tbx2.* Dev Biol, 2000. **228**(1): p. 95-105.
157. Derynck, R. and Y.E. Zhang, *Smad-dependent and Smad-independent pathways in TGF-beta family signalling.* Nature, 2003. **425**(6958): p. 577-84.
158. Yamaguchi, K., et al., *Identification of a member of the MAPKKK family as a potential mediator of TGF-beta signal transduction.* Science, 1995. **270**(5244): p. 2008-11.
159. Zhang, Y.E., *Non-Smad pathways in TGF-beta signaling.* Cell Res, 2009. **19**(1): p. 128-39.

160. Wang, R.N., et al., *Bone Morphogenetic Protein (BMP) signaling in development and human diseases.* Genes Dis, 2014. **1**(1): p. 87-105.
161. Batts, L.E., et al., *Bmp signaling is required for intestinal growth and morphogenesis.* Dev Dyn, 2006. **235**(6): p. 1563-70.
162. Jiao, K., et al., *An essential role of Bmp4 in the atrioventricular septation of the mouse heart.* Genes Dev, 2003. **17**(19): p. 2362-7.
163. Winnier, G., et al., *Bone morphogenetic protein-4 is required for mesoderm formation and patterning in the mouse.* Genes Dev, 1995. **9**(17): p. 2105-16.
164. Zhang, H. and A. Bradley, *Mice deficient for BMP2 are nonviable and have defects in amnion/chorion and cardiac development.* Development, 1996. **122**(10): p. 2977-86.
165. Gualdi, R., et al., *Hepatic specification of the gut endoderm in vitro: cell signaling and transcriptional control.* Genes Dev, 1996. **10**(13): p. 1670-82.
166. Deutsch, G., et al., *A bipotential precursor population for pancreas and liver within the embryonic endoderm.* Development, 2001. **128**(6): p. 871-81.
167. Chung, W.S., C.H. Shin, and D.Y. Stainier, *Bmp2 signaling regulates the hepatic versus pancreatic fate decision.* Dev Cell, 2008. **15**(5): p. 738-48.
168. Sugimoto, H., et al., *BMP-7 functions as a novel hormone to facilitate liver regeneration.* FASEB J, 2007. **21**(1): p. 256-64.
169. Do, N., et al., *BMP4 is a novel paracrine inhibitor of liver regeneration.* Am J Physiol Gastrointest Liver Physiol, 2012. **303**(11): p. G1220-7.
170. Tsugawa, D., et al., *Specific activin receptor-like kinase 3 inhibitors enhance liver regeneration.* J Pharmacol Exp Ther, 2014. **351**(3): p. 549-58.
171. Norton, J.D., *ID helix-loop-helix proteins in cell growth, differentiation and tumorigenesis.* J Cell Sci, 2000. **113 (Pt 22)**: p. 3897-905.
172. Benezra, R., et al., *The protein Id: a negative regulator of helix-loop-helix DNA binding proteins.* Cell, 1990. **61**(1): p. 49-59.
173. Perk, J., A. Iavarone, and R. Benezra, *Id family of helix-loop-helix proteins in cancer.* Nat Rev Cancer, 2005. **5**(8): p. 603-14.
174. Bain, G., et al., *E2A proteins are required for proper B cell development and initiation of immunoglobulin gene rearrangements.* Cell, 1994. **79**(5): p. 885-92.
175. Lee, J.E., et al., *Conversion of Xenopus ectoderm into neurons by NeuroD, a basic helix-loop-helix protein.* Science, 1995. **268**(5212): p. 836-44.
176. Zhuang, Y., P. Soriano, and H. Weintraub, *The helix-loop-helix gene E2A is required for B cell formation.* Cell, 1994. **79**(5): p. 875-84.
177. Jen, Y., H. Weintraub, and R. Benezra, *Overexpression of Id protein inhibits the muscle differentiation program: in vivo association of Id with E2A proteins.* Genes Dev, 1992. **6**(8): p. 1466-79.
178. Massari, M.E. and C. Murre, *Helix-loop-helix proteins: regulators of transcription in eucaryotic organisms.* Mol Cell Biol, 2000. **20**(2): p. 429-40.
179. Meyer, K.B., et al., *Repression of the immunoglobulin heavy chain 3' enhancer by helix-loop-helix protein Id3 via a functionally important E47/E12 binding site: implications for developmental control of enhancer function.* Eur J Immunol, 1995. **25**(6): p. 1770-7.
180. Sun, X.H., et al., *Id proteins Id1 and Id2 selectively inhibit DNA binding by one class of helix-loop-helix proteins.* Mol Cell Biol, 1991. **11**(11): p. 5603-11.
181. Fong, S., et al., *Id-1 as a molecular target in therapy for breast cancer cell invasion and metastasis.* Proc Natl Acad Sci U S A, 2003. **100**(23): p. 13543-8.

182. Iavarone, A., et al., *The helix-loop-helix protein Id-2 enhances cell proliferation and binds to the retinoblastoma protein.* Genes Dev, 1994. **8**(11): p. 1270-84.
183. Lasorella, A., et al., *Id2 is a retinoblastoma protein target and mediates signalling by Myc oncoproteins.* Nature, 2000. **407**(6804): p. 592-8.
184. Ohtani, N., et al., *Opposing effects of Ets and Id proteins on p16INK4a expression during cellular senescence.* Nature, 2001. **409**(6823): p. 1067-70.
185. Christy, B.A., et al., *An Id-related helix-loop-helix protein encoded by a growth factor-inducible gene.* Proc Natl Acad Sci U S A, 1991. **88**(5): p. 1815-9.
186. Riechmann, V., I. van Cruchten, and F. Sablitzky, *The expression pattern of Id4, a novel dominant negative helix-loop-helix protein, is distinct from Id1, Id2 and Id3.* Nucleic Acids Res, 1994. **22**(5): p. 749-55.
187. Fajerman, I., A.L. Schwartz, and A. Ciechanover, *Degradation of the Id2 developmental regulator: targeting via N-terminal ubiquitination.* Biochem Biophys Res Commun, 2004. **314**(2): p. 505-12.
188. Florio, M., et al., *Id2 promotes apoptosis by a novel mechanism independent of dimerization to basic helix-loop-helix factors.* Mol Cell Biol, 1998. **18**(9): p. 5435-44.
189. Kurooka, H. and Y. Yokota, *Nucleo-cytoplasmic shuttling of Id2, a negative regulator of basic helix-loop-helix transcription factors.* J Biol Chem, 2005. **280**(6): p. 4313-20.
190. Lasorella, A., et al., *Id2 is critical for cellular proliferation and is the oncogenic effector of N-myc in human neuroblastoma.* Cancer Res, 2002. **62**(1): p. 301-6.
191. Kleeff, J., et al., *The helix-loop-helix protein Id2 is overexpressed in human pancreatic cancer.* Cancer Res, 1998. **58**(17): p. 3769-72.
192. Coppe, J.P., et al., *Id-1 and Id-2 proteins as molecular markers for human prostate cancer progression.* Clin Cancer Res, 2004. **10**(6): p. 2044-51.
193. Uribe, R.A. and J.M. Gross, *Id2a influences neuron and glia formation in the zebrafish retina by modulating retinoblast cell cycle kinetics.* Development, 2010. **137**(22): p. 3763-74.
194. Oates, A.C., et al., *Zebrafish stat3 is expressed in restricted tissues during embryogenesis and stat1 rescues cytokine signaling in a STAT1-deficient human cell line.* Dev Dyn, 1999. **215**(4): p. 352-70.
195. Darnell, J.E., Jr., *STATs and gene regulation.* Science, 1997. **277**(5332): p. 1630-5.
196. Wen, Z. and J.E. Darnell, Jr., *Mapping of Stat3 serine phosphorylation to a single residue (727) and evidence that serine phosphorylation has no influence on DNA binding of Stat1 and Stat3.* Nucleic Acids Res, 1997. **25**(11): p. 2062-7.
197. Liu, L., K.M. McBride, and N.C. Reich, *STAT3 nuclear import is independent of tyrosine phosphorylation and mediated by importin-alpha3.* Proc Natl Acad Sci U S A, 2005. **102**(23): p. 8150-5.
198. Hirano, T., K. Ishihara, and M. Hibi, *Roles of STAT3 in mediating the cell growth, differentiation and survival signals relayed through the IL-6 family of cytokine receptors.* Oncogene, 2000. **19**(21): p. 2548-56.
199. Radaeva, S., et al., *Interferon-alpha activates multiple STAT signals and down-regulates c-Met in primary human hepatocytes.* Gastroenterology, 2002. **122**(4): p. 1020-34.
200. Niemand, C., et al., *Activation of STAT3 by IL-6 and IL-10 in primary human macrophages is differentially modulated by suppressor of cytokine signaling 3.* J Immunol, 2003. **170**(6): p. 3263-72.

201. Yasukawa, H., et al., *IL-6 induces an anti-inflammatory response in the absence of SOCS3 in macrophages.* Nat Immunol, 2003. **4**(6): p. 551-6.
202. Narazaki, M., et al., *Three distinct domains of SSI-1/SOCS-1/JAB protein are required for its suppression of interleukin 6 signaling.* Proc Natl Acad Sci U S A, 1998. **95**(22): p. 13130-4.
203. Frantsve, J., et al., *Socs-1 inhibits TEL-JAK2-mediated transformation of hematopoietic cells through inhibition of JAK2 kinase activity and induction of proteasome-mediated degradation.* Mol Cell Biol, 2001. **21**(10): p. 3547-57.
204. Baetz, A., et al., *Suppressor of cytokine signaling (SOCS) proteins indirectly regulate toll-like receptor signaling in innate immune cells.* J Biol Chem, 2004. **279**(52): p. 54708-15.
205. He, Y., et al., *SOCS1 inhibits tumor necrosis factor-induced activation of ASK1-JNK inflammatory signaling by mediating ASK1 degradation.* J Biol Chem, 2006. **281**(9): p. 5559-66.
206. Kamura, T., et al., *VHL-box and SOCS-box domains determine binding specificity for Cul2-Rbx1 and Cul5-Rbx2 modules of ubiquitin ligases.* Genes Dev, 2004. **18**(24): p. 3055-65.
207. Campbell, J.S., et al., *Expression of suppressors of cytokine signaling during liver regeneration.* J Clin Invest, 2001. **107**(10): p. 1285-92.
208. Riehle, K.J., et al., *Regulation of liver regeneration and hepatocarcinogenesis by suppressor of cytokine signaling 3.* J Exp Med, 2008. **205**(1): p. 91-103.
209. Nishina, T., et al., *Interleukin-11 links oxidative stress and compensatory proliferation.* Sci Signal, 2012. **5**(207): p. ra5.
210. Radaeva, S., et al., *Interleukin 22 (IL-22) plays a protective role in T cell-mediated murine hepatitis: IL-22 is a survival factor for hepatocytes via STAT3 activation.* Hepatology, 2004. **39**(5): p. 1332-42.
211. Cressman, D.E., et al., *Liver failure and defective hepatocyte regeneration in interleukin-6-deficient mice.* Science, 1996. **274**(5291): p. 1379-83.
212. Sakamoto, T., et al., *Mitosis and apoptosis in the liver of interleukin-6-deficient mice after partial hepatectomy.* Hepatology, 1999. **29**(2): p. 403-11.
213. Ogata, H., et al., *Loss of SOCS3 in the liver promotes fibrosis by enhancing STAT3-mediated TGF-beta1 production.* Oncogene, 2006. **25**(17): p. 2520-30.
214. Yeoh, G.C., et al., *Opposing roles of gp130-mediated STAT-3 and ERK-1/ 2 signaling in liver progenitor cell migration and proliferation.* Hepatology, 2007. **45**(2): p. 486-94.
215. Lemaigre, F.P., *Development of the biliary tract.* Mech Dev, 2003. **120**(1): p. 81-7.
216. Si-Tayeb, K., F.P. Lemaigre, and S.A. Duncan, *Organogenesis and development of the liver.* Dev Cell, 2010. **18**(2): p. 175-89.
217. Lokmane, L., et al., *Crucial role of vHNF1 in vertebrate hepatic specification.* Development, 2008. **135**(16): p. 2777-86.
218. Matthews, R.P., et al., *The zebrafish onecut gene hnf-6 functions in an evolutionarily conserved genetic pathway that regulates vertebrate biliary development.* Dev Biol, 2004. **274**(2): p. 245-59.
219. Jones, S., *An overview of the basic helix-loop-helix proteins.* Genome Biol, 2004. **5**(6): p. 226.
220. Sumazaki, R., et al., *Conversion of biliary system to pancreatic tissue in Hes1-deficient mice.* Nat Genet, 2004. **36**(1): p. 83-7.

221. Kodama, Y., et al., *The role of notch signaling in the development of intrahepatic bile ducts.* Gastroenterology, 2004. **127**(6): p. 1775-86.
222. Yin, C., et al., *The basic helix-loop-helix transcription factor, heart and neural crest derivatives expressed transcript 2, marks hepatic stellate cells in zebrafish: analysis of stellate cell entry into the developing liver.* Hepatology, 2012. **56**(5): p. 1958-70.
223. Nath, B. and G. Szabo, *Hypoxia and hypoxia inducible factors: diverse roles in liver diseases.* Hepatology, 2012. **55**(2): p. 622-33.
224. Lin, T.Y., et al., *Hypoxia-inducible factor 2 alpha is essential for hepatic outgrowth and functions via the regulation of leg1 transcription in the zebrafish embryo.* PLoS One, 2014. **9**(7): p. e101980.
225. Sikder, H.A., et al., *Id proteins in cell growth and tumorigenesis.* Cancer Cell, 2003. **3**(6): p. 525-30.
226. Hua, H., et al., *BMP4 regulates pancreatic progenitor cell expansion through Id2.* J Biol Chem, 2006. **281**(19): p. 13574-80.
227. Yokota, Y., et al., *Development of peripheral lymphoid organs and natural killer cells depends on the helix-loop-helix inhibitor Id2.* Nature, 1999. **397**(6721): p. 702-6.
228. Bussmann, J. and S. Schulte-Merker, *Rapid BAC selection for tol2-mediated transgenesis in zebrafish.* Development, 2011. **138**(19): p. 4327-32.
229. Beis, D., et al., *Genetic and cellular analyses of zebrafish atrioventricular cushion and valve development.* Development, 2005. **132**(18): p. 4193-204.
230. Chung, W.S. and D.Y. Stainier, *Intra-endodermal interactions are required for pancreatic beta cell induction.* Dev Cell, 2008. **14**(4): p. 582-93.
231. Das, A. and J.G. Crump, *Bmps and id2a act upstream of Twist1 to restrict ectomesenchyme potential of the cranial neural crest.* PLoS Genet, 2012. **8**(5): p. e1002710.
232. Uribe, R.A., et al., *Id2a functions to limit Notch pathway activity and thereby influence the transition from proliferation to differentiation of retinoblasts during zebrafish retinogenesis.* Dev Biol, 2012. **371**(2): p. 280-92.
233. Field, H.A., et al., *Formation of the digestive system in zebrafish. I. Liver morphogenesis.* Dev Biol, 2003. **253**(2): p. 279-90.
234. Cheng, P.Y., et al., *Zebrafish cdx1b regulates expression of downstream factors of Nodal signaling during early endoderm formation.* Development, 2008. **135**(5): p. 941-52.
235. Argenton, F., E. Zecchin, and M. Bortolussi, *Early appearance of pancreatic hormone-expressing cells in the zebrafish embryo.* Mech Dev, 1999. **87**(1-2): p. 217-21.
236. Zhang, D.H., et al., *Identification of Annexin A4 as a hepatopancreas factor involved in liver cell survival.* Developmental Biology, 2014. **395**(1): p. 96-110.
237. Bai, G., et al., *Id sustains Hes1 expression to inhibit precocious neurogenesis by releasing negative autoregulation of Hes1.* Dev Cell, 2007. **13**(2): p. 283-97.
238. Robu, M.E., et al., *p53 activation by knockdown technologies.* PLoS Genet, 2007. **3**(5): p. e78.
239. Westerfield, M. and ZFIN., *The zebrafish book a guide for the laboratory use of zebrafish Danio (Brachydanio) rerio*. 2000, ZFIN,: Eugene, Or.
240. Godinho, L., et al., *Targeting of amacrine cell neurites to appropriate synaptic laminae in the developing zebrafish retina.* Development, 2005. **132**(22): p. 5069-79.
241. Langheinrich, U., et al., *Zebrafish as a model organism for the identification and characterization of drugs and genes affecting p53 signaling.* Curr Biol, 2002. **12**(23): p. 2023-8.

242. Alexander, J., D.Y. Stainier, and D. Yelon, *Screening mosaic F1 females for mutations affecting zebrafish heart induction and patterning.* Dev Genet, 1998. **22**(3): p. 288-99.
243. Ho, C.Y., et al., *A role for the extraembryonic yolk syncytial layer in patterning the zebrafish embryo suggested by properties of the hex gene.* Curr Biol, 1999. **9**(19): p. 1131-4.
244. Glasgow, E. and S.I. Tomarev, *Restricted expression of the homeobox gene prox 1 in developing zebrafish.* Mech Dev, 1998. **76**(1-2): p. 175-8.
245. Her, G.M., Y.H. Yeh, and J.L. Wu, *435-bp liver regulatory sequence in the liver fatty acid binding protein (L-FABP) gene is sufficient to modulate liver regional expression in transgenic zebrafish.* Dev Dyn, 2003. **227**(3): p. 347-56.
246. Kudoh, T., et al., *A gene expression screen in zebrafish embryogenesis.* Genome Res, 2001. **11**(12): p. 1979-87.
247. Flores, M.V., et al., *Intestinal differentiation in zebrafish requires Cdx1b, a functional equivalent of mammalian Cdx2.* Gastroenterology, 2008. **135**(5): p. 1665-75.
248. Zhao, X., et al., *Klf6/copeb is required for hepatic outgrowth in zebrafish and for hepatocyte specification in mouse ES cells.* Dev Biol, 2010. **344**(1): p. 79-93.
249. Stuckenholz, C., et al., *Sfrp5 modulates both Wnt and BMP signaling and regulates gastrointestinal organogenesis [corrected] in the zebrafish, Danio rerio.* PLoS One, 2013. **8**(4): p. e62470.
250. Klein, C., et al., *Neuron navigator 3a regulates liver organogenesis during zebrafish embryogenesis.* Development, 2011. **138**(10): p. 1935-45.
251. Lasorella, A., R. Benezra, and A. Iavarone, *The ID proteins: master regulators of cancer stem cells and tumour aggressiveness.* Nat Rev Cancer, 2014. **14**(2): p. 77-91.
252. Biggs, J., E.V. Murphy, and M.A. Israel, *A human Id-like helix-loop-helix protein expressed during early development.* Proc Natl Acad Sci U S A, 1992. **89**(4): p. 1512-6.
253. Ellmeier, W., et al., *Mutually exclusive expression of a helix-loop-helix gene and N-myc in human neuroblastomas and in normal development.* EMBO J, 1992. **11**(7): p. 2563-71.
254. Jung, S., et al., *Id proteins facilitate self-renewal and proliferation of neural stem cells.* Stem Cells Dev, 2010. **19**(6): p. 831-41.
255. Cooper, C.L., et al., *Expression of the Id family helix-loop-helix regulators during growth and development in the hematopoietic system.* Blood, 1997. **89**(9): p. 3155-65.
256. Norton, J.D. and G.T. Atherton, *Coupling of cell growth control and apoptosis functions of Id proteins.* Mol Cell Biol, 1998. **18**(4): p. 2371-81.
257. Mori, S., S.I. Nishikawa, and Y. Yokota, *Lactation defect in mice lacking the helix-loop-helix inhibitor Id2.* EMBO J, 2000. **19**(21): p. 5772-81.
258. Deed, R.W., et al., *Regulation of Id3 cell cycle function by Cdk-2-dependent phosphorylation.* Mol Cell Biol, 1997. **17**(12): p. 6815-21.
259. Rodriguez, J.L., et al., *Id2 leaves the chromatin of the E2F4-p130-controlled c-myc promoter during hepatocyte priming for liver regeneration.* Biochem J, 2006. **398**(3): p. 431-7.
260. Langlands, K., et al., *Differential interactions of Id proteins with basic-helix-loop-helix transcription factors.* J Biol Chem, 1997. **272**(32): p. 19785-93.
261. Miyajima, A., M. Tanaka, and T. Itoh, *Stem/progenitor cells in liver development, homeostasis, regeneration, and reprogramming.* Cell Stem Cell, 2014. **14**(5): p. 561-74.
262. Greenbaum, L.E., *The ductal plate: a source of progenitors and hepatocytes in the adult liver.* Gastroenterology, 2011. **141**(4): p. 1152-5.

263. Lu, W.-Y., et al., *Hepatic progenitor cells of biliary origin with liver repopulation capacity.* Nature Cell Biology, 2015. **17**(8): p. 971-83.
264. Lowes, K.N., et al., *Oval cell numbers in human chronic liver diseases are directly related to disease severity.* American Journal of Pathology, 1999. **154**(2): p. 537-541.
265. Bird, T.G.T., et al., *Bone marrow injection stimulates hepatic ductular reactions in the absence of injury via macrophage-mediated TWEAK signaling.* Proc Natl Acad Sci U S A, 2013. **110**(16): p. 6542-6547.
266. Ko, S., et al., *Bromodomain and extraterminal (BET) proteins regulate biliary-driven liver regeneration.* J Hepatol, 2016. **64**(2): p. 316-325.
267. Xu, C.P., et al., *Bone morphogenetic protein-2 is a negative regulator of hepatocyte proliferation downregulated in the regenerating liver.* World Journal of Gastroenterology, 2006. **12**(47): p. 7621-7625.
268. Sugimoto, H., et al., *BMP-7 functions as a novel hormone to facilitate liver regeneration.* Faseb Journal, 2007. **21**(1): p. 256-264.
269. Wu, C.C., et al., *Spatially Resolved Genome-wide Transcriptional Profiling Identifies BMP Signaling as Essential Regulator of Zebrafish Cardiomyocyte Regeneration.* Dev Cell, 2016. **36**(1): p. 36-49.
270. Sakaguchi, T.F., et al., *Endothelial signals modulate hepatocyte apicobasal polarization in zebrafish.* Curr Biol, 2008. **18**(20): p. 1565-71.
271. Delous, M., et al., *Sox9b is a key regulator of pancreaticobiliary ductal system development.* PLoS Genet, 2012. **8**(6): p. e1002754.
272. Massague, J. and D. Wotton, *Transcriptional control by the TGF-beta/Smad signaling system.* EMBO J, 2000. **19**(8): p. 1745-54.
273. Kramer, C., et al., *Maternally supplied Smad5 is required for ventral specification in zebrafish embryos prior to zygotic Bmp signaling.* Dev Biol, 2002. **250**(2): p. 263-79.
274. Ludtke, T.H., et al., *Tbx3 promotes liver bud expansion during mouse development by suppression of cholangiocyte differentiation.* Hepatology, 2009. **49**(3): p. 969-78.
275. Shirai, M., et al., *T-box 2, a mediator of Bmp-Smad signaling, induced hyaluronan synthase 2 and Tgfbeta2 expression and endocardial cushion formation.* Proc Natl Acad Sci U S A, 2009. **106**(44): p. 18604-9.
276. Snelson, C.D., et al., *Tbx2b is required for the development of the parapineal organ.* Development, 2008. **135**(9): p. 1693-702.
277. Nakahiro, T., et al., *Identification of BMP-responsive elements in the mouse Id2 gene.* Biochem Biophys Res Commun, 2010. **399**(3): p. 416-21.
278. Das, A. and J.G. Crump, *Bmps and Id2a Act Upstream of Twist1 To Restrict Ectomesenchyme Potential of the Cranial Neural Crest.* PLoS Genet, 2012. **8**(5).
279. Khaliq, M., et al., *Id2a is required for hepatic outgrowth during liver development in zebrafish.* Mech Dev, 2015. **138 Pt 3**: p. 399-414.
280. Urasaki, A., G. Morvan, and K. Kawakami, *Functional dissection of the Tol2 transposable element identified the minimal cis-sequence and a highly repetitive sequence in the subterminal region essential for transposition.* Genetics, 2006. **174**(2): p. 639-49.
281. Sugiyama, M., et al., *Illuminating cell-cycle progression in the developing zebrafish embryo.* Proc Natl Acad Sci U S A, 2009. **106**(49): p. 20812-20817.
282. Kwan, K.M., et al., *The Tol2kit: a multisite gateway-based construction kit for Tol2 transposon transgenesis constructs.* Dev Dyn, 2007. **236**(11): p. 3088-99.

283. de Groh, E.D., et al., *Inhibition of histone deacetylase expands the renal progenitor cell population.* J Am Soc Nephrol, 2010. **21**(5): p. 794-802.
284. Okabe, M., et al., *Potential hepatic stem cells reside in EpCAM(+) cells of normal and injured mouse liver.* Development, 2009. **136**(11): p. 1951-1960.
285. Nejak-Bowen, K.N., et al., *Accelerated liver regeneration and hepatocarcinogenesis in mice overexpressing serine-45 mutant beta-catenin.* Hepatology, 2010. **51**(5): p. 1603-13.
286. Padrissa-Altes, S., et al., *Control of hepatocyte proliferation and survival by Fgf receptors is essential for liver regeneration in mice.* Gut, 2015. **64**(9): p. 1444-53.
287. Apte, U., et al., *Wnt/beta-catenin signaling mediates oval cell response in rodents.* Hepatology, 2008. **47**(1): p. 288-295.
288. Fan, J., et al., *Bone morphogenetic protein-4 induced rat hepatic progenitor cell (WB-F344 cell) differentiation toward hepatocyte lineage.* J Cell Physiol, 2009. **220**(1): p. 72-81.
289. Zhang, L., et al., *BMP4 administration induces differentiation of CD133+ hepatic cancer stem cells, blocking their contributions to hepatocellular carcinoma.* Cancer Res, 2012. **72**(16): p. 4276-85.
290. Rossi, A., et al., *Genetic compensation induced by deleterious mutations but not gene knockdowns.* Nature, 2015. **524**(7564): p. 230-3.
291. Ding, B.S., et al., *Inductive angiocrine signals from sinusoidal endothelium are required for liver regeneration.* Nature, 2010. **468**(7321): p. 310-5.
292. Ding, B.S., et al., *Divergent angiocrine signals from vascular niche balance liver regeneration and fibrosis.* Nature, 2014. **505**(7481): p. 97-102.
293. Boulter, L., et al., *Macrophage-derived Wnt opposes Notch signaling to specify hepatic progenitor cell fate in chronic liver disease.* Nature Medicine, 2012. **18**(4): p. 572-579.
294. Huang, M.B., et al., *Antagonistic Interaction Between Wnt and Notch Activity Modulates the Regenerative Capacity of a Zebrafish Fibrotic Liver Model.* Hepatology, 2014. **60**(5): p. 1753-1766.
295. Michalopoulos, G.K. and M.C. DeFrances, *Liver regeneration.* Science, 1997. **276**(5309): p. 60-6.
296. Kochanek KD, M.S., Xu JQ, Tejada-Vera B, *Deaths: Final Data for 2014*, in *National Vital Statistical Reports*. 2016, National Center for Health Statistics: Hyattsville, MD.
297. Knight, B., et al., *Liver inflammation and cytokine production, but not acute phase protein synthesis, accompany the adult liver progenitor (oval) cell response to chronic liver injury.* Immunol Cell Biol, 2005. **83**(4): p. 364-74.
298. Libbrecht, L., et al., *Deep intralobular extension of human hepatic 'progenitor cells' correlates with parenchymal inflammation in chronic viral hepatitis: can 'progenitor cells' migrate?* J Pathol, 2000. **192**(3): p. 373-8.
299. Lowes, K.N., et al., *Oval cell numbers in human chronic liver diseases are directly related to disease severity.* Am J Pathol, 1999. **154**(2): p. 537-41.
300. Yin, L., D. Lynch, and S. Sell, *Participation of different cell types in the restitutive response of the rat liver to periportal injury induced by allyl alcohol.* J Hepatol, 1999. **31**(3): p. 497-507.
301. Hemmann, U., et al., *Differential activation of acute phase response factor/Stat3 and Stat1 via the cytoplasmic domain of the interleukin 6 signal transducer gp130. II. Src homology SH2 domains define the specificity of stat factor activation.* J Biol Chem, 1996. **271**(22): p. 12999-3007.

302. Zhong, Z., Z. Wen, and J.E. Darnell, Jr., *Stat3: a STAT family member activated by tyrosine phosphorylation in response to epidermal growth factor and interleukin-6.* Science, 1994. **264**(5155): p. 95-8.
303. Sanchez, A., et al., *Activation of NF-kappaB and STAT3 in rat oval cells during 2-acetylaminofluorene/partial hepatectomy-induced liver regeneration.* Hepatology, 2004. **39**(2): p. 376-85.
304. Moh, A., et al., *Role of STAT3 in liver regeneration: survival, DNA synthesis, inflammatory reaction and liver mass recovery.* Lab Invest, 2007. **87**(10): p. 1018-28.
305. Elsaeidi, F., et al., *Jak/Stat signaling stimulates zebrafish optic nerve regeneration and overcomes the inhibitory actions of Socs3 and Sfpq.* J Neurosci, 2014. **34**(7): p. 2632-44.
306. Zhao, X.F., et al., *Leptin and IL-6 family cytokines synergize to stimulate Muller glia reprogramming and retina regeneration.* Cell Rep, 2014. **9**(1): p. 272-84.
307. Gerloff, T., et al., *The sister of P-glycoprotein represents the canalicular bile salt export pump of mammalian liver.* J Biol Chem, 1998. **273**(16): p. 10046-50.
308. Carten, J.D., M.K. Bradford, and S.A. Farber, *Visualizing digestive organ morphology and function using differential fatty acid metabolism in live zebrafish.* Dev Biol, 2011. **360**(2): p. 276-85.
309. Sakaue-Sawano, A., et al., *Visualizing spatiotemporal dynamics of multicellular cell-cycle progression.* Cell, 2008. **132**(3): p. 487-98.
310. Liu, Y., D.S. Sepich, and L. Solnica-Krezel, *Stat3/Cdc25a-dependent cell proliferation promotes embryonic axis extension during zebrafish gastrulation.* PLoS Genet, 2017. **13**(2): p. e1006564.
311. Ninov, N., M. Borius, and D.Y. Stainier, *Different levels of Notch signaling regulate quiescence, renewal and differentiation in pancreatic endocrine progenitors.* Development, 2012. **139**(9): p. 1557-67.
312. Akira, S., *Roles of STAT3 defined by tissue-specific gene targeting.* Oncogene, 2000. **19**(21): p. 2607-11.
313. Alonzi, T., et al., *Essential role of STAT3 in the control of the acute-phase response as revealed by inducible gene inactivation [correction of activation] in the liver.* Mol Cell Biol, 2001. **21**(5): p. 1621-32.
314. Li, W., et al., *STAT3 contributes to the mitogenic response of hepatocytes during liver regeneration.* J Biol Chem, 2002. **277**(32): p. 28411-7.
315. Sun, L., et al., *JAK1-STAT1-STAT3, a key pathway promoting proliferation and preventing premature differentiation of myoblasts.* J Cell Biol, 2007. **179**(1): p. 129-38.
316. Wang, K., et al., *JAK2/STAT2/STAT3 are required for myogenic differentiation.* J Biol Chem, 2008. **283**(49): p. 34029-36.
317. Tierney, M.T., et al., *STAT3 signaling controls satellite cell expansion and skeletal muscle repair.* Nat Med, 2014. **20**(10): p. 1182-6.
318. He, G. and M. Karin, *NF-kappaB and STAT3 - key players in liver inflammation and cancer.* Cell Res, 2011. **21**(1): p. 159-68.
319. Kanther, M., et al., *Microbial colonization induces dynamic temporal and spatial patterns of NF-kappaB activation in the zebrafish digestive tract.* Gastroenterology, 2011. **141**(1): p. 197-207.
320. Ninov, N., M. Borius, and D.Y.R. Stainier, *Different levels of Notch signaling regulate quiescence, renewal and differentiation in pancreatic endocrine progenitors.* Development, 2012. **139**(9): p. 1557-1567.

321. Mosimann, C., et al., *Ubiquitous transgene expression and Cre-based recombination driven by the ubiquitin promoter in zebrafish.* Development, 2011. **138**(1): p. 169-77.
322. Ninov, N., et al., *Metabolic Regulation of Cellular Plasticity in the Pancreas.* Current Biology, 2013. **23**(13): p. 1242-1250.
323. Cheung, I.D., et al., *Regulation of intrahepatic biliary duct morphogenesis by Claudin 15-like b.* Developmental Biology, 2012. **361**(1): p. 68-78.
324. Pyati, U.J., et al., *Sustained Bmp signaling is essential for cloaca development in zebrafish.* Development, 2006. **133**(11): p. 2275-84.
325. Shimizu, N., K. Kawakami, and T. Ishitani, *Visualization and exploration of Tcf/Lef function using a highly responsive Wnt/beta-catenin signaling-reporter transgenic zebrafish.* Developmental Biology, 2012. **370**(1): p. 71-85.
326. Zhang, C., et al., *Interleukin-6/signal transducer and activator of transcription 3 (STAT3) pathway is essential for macrophage infiltration and myoblast proliferation during muscle regeneration.* J Biol Chem, 2013. **288**(3): p. 1489-99.
327. Shiau, C.E., et al., *Differential requirement for irf8 in formation of embryonic and adult macrophages in zebrafish.* PLoS One, 2015. **10**(1): p. e0117513.